This electronic thesis or dissertation has been downloaded from the King's Research Portal at https://kclpure.kcl.ac.uk/portal/

KING'S College LONDON

A Multi-Modal Assessment of Brain Alterations in Young Adults with Psychotic Experiences
Results from the Avon Longitudinal Study of Parents and Children

Fonville, Leon Michel

Awarding institution:
King's College London

The copyright of this thesis rests with the author and no quotation from it or information derived from it may be published without proper acknowledgement.

END USER LICENCE AGREEMENT

Unless another licence is stated on the immediately following page this work is licensed

under a Creative Commons Attribution-NonCommercial-NoDerivatives 4.0 International

licence. https://creativecommons.org/licenses/by-nc-nd/4.0/

You are free to copy, distribute and transmit the work

Under the following conditions:

- Attribution: You must attribute the work in the manner specified by the author (but not in any way that suggests that they endorse you or your use of the work).
- Non Commercial: You may not use this work for commercial purposes.
- No Derivative Works - You may not alter, transform, or build upon this work.

Any of these conditions can be waived if you receive permission from the author. Your fair dealings and other rights are in no way affected by the above.

Take down policy

If you believe that this document breaches copyright please contact librarypure@kcl.ac.uk providing details, and we will remove access to the work immediately and investigate your claim.

Download date: 05. May. 2023

A Multi-Modal Assessment of Brain Alterations in Young Adults with Psychotic Experiences: Results from the Avon Longitudinal Study of Parents and Children

Leon Michel Fonville

Institute of Psychiatry, Psychology, and Neuroscience

SUBMITTED FOR THE DEGREE OF

DOCTOR OF PHILOSOPHY

KING'S COLLEGE LONDON

Abstract

The work presented in this doctoral thesis examines magnetic resonance imaging (MRI) data on a sample of young adults who were assessed for the presence of psychotic experiences (PEs) such as delusions, hallucinations, and thought interference. The manifestation of PEs is considered a risk factor for psychosis that becomes greater with persistence of symptoms. The aim of this body of work was to examine the state of the brain using MRI in individuals with PEs, taking into account previous reports on psychosis as well as typical neurodevelopment. We have carried out a range of imaging techniques and analyses on a large multi-modal imaging dataset of 111 healthy controls, 67 with transient PEs, and 69 with persistent PEs.

I initially set out to examine brain structure and function in relation to working memory through voxel-based morphometry of grey matter and investigating neurofunctional signalling in relation to a working memory task. In addition, I sought to characterise the temporal dynamics of regional activation in frontal and parietal regions involved in working memory using dynamic causal modelling. Next, we carried out an in-depth analysis of the cortical surface morphometry and sought to characterise the underlying white matter connectivity using atlas-based tractography. Finally, we carried out virtual dissections of the corpus callosum, the inferior fronto-occipital fasciculus, and the superior longitudinal fasciculus.

We found qualitative evidence of protracted development of working memory network configuration in relation to duration of PEs but neuroanatomical evidence did not show consistent support. We found evidence of disturbances in cortical folding in relation to persistence of PEs but little evidence of accompanying alterations in white matter. Analyses of dissected tracts did highlight differences along the tract in relation to PEs. We discuss these findings in relation to their implication for PEs as a risk factor for a psychotic disorder and as a manifestation of an atypical neurodevelopment trajectory.

Acknowledgements

It would not have been possible to commit several years to a project like this without the support and guidance of the many kind people that are in my life. There are too many names and examples to list here but there are several that deserve and need to be mentioned.

First and foremost I need to thank my principal supervisor Professor Anthony David for not only providing this opportunity but to offer continued support and guidance during my PhD and having the patience to allow me to make the most of this experience. I am also thankful to my second supervisor, Professor Derek Jones, who welcomed me to Cardiff and invested his time and effort in my development.

I need to extend my thanks to Dr. Mark Drakesmith and Dr. Greg Parker at CUBRIC for their continued assistance in all my imaging-related queries. Your input and help was always greatly appreciated. I am grateful to all the wonderful people I've shared an office with in our little section of Cognitive Neuropsychiatry, whether I needed help or just a friendly chat you've always been happy to help. I'll miss the cake.

To all my friends at the IoPPN with whom I've shared the highs and lows of our pursuit of 'academic excellence', you've helped keep me sane many times over. My friends outside of academia, especially my teammates in jiu-jitsu, thank you for making me remember the world outside of my PhD.

Last but not least a big thank you to my family. To my parents who despite my best efforts managed to guide me in this direction and continued to support me throughout. Without them I would never have been in this position. To my wife Candace, without her I would never have lasted in this foreign city nor would I ever have been able to call it my home.

This thesis is dedicated to my parents, Arnold and Henny,

and to my wonderful wife Candace.

Statement of Contribution

In this thesis I set out to examine the impact of psychotic experiences (PEs) during late adolescence and early adulthood on brain structure, function, and organisation using multi-modal magnetic resonance imaging (MRI). Data acquisition had already been completed and I joined during the data analysis phase of the project.

I took lead on analysis of the functional MRI data and carried out the pre-processing of structural and functional MRI data, statistical analyses of fMRI and behavioural data, and modelling of the temporal dynamics during fMRI within a fronto-parietal network. In addition, I carried out a complementary analysis of the segmented grey matter images from the structural MRI data.

On the remainder of the structural and diffusion MRI data that had been implemented in other analyses I coordinated with colleagues on how to best incorporate work that had already been carried out in my own analyses. I picked up a prior analysis on the cortical surface morphometry and ran additional preprocessing steps prior to my own statistical analyses. I then incorporated the diffusion imaging data that had already been preprocessed to analyse the underlying white matter using atlas-based tractography. I carried out the virtual dissections and automated shape modelling of specific white matter bundles and conducted statistical modelling on these tracts.

Table of Contents

Table of Tables

Table of Figures

Chapter 1

Magnetic Resonance Imaging across the Psychosis Spectrum

One of the ongoing challenges in psychiatry has been to accurately identify individuals who are prone to developing a serious mental health problem. In particular, the timely recognition of those at risk of developing a psychotic disorder, such as schizophrenia, has become an important field of study; the duration of untreated psychosis has been linked to poor treatment response, higher chances of relapse and a poorer prognosis overall (Drake et al., 2000; Perkins et al., 2005). Furthermore, much of the disability that is commonly seen in those with psychotic disorders slowly begins to form during this pre-psychotic phase (McGorry et al., 2008). As such, early intervention programs for psychosis have become common practice, with international clinical guidelines introduced (International Early Psychosis Association Writing Group, 2005), and a substantial amount of research has been dedicated to the identification of individuals considered at high risk to prevent or delay the onset of a psychotic disorder (McGorry et al., 2008). Operational criteria have been defined to describe those considered at ultra-high risk for psychosis (Yung et al., 1998; Phillips et al., 2000) which combine state and trait risk factors including attenuated psychotic symptoms, brief limited intermittent psychotic episode, a significant decline in general functioning paired with a greater familial risk of psychosis, or basic symptoms (Yung et al., 1998; Phillips et al., 2000). These criteria capture a relatively heterogeneous cohort as they were formulated to identify those with a high likelihood of transitioning to psychosis and it has been found that roughly 1 out of 4 goes on to develop a psychotic disorder, the majority of which being diagnosed with schizophrenia (Fusar-Poli et al., 2012a).

More recently, it has been proposed that psychotic symptoms can be expressed at levels below the traditional high threshold of clinical significance and are far more prevalent in the general population than the clinical disorder (van Os et al., 2000; van Os, 2003; van Os et al., 2009). These symptoms, frequently cited as subclinical psychotic experiences (PEs), have forced a reappraisal of the psychosis phenotype in which the expression lies along a continuum with psychotic disorders representing an extreme variant. Such a reappraisal provides for an elegant account of differing degrees of severity and specificity and tends towards the consideration of the psychosis phenotype as a transdiagnostic feature of mental health rather than a discrete disorder. This is also reflected in the fact that, as in schizophrenia, individuals with PEs frequently report at least one diagnosable non-psychotic disorder (Buckley, Miller, Lehrer, & Castle, 2009; Kelleher et al., 2012). However, PEs are associated with an elevated risk of transitioning to a psychotic disorder that follows a dose-response relationship with increasing persistence of symptoms (Kaymaz et al., 2012). The manifestation of PEs also shows similar associations with demographic risk factors as those known for schizophrenia, such as urbanicity, lower childhood trauma, ethnic minority status, and cannabis use (van Os et al., 2009). There is less clear evidence of a common underlying genetic risk for PEs; while familial clustering has been reported (van Os et al., 2009), there has been a lack of strong associations between polygenic risk for schizophrenia and the presence of PEs (Zammit et al., 2013a; Jones et al., 2016). Furthermore, the cognitive profile of adults with PEs differs from that seen in those with psychotic disorders (Mollon et al., 2016) and though it is possible that much of the deterioration associated with schizophrenia occurs after onset, such a decline has not been reported in studies of high risk and first-episode patients (Bora & Murray, 2014). Debate surrounding the proposed extended psychosis phenotype is ongoing (David, 2010; Lawrie et al., 2010; Kaymaz & van Os, 2010; Yung & Lin, 2016; Tandon, 2016) and the utility of PEs in psychiatric research, particularly for psychosis, as well as clinical practice remains an active field of study. If PEs are qualitatively similar to clinical psychotic phenomena, and manifest as a result of similar

aetiological factors, comparable disturbances in neuroanatomy should be observable using imaging techniques. The following sections aim to summarise the literature on PEs, their correspondence to the high risk prodrome, and how both relate to schizophrenia.

1.2 Magnetic Resonance Imaging in Schizophrenia

Psychotic disorders such as schizophrenia are considered to have a neuropathological basis associated with dynamic changes through the course of psychosis, consisting of both early neurodevelopmental aberrations and progressive accelerated maturational processes that take place around the time of transition to illness (Lewis & Levitt, 2002; Pantelis et al., 2005; Walker et al., 2013). Evidence for progressive changes comes from longitudinal studies that have examined brain anatomy in first-episode and early-onset schizophrenia and found accelerated loss of cortical grey matter volume, relative to healthy controls, over time that was not uniform across the whole brain. Some of these studies showed that the decrease in grey matter volume was more pronounced in the superior temporal gyrus, particularly in the left hemisphere, and age of onset was found to be a moderator of overall volume loss as well as reductions in the temporal lobe (Vita et al., 2012). Examining first-episode patients highlighted a greater difference in volume loss in all of the cerebral lobes and this suggests major reductions in cortical grey matter occur during the initial stage of psychosis. Earlier onset on the other hand was found to moderate both whole brain as well as temporal grey matter volume leading to a more pronounced trajectory of volume loss. Similarly, enlargement of the lateral ventricles over time has been found to be greater in those with chronic schizophrenia (Kempton et al., 2010). Though the link to volume changes is not fully understood, progressive disturbances in cortical complexity have been reported and has predominantly implicated the frontal lobe (White & Hilgetag, 2011; White &

Gottesman, 2012). The underlying white matter connectivity in schizophrenia is also thought to be critical as it has been proposed that schizophrenia arises from dysfunction of connectivity, often described as 'dysconnectivity', that involves frontal, frontotemporal and frontolimbic circuitry (Pettersson-Yeo et al., 2011; Wheeler & Voineskos, 2014). Though there is a lack of longitudinal studies on white matter, cross-sectional findings show a strong degree of overlap in location and direction of the effects between early-onset, first-episode and chronic schizophrenia, highlighting reduced fractional anisotropy in the corpus callosum, the inferior fronto-occipital fasciculus, the internal capsule, and the superior and inferior longitudinal fasciculi (Pettersson-Yeo et al., 2011; Wheeler & Voineskos, 2014). Unlike anatomical imaging, functional imaging studies have produced more conflicting results regarding schizophrenia that has been unable to produce a uniform regional explanation for the heterogeneous alterations in functional response that have been reported (Glahn et al., 2005). Instead, recent advances have aimed to interpret focal disturbances as part of interconnected networks where abnormalities are due to dysconnectivity within specific networks (Stephan et al., 2006a, 2006b; Crossley et al., 2016). Reframing functional activation using graph theory has led to the notion that in schizophrenia both network connectivity and topological organisation is affected and the typically seen hyper- and hypoactivation is reflective of compensatory mechanisms due to poorer integration that centres around highly connected brain regions, or 'hubs' (van den Heuvel & Fornito, 2014; Crossley et al., 2016).

1.3 Magnetic Resonance Imaging in the Psychosis Prodrome

It is assumed that the observed aberrations in the brain that are present in schizophrenia begin prior to the onset of the illness, though the exact nature and timing of these events is not yet fully understood (Pantelis et al., 2005). Disturbances in grey matter volume have consistently been reported by cross-sectional studies

that have assessed those considered at high risk and typically report on volume reductions in the prefrontal and cingulate regions, but have also listed temporal and parietal regions (Jung et al., 2010; Chan et al., 2011; Fusar-Poli et al., 2011a; Mechelli et al., 2011; Schmidt et al., 2013; Bois et al., 2015). As mentioned, around one quarter of individuals considered at ultra-high risk, transition to a psychotic disorder (Fusar-Poli et al., 2012a) and several studies have distinguished between transition outcomes within those at high risk using cross-sectional or longitudinal designs. Cross-sectional studies reveal that those who do end up transitioning show greater reductions in grey matter volume in the frontal, cingulate and temporal cortex compared to those who do not transition. Furthermore, longitudinal assessments have found a different pattern of volume reduction over time in those who end up transitioning in these same regions as well as in the cerebellum (Wood et al., 2008; Smieskova et al., 2010; Bois et al., 2015). These findings match well with comparisons of the high risk prodrome and first-episode patients (Fusar-Poli et al., 2011a). Imaging findings on white matter are not as clear yet; though similar fronto-temporal and fronto-limbic connections have been highlighted as showing abnormalities (Fusar-Poli et al., 2011a; Vita et al., 2012) there is a lack of further comparisons between high risk and schizophrenia as well a further distinction between transition outcomes in those at risk. As expected, alongside these reported volume reductions and aberrant connectivity there are abnormalities in cortical complexity (Stanfield et al., 2008) and these have been suggested to be indicative of a transition to a psychotic disorder (Harris et al., 2004, 2007). Interestingly, with respect to gyrification, the findings in schizophrenia tend to be mixed whereas in the high risk prodrome there have only been reported increases in gyrification in the prefrontal lobe. Though fMRI studies have commonly highlighted aberrations in functional response in high risk individuals across cognitive paradigms (Fusar-Poli et al., 2007), further corroborated by recent work from our group (Dutt et al., 2015), current evidence for 'dysconnectivity' has mostly been limited to individual studies implicating aberrant functional connectivity of the so-called default mode network (Shim et al., 2010),

fronto-temporal (Allen et al., 2010), fronto-parietal (Schmidt et al., 2014a), and fronto-striatal network coupling (Dandash et al., 2014).

1.4 Magnetic Resonance Imaging in Psychotic Experiences

The study of psychotic experiences using MRI is fairly recent and the majority of early studies that have looked at PEs in comparison to healthy controls (HC) have not been consistent in their findings (see table 1). This inconsistency is most likely due to confounding by differing assessments of PEs as well as lack of statistical power due to inadequate sample sizes.

Table 1. Overview of early neuroimaging studies on PEs. Red arrows indicate reductions found in PEs in comparison to healthy controls and green arrows indicate increases.

Author	Sample	Modality (Measure)	Results (in PEs)		Comments
Jacobson et al. (2010)	11 PEs, 14 HC	fMRI (BOLD)	↓	Frontal, cingulate and temporal areas	PEs were screened using a questionnaire but confirmed via clinical interview. Study was on schoolchildren.
		sMRI (GMV)	↑	Orbitofrontal, angular, middle and superior temporal gyri	
			↓	Middle temporal gyrus	
		DTI (FA)	↓	IFOF, ILF and CB	
Modinos et al., (2010b)	17 PEs, 17 HC	fMRI (BOLD)	↑	Prefrontal areas	PEs were selected based on high scores on a self-report screening tool for PE. The entire sample consisted of undergraduates.
			↓	Prefrontal-amygdala coupling	
Modinos et al. (2010a)	18 PEs, 20 HC	sMRI (GMV)	↑	Posterior cingulate and precuneus	Same cohort as above

Table 1. Continued from previous page

Author	Sample	Modality (Measure)	Results (in PEs)		Comments
Modinos et al. (2011)	18 PEs, 18 HC	fMRI (BOLD)	↑	Insula, prefrontal, and anterior cingulate cortex	Same cohort as above
Modinos et al. (2012)	20 PEs, 20 HC	fMRI (BOLD)	-	No differences	Same cohort as above
				75% Accuracy in classification	
Corlett & Fletcher (2012)	18 HC	fMRI (BOLD)	↓	Correlation between BOLD signal and 'magical ideation' in frontal and striatal regions	The participants completed several self-report measures on schizotypy.
DeRosse et al. (2014)	112 HC	DTI (FA)	↓	Correlation between PEs score and FA in the SLF	PEs defined using a self-report measure
Orr et al. (2014)	25 PEs, 27 HC	fMRI (BOLD)	↓	Fronto-parietal network coupling Default mode network coupling Cingulo-opercular network coupling Cerebellar network coupling	PEs were selected based on high scores on a self-report screening tool for PE.
			↑	Fronto-parietal network coupling (in different clusters)	
Córdova-Palomera et al. (2014)	48 HC	sMRI (CT)	-	No correlation between cortical thickness and PEs score	Sample was made of monozygotic twin pairs A PEs score was obtained from a self-report measure.
Pelletier-Baldelli et al. (2014)	20 PEs, 20 HC	sMRI (GMV)	↓	Orbitofrontal cortex	PEs were selected based on high scores on a self-report screening tool for PE.

As PEs are assumed to be prevalent in the general population, more recent studies have adopted a population-based approach (rather than based on help-seeking individuals) and have been able to recruit from a much larger sample.

A population-based sample of youths aged 11 to 22 years old, part of the Philadelphia Neurodevelopmental Cohort, has taken part in studies of anatomical and functional differences in the brain in relation to symptoms along the psychosis spectrum (Satterthwaite et al., 2014). An fMRI study on working memory in this sample highlighted a lower BOLD signal in those with PEs in response to a working memory task across a range of regions involved in working memory, including the superior parietal lobule and middle and superior frontal regions, as well as the precuneus, lateral occipital lobe, cerebellum and insula (Wolf et al., 2015). Interestingly, this study also incorporated an emotion identification task and here those with PEs were found to demonstrate a greater functional response in the amygdala as well as in superior and middle frontal gyri and the fusiform gyrus. Looking at the activation within the PE group, it was found that severity of symptoms during the emotion identification paradigm was found to correlate with the response in the amygdala but not with the cognitive deficits. During the working memory paradigm, it was found that the response in the prefrontal lobe was correlated with cognitive deficits rather than symptom severity. A more sophisticated analysis of the underlying connectivity of functional networks instead highlighted abnormalities within both the default-mode network and a cingulo-opercular network, which is considered to underlie attentional control (Satterthwaite et al., 2015). Interestingly the finding of reduced connectivity within the cingulo-opercular network, but not the increased connectivity of the default-mode network, is in agreement with a previous smaller study on PEs by Orr et al. (2014) that is listed in table 1.

Other imaging studies on this sample from the Philadelphia Neurodevelopmental Cohort have reported structural abnormalities as well, individuals with PEs were found to have a global reduction grey matter volume and an increase in white matter volume (Satterthwaite et al., 2016). Further voxel-based analyses found that even when taking intracranial volume into account there were volumetric reductions spanning temporal, prefrontal, orbitofrontal and posterior cingulate regions. Interestingly, in the medial temporal lobe there was a group-by-age interaction

effect where volume was initially greater during childhood but dropped below that of their typical peers during adolescence. However, a second in-depth study of specific regions of interest did not find strong evidence of volumetric differences in those with PEs (Roalf et al., 2016). This study examined the amygdala, hippocampus, interior and superior temporal gyrus, temporal pole, parahippocampal gyrus, and entorhinal cortex in both hemispheres and volumetric reductions were limited to just the left entorhinal cortex. A recent population-based study from our group that examined young adults with PEs instead found reduced grey matter volume in the supramarginal gyrus and, using an ordinal approach to severity of PEs, disturbances in cortical myelination in temporo-parietal and frontal areas (Drakesmith et al., 2016b).

A recent study on white matter, part of the Adolescent Brain Development Study (Kelleher et al. 2012), examined adolescents with PEs and reported voxel-based alterations that converged in the areas covering the superior longitudinal fasciculus (SLF), the inferior fronto-occipital fasciculus (IFOF), and the uncinate fasciculus (UF) (O'Hanlon et al. 2015). Further examination of these tracts highlighted increased fractional anisotropy (FA) and axial diffusivity in the UF and along-tract statistics further revealed alterations at several positions along the tract in the frontal section of the IFOF. A recent population-based study from our group also highlighted voxel-based disturbances that implicate the IFOF and SLF as well as the corona radiata, corpus callosum, and internal capsule (Drakesmith et al., 2016a). More importantly this study found a similar pattern of reduced FA in frontal medial pathways using either a binary comparison of people with PEs versus controls with no PEs, as well as using an ordinal definition related to the severity of PEs.

Though it is easy to recognise some overlap with the psychosis literature, it should be noted that the findings in PEs do not follow the typical widespread pattern of alterations across the brain. It is clear the current literature on PEs using MRI is limited and still lacking in robust data. While there is some evidence of qualitative

similarities with the general psychosis literature, more work is needed to establish a neuroimaging profile of PEs and to fill in the gaps that currently exist. Furthermore, there is a lack of consideration for the neurodevelopmental origin of disturbances in the brain and this is of particular importance for PEs which can be placed conceptually at one of the early stages in the illness progression.

1.5 Objectives and Outline

The study of brain structure, function, and organisation in individuals with psychotic experiences is a recent field of enquiry. By examining those who express subclinical symptoms, and are at elevated risk of developing a psychotic disorder, it might be possible to identify anatomical and functional abnormalities that play a role in the manifestation of these symptoms. Moreover, the persistence of PEs is associated with a further elevated risk of developing a psychotic disorder and little is known about the effect of persistent PEs on the brain. Finally, the mere presence of PEs during development highlights an atypical trajectory that is likely to be observable in the brain and could provide novel insights into the manifestation of subclinical and clinical levels of hallucinations, delusions, and thought interference. The objective of this study was to examine the brain of those with PEs to gain insight on what drives the manifestation of these symptoms and, for the first time, investigate the profile of abnormally persistent PEs using a multi-modal approach. In this thesis I aim to report our findings on brain function and structure in PEs and to examine them from a neurodevelopmental perspective.

In the third chapter, we utilise functional and structural magnetic resonance imaging to assess working memory function in PEs using a letter variant of the n-back task to test for differences in blood-oxygenation level dependent (BOLD) signal and to examine the network configuration of the engaged fronto-parietal brain network as well as the underlying brain structure in terms of grey matter volume.

The fourth chapter further investigates the structural integrity of the cortex, this time examining cortical thickness and cortical folding patterns (gyrification), to gain insight into the developmental trajectory of cortical grey matter. We also sought to investigate the effect of genetic risk for schizophrenia alongside the effect of PEs. Deviations in cortical morphometry were linked to white matter, using atlas-based tractography, to further assess the nature of these disturbances.

The fifth chapter focuses on the structural connectivity of three major white matter bundles; the inferior fronto-occipital fasciculus, the corpus callosum, and the superior longitudinal fasciculus. Segmentation was carried out using a novel automated procedure that utilises shape modelling and an along-tract approach was carried out to examine the microstructural qualities along each white matter pathway in relation to PEs.

Overall, we expected to find abnormalities that overlap with those found in schizophrenia and high risk cohorts. This entails reductions in BOLD response as well as differences in the modulatory connections of the working memory network during the task. Though typically reductions are present in grey matter volume in association with psychosis, prior studies have not been conclusive so we had no specific regional hypothesis and took an exploratory data driven approach. Nevertheless, on the basis of existing literature, we hypothesised that cortical morphometry would be affected in those with PEs in frontal, parietal, and temporal regions of the brain in relation to cortical folding but not cortical thickness. However, in those with persisting PEs and high genetic risk for schizophrenia we did expect to find reductions in cortical thickness. We further anticipated disturbances in structural connectivity in regions that showed aberrant cortical folding.

Within this programme of research, we had a rating of the presence of PEs at two separate assessments roughly 2 years apart. These ratings were combined to classify the transient or persistent nature of the PEs in individuals. Across all our analyses, we considered those with persistent PEs to be at greater risk and expected this group to

show a stronger deviation from healthy controls in terms of MRI indices that is more comparable to those with schizophrenia. Thus in all our work we hypothesised a linear relation between the transient and persistent nature of PEs relative to healthy controls where the size of an effect will be greater in those with persisting symptoms.

Chapter 2

General Methodology

This chapter provides a detailed description of the methodology used in this thesis. Many of the findings throughout this thesis will or have become published academic works and have been written with this in mind. First, we describe our study sample in greater detail to avoid unnecessary repetition of minor details in later chapters. Second, we provide a general frame of reference on the principles and assumptions of MRI so that the following chapters can focus on the application of these methods and the interpretation of our findings.

2.1 Study Sample

2.1.1 Background

All participants were part of The Avon Longitudinal Study of Parents and Children (ALSPAC; http://www.bristol.ac.uk/alspac/) birth cohort that originated in the early 1990s and involved over 14,000 pregnant women from Avon in the southwest of England. These women, their children, and their partners have been extensively followed up on for the past two decades to examine the effect of genetic and environmental factors on health. As part of the ALSPAC study, children were assessed for the presence of psychotic experiences at ages 12 and 18 using the semi-structured Psychosis-Like Symptoms Interview (PLIKSi; Horwood et al., 2008).

The PLIKSi is made up of questions derived from the Diagnostic Interview Schedule for Children (DISC; Shaffer et al., 2000) and the Schedules for Clinical Assessment in Neuropsychiatry (SCAN; Wing et al., 1990). It consists of 12 core questions that assess the presence of key PEs over the past 6 months and these questions cover the

occurrence of hallucinations (auditory and visual), delusions (being spied on, persecuted, thoughts being read, control, grandiose ability, reference and other unspecified delusions) and thought interference (broadcasting, insertion, and withdrawal). Further cross-questioning and probing can be used to establish the presence of PEs and ratings follow glossary definitions and rules for SCAN. The interviewer rated experiences as absent, suspected, or definitely psychotic. Experiences were only rated as definite when the interviewee was able to provide a clear example and unclear responses are always rated down. The interviews were carried out by psychology graduates trained in assessments using the SCAN psychosis section and the PLIKSi.

2.1.2 Participants

A total of 4,724 young adults were assessed for the presence of PEs using the PLIKSi when they were around 18 years old and 433 (9.2%) individuals were rated as having suspected or definite PEs (Zammit et al., 2013b). From this sample, 126 individuals were recruited to take part in the imaging study and were reassessed for the presence of PEs on the day of the scan. A control group of 126 participants was recruited out of the 4,291 individuals who were rated as not having had PEs at age 18. This control group was recruited at random until the two groups were balanced. Controls were also reassessed for the presence of psychotic experiences on the day of the scan. Figure 1 gives an overview of the amount of individuals involved and the criteria used in classifying participants.

At the time of the imaging study and PLIKSi reassessment all participants were approximately 20 years old. Out of the 252 individuals recruited to take part in the study, only 247 were reassessed for PEs which leads to a regrouping of 122 controls and 125 with PEs. The PLIKSi at age 20 revealed that 111 out of the 122 controls were still rated as not having had any PEs. Out of the 126 individuals with PEs, 69 were still rated as having had suspected or definite PEs in the past 6 months and 56 were no

longer rated as having had PEs. Conversely, 11 of the original control sample were now rated as having had suspected or definite PEs.

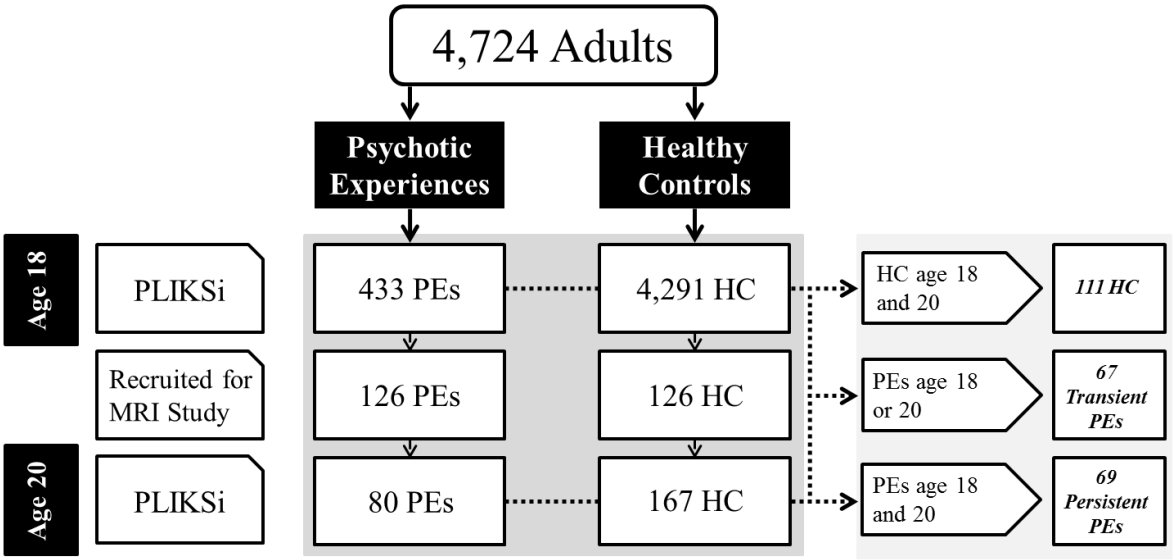

Figure 1. Flowchart describing the assessment using the PLIKSi and the recruitment of participants.[1] Though a total of 252 individuals were recruited to undergo MRI scanning, only 247 of them were re-assessed on the day for the presence of PEs.

2.1.3 Psychotic Experiences

As mentioned, the PLIKSi was used to evaluate the presence of PEs in the domains of hallucinations, delusions and thought interference. The most frequently reported PEs were in the hallucinations domain, though a large portion of the sample were rated as having had PEs in several domains. A summary of the percentage of individuals who reported PEs in each domain is given in table 2 and figure 2 highlights the numerous changes over time in the distribution of the reported PEs per domain.

[1] Figure 1 was adapted from a flowchart that is originally part of our published manuscript, represented in this thesis as chapter 3. The numbers have been adapted to describe the overall sample rather than the subsample used in that study.

Table 2. An overview of the PEs that were reported at assessments. The number between parentheses represents the proportion that reported PEs solely in that domain.

Domain	Age 18	Age 20
	n = 125	n = 80
Hallucinations	84.8%	77.5%
	(51.2%)	(42.5%)
Thought Interferences	33.6%	33.8%
	(4.0%)	(1.3%)
Delusions	26.4%	35.0%
	(8.8%)	(20.0%)

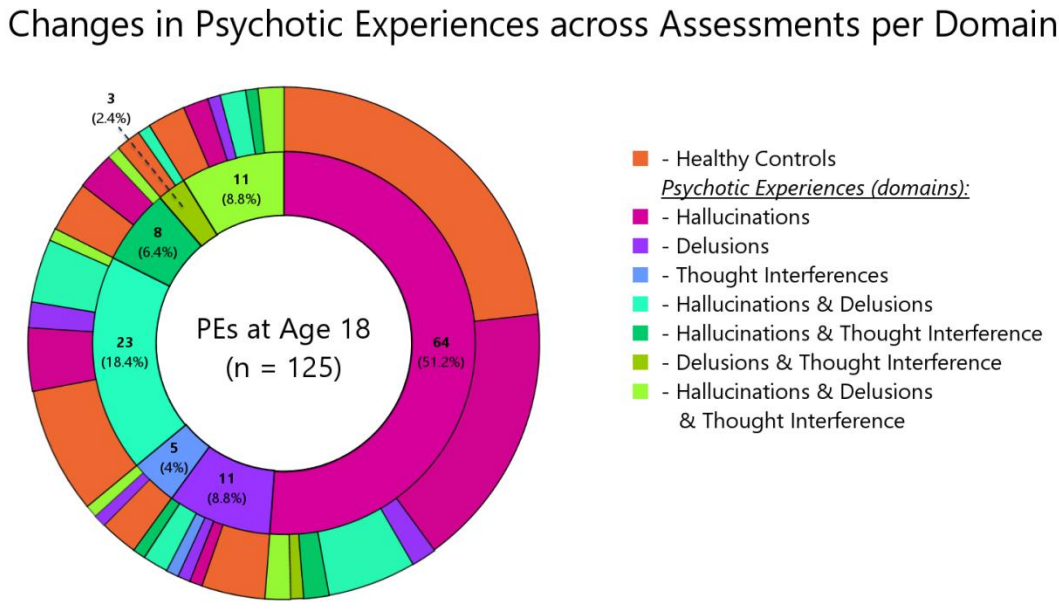

Figure 2. Prevalence and change in reported PEs. **Inner circle:** Prevalence of the reported PEs at age 18 per domain giving the actual numbers of participants and the percentage out of the total in parentheses. **Outer circle:** Breakdown of the change in reported PEs at age 20 for each of the initial domains that PEs fell under at age 18.

2.2 Informed Consent

Written consent was obtained prior to assessment at age 18 and ethical approval was obtained from the ALSPAC Law and Ethics Committee and the local research ethics committees. All participants gave informed consent prior to scanning and reassessment at age 20 and ethical approval was granted by the Cardiff University School of Psychology Ethics Committee and the ALSPAC Ethics and Law Committee.

2.3 ALSPAC Variables

Several measures were obtained from the ALSPAC database to be included in imaging analyses. These included gender, handedness, and childhood IQ, Childhood IQ was obtained using the Wechsler Intelligence Scale for Children (WISC-III; Wechsler, Golombok, & Rust, 1992) and was administered at age 8. The WISC-III was shortened to only carry out the alternate items with the exception of the coding subtest which did get administered in its standard form (Horwood et al., 2008).

2.4 Magnetic Resonance Imaging

2.4.1 Background

The following section provides a rough overview of the principles and application of magnetic resonance imaging (MRI). For a detailed description of these processes and more we refer to established bodies of work by Westbrook and Kaut (1998) and the work of McRobbie et al. (2003). MRI is a medical imaging technique that allows for a non-invasive assessment of anatomy and physiological processes in the body *in vivo*. It relies on the property of nuclear magnetic resonance, which is the phenomenon of MR active nuclei absorbing and re-emitting electromagnetic radiation. Hydrogen is most commonly targeted due to the abundance of water in the human body.

Hydrogen has an MR active nucleus[2] that contains a single positively charged proton that spins and has a magnetic field induced around it with a north and south pole of equal strength. The north and south poles of each nucleus are represented by the magnetic moment and in absence of an applied magnetic field the magnetic moments of hydrogen nuclei are randomly orientated. When placed in an external magnetic field B_0, such as an MRI scanner, the magnetic moments align along the axis of B_0. Hydrogen nuclei possess energy in one of two discrete quantities; *i)* low-energy nuclei that align their magnetic moments parallel to the longitudinal plane and are often referred to as spin-up nuclei and *ii)* high-energy nuclei that align their magnetic moments in anti-parallel direction and are termed spin-down nuclei. The thermal energy (low/high) of a nucleus is mainly determined by the temperature of the individual undergoing MR scanning and cannot be significantly altered, often referred to as thermal equilibrium. As such, at higher magnetic field strengths there are fewer nuclei with enough energy to align anti-parallel to B_0. Additionally, under thermal equilibrium there are always a larger number of spin-up nuclei and this produces a net magnetic vector M_0 in alignment with the external magnetic field B_0 that reflects the balance between spin-up and spin-down nuclei. Regardless of their alignment, the presence of a strong magnetic field produces an additional spin, or wobbling motion, of the magnetic moments around B_0 which is called precession. This secondary spin follows a circular path around B_0 and spins at a specific frequency. The Larmor frequency of precession (ω_0) for hydrogen nuclei is the product of the strength of the magnetic field B_0 and the gyro-magnetic ratio (γ), which expresses the ratio of a nucleus' angular momentum and magnetic moment. The gyro-magnetic ratio of hydrogen nuclei is 42.57MHz/T.

[2] MR active nuclei are any nuclei that have an angular momentum, or spin, due to either a greater or lesser amount of neutrons than protons that leads to unequal opposite spin directions. Nuclei with an even mass number have an equal number of protons and neutrons and the opposite spin directions cancel each other out.

Because we know the frequency of precession for hydrogen nuclei it is possible to apply an oscillating perturbation in the form of a radio frequency (RF) pulse at the same frequency. This RF pulse causes the nuclei to resonate and absorb the energy from the external frequency, which causes an increase in the number of spin-down nuclei. The change in balance between spin-up and spin-down nuclei causes the net magnetization vector M_0 to move away from B_0 and results in a net magnetization vector M_1 in the transverse plane. Another result of resonance is that the magnetic moments of hydrogen nuclei move into phase with each other, which means they are in the same position on the precessional path. This in phase precessing magnetization is picked up in the transverse plane by a receiver coil and produces magnetic field fluctuations inside the coil that induce an electrical voltage that constitutes the MR signal. The amplitude of this induced signal is related to the magnitude of coherent magnetization in the transverse plane. When the RF pulse is switched off, the magnetization vector will begin to realign with B_0 by giving up the absorbed RF energy to the surrounding environment. This relaxation results in *i)* spin-lattice relaxation or T_1 recovery: Nuclei giving up their energy to the surrounding environment which causes the recovery of M_0. The rate of recovery is an exponential process described by the time constant T_1. ii) spin-spin relaxation or T_2 decay: A loss of phase coherency in M_1 due to direct interactions between nuclei that spin at different precessional frequencies due to local differences in the magnetic field. The rate of decay is also exponential and is described by the time constant T_2. These time constants represent the time it takes for 63% of magnetization to be recovered in the longitudinal plane (T_1) or be lost in the transverse plane (T_2).

In order to spatially locate a signal in three dimensions, gradient coils are used to linearly alter the magnetic field strength and precessional frequency along the axis of the gradient. This facilitates selective excitation of a slice of the magnetic field by transmitting an RF pulse with a band of frequencies that coincides with the precessional frequencies of nuclei in that slice. The slope and transmission bandwidth of the applied gradient for slice selection determines the thickness of the slice as well

as the gap between slices. Within each slice there is a range of frequencies that are excited and rephased. To locate a signal along the remaining axes of the image, a frequency encoding and a phase encoding gradient are applied. The phase encoding gradient allows for a signal to be located along its axis according to the phase differences and the signal is located along the other axis according to its frequency after applying a frequency encoding gradient.

Further details on MRI acquisitions will be discussed in the context of their specific application. Acquisition sequences used in this study are reported in detail in each respective chapter.

2.4.2 Structural MRI

The relaxation process that is captured in T_1 recovery and T_2 decay differs for hydrogen nuclei depending on the surrounding tissue. At the extreme ends of this are water, with long T_1 and T_2 times, and fat, with short T_1 and T_2 times. By manipulating the amount of relaxation that occurs before acquiring a signal, it is possible to contrast tissues based on their fat or water content. A T_1-weighted image is one where the contrast in signal is predominantly based on differences in the longitudinal relaxation of fat and water. A T_1-weighted imaging sequence aims to maximize this contrast and neither fat nor water should have time to fully recover longitudinal magnetization.

In this study a fast spoiled-gradient echo (FSPGR) imaging sequence was used to acquire T_1-weighted images. By keeping the repetition time, the time from one pulse sequence to the next one, shorter than the T_1 and T_2 relaxation times there is lingering transverse magnetization (M_1) as there is not enough time for it to fully decay. Each sequential RF pulse will push the residual M_1 in to the longitudinal plane and at the same time flip part of the longitudinal magnetization (M_0) in to the transverse plane. This keeps the magnetization components in a steady state where in each cycle hydrogen nuclei release and gain a similar amount of energy.

Additionally, a spoiling gradient is applied before the next RF pulse with variable amplitudes in order to dephase M_1 from cycle to cycle and optimize the T_1 contrast.

2.4.3 Functional MRI

MRI can be utilised to infer neural activity in brain regions by assessing changes in blood oxygen levels. Neuronal firing causes small changes in local metabolism and because neurons do not have an internal energy reserve there is a disproportionate increase in blood flow to supply oxygen and glucose. Haemoglobin is a protein molecule in red blood cells that binds and transports oxygen from the lungs to the rest of the body. When bound to oxygen we refer to it as oxyhaemoglobin and it is diamagnetic in response to a magnetic field. When oxyhaemoglobin unloads its oxygen molecules, it is referred to as deoxyhaemoglobin and becomes paramagnetic in response to a magnetic field. When a region of the brain becomes more active, there is an initial increase in oxygen consumption, which increases the amount of deoxyhaemoglobin relative to oxyhaemoglobin, and an overcompensating increase in blood flow which provides an oversupply of oxygenated blood, causes vasodilation, and expedites the transport of deoxyhaemoglobin away from the region. The initial increase in deoxyhaemoglobin produces magnetic field inhomogeneities that are restricted to the blood vessels surrounding the brain tissue and these inhomogeneities can be utilised as an endogenous MRI contrast known as the blood oxygenation-level dependent (BOLD).

The BOLD signal is used to assess the complex dynamics of cerebral blood flow, blood volume and oxygenation levels with regards to localised neuronal activity and this is modelled as the haemodynamic response function (HRF). The HRF is typically described as an initial dip in BOLD signal caused by the increase in deoxyhaemoglobin, followed by a sharp rise, reflective of the increase in blood flow, that peaks at arounds 6 seconds before dropping at a similar rate and finally presenting a lingering undershoot, thought to reflect the slower return to baseline of blood volume. Differences in BOLD signal are measured using T_2*-weighted images;

a combination of T_2 decay and dephasing due to magnetic inhomogeneities.[3] In T_2*-weighted images, the presence of deoxyhaemoglobin causes a darkening of the image in those voxels and the haemodynamic response function is captured in these images as a brighter signal due to a strong increase in oxyhaemoglobin.

Functional MRI is a method of imaging the changes in BOLD signal across time using fast imaging pulse sequences that are sensitive to magnetic field inhomogeneities. Echo-planar imaging (EPI) allows for imaging of the whole brain within a single excitatory RF pulse. It does this by rapidly turning off and changing the direction of the frequency encoding and phase encoding gradients. The frequency encoding gradient switches from positive to negative and vice versa at each signal readout and the phase encoding gradient slowly changes amplitude from maximum positive to maximum negative polarity. This study used a gradient-echo echo-planar imaging sequence, which is an EPI sequence that begins with a variable RF excitation pulse.

2.4.4 Diffusion MRI

In the context of MRI, when we talk about diffusion we are referring to the random transport phenomenon of water molecules from one spatial location to another over time. Statistically this is captured as the diffusion coefficient and is dependent on the mass of the molecules, the temperature, and the viscosity. In biological tissues, diffusion is hindered and modulated by the properties and interactions with surrounding tissues on a microscopic level. The directedness of diffusion can be described as isotropic when water molecules diffuse equally free in every direction or as anisotropic when diffusion is restricted or hindered in certain directions. At the image resolution used in MRI diffusion of water molecules in grey matter appears isotropic whereas the myelinated axon bundles of white matter are considered more anisotropic as diffusion is restricted in directions perpendicular to the white matter tracts.

[3] This is the sum of the true transverse relaxation rate $(1/T2)$ and the product of the local field inhomogeneity and the gyromagnetic ratio, which can shortened to: $1/T2^* = 1/T2 + 1/T2'$

An imaging sequence can be modified to become sensitive to diffusion by applying a bipolar gradient after excitation and before signal acquisition. After RF excitation hydrogen nuclei spins are precessing in phase. By applying a positive gradient the precessional frequency of spins increases and causes spins to accumulate phase along the gradient relative to their position. The negative gradient causes an opposite gain in phase along the direction of the gradient. In the absence of motion there is no net effect on the phase of spins and net magnetization remains the same. In the presence of diffusion-induced displacement the negative gradient does not remove all of the dephasing accrued after the positive gradient and there is a net loss in magnetization that can be captured by a receiver coil. The amount of signal attenuation is reliant on both the diffusion and the amplitude of the diffusion-weighted gradient.

Because the displacement can only be measured along the direction of the gradient the imaging sequence needs to be repeated. By acquiring images sensitised to six or more different orientations, it becomes possible to estimate the diffusion tensor. Here the tensor describes an ellipsoid shape and is often represented as a 3x3 matrix.[4] The three orthogonal axes of the ellipsoid can be represented by the tensor eigenvectors and the eigenvalues of the vectors, denoted by λ, describe the displacement. A typically isotropic tensor will have roughly equal eigenvalues in each main eigenvector whereas an anisotropic tensor will primarily show diffusion along one direction (λ_1). The displacement along the principal direction (λ_1) describes the axial diffusivity. The radial diffusivity is described by taking the average displacement in the non-principal directions (λ_2, λ_3) and the mean diffusivity simply takes the average across all directions. Lastly, the anisotropy of the diffusion process can be described as a scalar value that ranges from zero to one called the fractional anisotropy (FA); a value of one means that the diffusion occurs along one axis and is

[4] As a 3x3 symmetric matrix, the tensor describes the diffusion in three dimensions. The diagonal elements describe the diffusion variance along each axis and the off-diagonal elements describe the correlation between displacements.

fully restricted in the other directions whereas a value of zero means that the diffusion is equally restricted in all directions. FA is calculated from the eigenvalues of the tensor.

$$FA = \sqrt{\frac{1}{2}}\frac{\sqrt{(\lambda_1 - \lambda_2)^2 + (\lambda_1 - \lambda_3)^2 + (\lambda_2 - \lambda_3)^2}}{\sqrt{({\lambda_1}^2 + {\lambda_2}^2 + {\lambda_3}^2)}}$$

One of the major disadvantages of this approach is that the tensor assumes there is a single, major orientation of white matter in a voxel and as such it is not capable of accurately resolving multiple white matter fibre orientations within a voxel. A more accurate estimation of fibre populations is the fibre orientation distribution function (fODF) which quantifies the fraction of fibres within a voxel that are aligned along each orientation. By assuming the diffusion-weighted signal attenuation is the sum of each population's orientation weighted by their volume fraction, it is possible to deconvolve the signal attenuation for a single orientation from the total signal (Tournier et al., 2004). By sampling the diffusion in a large enough number of directions it becomes possible to estimate the fibre orientations within a voxel in an equal number of directions. High angular resolution diffusion-weighted imaging (HARDI) is an acquisition protocol that was designed to address the high intravoxel heterogeneity of fibre orientations by measuring the diffusion-weighted signal attenuation in a large number of uniformly distributed directions using high b-value diffusion gradients to detect multiple minima and maxima as a function of the gradient orientation (Tuch et al., 2002).

2.5 Preprocessing of MRI data

2.5.1 Structural MRI

On a T_1-weighted image, the image contrast is predominantly due to differences in longitudinal recovery of magnetization, T_1 relaxation time, and this will be fast for

tissues high in fat content and slow for tissues high in water content. Higher water content will show up darker on a T_1-weighted image whereas a high fat content will appear brighter. This contrast is suitable for identifying white matter, grey matter, and cerebrospinal fluid and can be used to study the morphometry of the brain.

Voxel-based morphometry (VBM) is an analytical approach to examining differences in composition of brain tissue on a localised level whilst disregarding global individual differences in anatomy. In order to compare the composition of each voxel between individuals the brain maps are transformed to fit in to the same stereotactic space. In this thesis, we carried out a VBM analysis using SPM8 (see http://www.fil.ion.ucl.ac.uk/spm), running under Matlab (The Mathworks Inc., 2016). First, images are segmented to produce separate maps per tissue class (white matter, grey matter and cerebrospinal fluid). This is done based on the intensity distribution of the image and prior probability maps of the spatial distribution of tissue classes in typical brains. Both probabilities are combined using a Bayesian rule to obtain a joint posterior probability. In this study VBM was utilised to examine grey matter volume. The segmentation parameters were then imported to DARTEL (Diffeomorphic Anatomical Registration using Exponentiated Lie algebra; Ashburner, 2007) to produce rigidly aligned grey matter images and a study-specific template was created and iteratively updated using the deformations from the template. The final template is then normalised to the Montreal Neurological Institute (MNI; Evans et al., 1993) standard stereotactic space, using an affine transformation, and the deformations from the template are then used to transform the grey matter images to MNI space. Grey matter images were modulated using a Jacobian determinant to correct for expansion and contraction due to non-linear components of spatial normalisation. The modulated grey matter images were then smoothed with an 8mm full width at half maximum (FWHM) isotropic Gaussian kernel. These smoothed, modulated images represent the regional grey matter volume. The parameters used to perform VBM analysis are described in chapter 3.

Unlike VBM, surface based analyses focus solely on the morphometry of the cortical surface. In this study, Freesurfer 5.3 (surfer.nmr.mgh.harvard.edu) was utilised to examine the cortex. The Freesurfer image processing pipeline is fully automated and has not changed drastically from previous publications that describe this in great detail (Dale, Fischl, & Sereno, 1999; Fischl, Sereno, & Dale, 1999; Fischl, 2012; Schaer et al., 2012). First, the data needs to be conformed to a suitable resolution[5] before computing the affine transformation parameters that map the input image to an MNI atlas. The intensities for all voxels are then mean centred on the assumed signal intensity of white matter[6] and the skull and other non-brain tissue is removed. A second intensity normalisation is performed on the skull-stripped image using predetermined control points to specify the range of white matter intensities and is then segmented to produce a white matter volume. This volume is then cut sagitally and axially to isolate the hemispheres and a connected components procedure is used to identify and binarize the white matter structure in each hemisphere. A surface tessellation, following a vertex configuration, is produced for each hemisphere that represents the boundary between white matter and other brain tissue. This triangular mesh is then smoothed and inflated to produce a representation of the cortical surface that retains its geometric properties but allows for visualisation of the areas within the cortical folds. Any topological errors are fixed by changing the number of vertices in the surface mesh. After this the surface is smoothed and inflated again. This already inflated surface is then further inflated to resemble a sphere which is then registered to a spherical brain atlas (Desikan et al., 2006) that is based on the average folding patterns of the cortex. This facilitates a point-to-point correspondence of coordinates that is based on the anatomy rather than the signal intensity and enables automated labelling of regions of interest on the cortical surface. Finally an estimate is produced for the pial surface and cortical parcellation statistics are computed for each of the structures present in the spherical

[5] The Freesurfer pipeline processes images at a 256 x 256 x 256 resolution with isotropic 1mm voxels and so the first step in preprocessing is to format the data to this resolution.

[6] The mean signal intensity of white matter is set to a fixed value of 110.

brain atlas. The cortical thickness can be calculated by measuring the distance between the pial surface and the white matter surface. Regional grey matter volume can simply be computed as the sum of the number of voxels. The local gyrification index (lGI; Schaer et al., 2012) measures the amount of cortex that is buried within the sulcal folds relative to the amount on the visible outer cortex. This requires the additional process of binarizing the pial surface and filling the sulcal folds before creating a new surface tessellation that tightly covers this outer hull. The lGI can then be computed as the ratio between the amount of surface of a circular region of interest (ROI) on the outer hull and the corresponding amount on the pial surface layer. This process is repeated for each vertex using overlapping circular region of interest with a diameter of 25mm. Each vertex on the pial surface then receives a weighted part of the lGI value it contributed to, inversely proportional to the distance between the points on the pial surface and the outer hull.

2.5.2 Functional MRI

Unlike structural MRI, functional MRI (fMRI) captures multiple MR images over a period of time that are sensitised to changes in BOLD signal. Thus, fMRI can be seen as a time-series of 3-dimensional images of the brain that capture changes in brain function as they are occurring, most often due to exposure to specific demands related to a psychological experiment. However, these images have a lower resolution due to the speed at which they need to be captured and require additional processing to prevent false inferences due to noise in the data. SPM8 (http://www.fil.ion.ucl.ac.uk/spm), running under Matlab (The Mathworks Inc., 2016), was used to process the imaging data.

To account for head movement during fMRI acquisition, the images that comprise the fMRI time-series are realigned to a reference point, often the first image in the time-series. The translations (motion in X, Y or Z direction) and rotations (motion over X, Y or Z direction) for each image in the time-series are stored and can be added later in the analysis to further account for head movement. A mean image of

the time-series is also produced to facilitate coregistration to a structural MR image. Following realignment, differences in timing of slice acquisition are addressed through slice timing correction. The mean image for each individual's time-series is then used as a reference in coregistration of the fMRI time-series to a T_1-weighted structural MR image using a normalised mutual information cost function. The same deformations from each individual structural image to the spatially normalised DARTEL template can be applied to the fMRI time-series following successful coregistration to spatially normalise the fMRI time-series to MNI space. As before with the structural MR images, a Gaussian smoothing kernel was applied with a FWHM of 8mm after normalisation.

2.5.3 Diffusion MRI

The initial diffusion imaging data is made up of diffusion weighted images with different gradient directions and a few non-weighted images (b = 0 s/mm^2). To correct for motion artefacts and eddy current induced distortion each volume image is coregistered to the first non-weighted image using an affine transformation based on mutual information. The B-matrix is rotated as well to preserve orientational information (Leemans & Jones, 2009). Distortions caused by the magnetic field inhomogeneities are corrected for by registering the diffusion volume to a T_1-weighted scan which will resample the diffusion data to the undistorted T_1 image. These steps are carried out in unison as part of distortion correction in ExploreDTI (Leemans et al., 2009; http://exploredti.com) and the transforms are concatenated into a single transformation and applied to the raw diffusion volumes.[7] The corrected diffusion data is then fitted to the diffusion tensor and corrected for partial volume effects due to cerebrospinal fluid contamination (Pasternak et al., 2009). Image maps of fractional anisotropy (FA), mean diffusivity (MD), axial diffusivity (AD), and radial diffusivity (RD) are then computed from the tensor.

[7] In this study the diffusion data was non-linearly warped to a synthetic T1 image that was computed from a mcDESPOT imaging pipeline using Elastix (Klein et al., 2010) using a distorted diffusion image of the fractional anisotropy as a reference. The warps were computed using normalised mutual information as the cost function and constrained the deformations to the phase-encoding direction.

As mentioned, the diffusion tensor model is inadequate in regions of the brain where multiple fibre population orientations are present and instead the fibre orientation density function (fODF) is obtained using spherical deconvolution (Tournier et al., 2004). This approach assumes that the observed diffusion signal is the result of a convolution of an fODF with a known symmetrical fibre response function and, given that the response function and signal are known, the fODF can be retrieved by deconvolving the response from the signal. A damping component is further introduced to suppress artefacts caused by partial volume effects from isotropic tissue (Dell'Acqua et al., 2010).

The reconstruction of estimated white matter tracts was carried out using deterministic tractography by first placing seed points at the vertices of a grid superimposed over the fODF diffusion image and interpolating an estimate of the fODF at each seed point to determine the likely orientations. At each peak that is greater than a chosen threshold proceed along that direction and interpolate a new fODF at the next location and find the peak that minimises the subtended angle. This process continues while a peak fODF subtends at an angle below a set threshold and if the fODF peak exceeds the chosen magnitude. Finally, all streamlines that are below or above a chosen length are also excluded. In this study streamline reconstruction was carried out by placing seedponts over a 3x3x3 mm grid with a 1 mm stepsize and streamlines were terminated if the angular threshold exceeded 45° or if the fODF amplitude exceeded 0.05. Streamlines were restricted to those between 30 to 300 mm in length.

2.6 General Linear Model

Statistical analysis of MR imaging data is frequently done using a general linear model (GLM) approach. In essence, the GLM can be considered an extension of multiple linear regression but for a single dependent variable. At its most basic level,

the GLM tries to model an observed variable Y as a linear combination of a set of predictor variables X weighted by their independent contributions β.

$$Y = \beta_0 + \beta_1 X_1 + \cdots \beta_k X_k + \varepsilon$$

Using this equation, the observed value of Y can be expressed in terms of a constant (β_0) and a slope ($\beta_1 \ldots \beta_k$) that capture the independent contribution of each predictor variable ($X_1 \ldots X_k$). An error term (ε) is included that captures the random disturbances. At the group level, this equation is more efficiently expressed using matrix notation.

$$Y = X\beta + \varepsilon$$

In this format, Y is an *n*-by-*1* vector of observed data for *n* participants, X is an *n*-by-*m* matrix with *n* observations of *m* predictor variables, β is an *m*-by-1 vector and ε is an *n*-by-*1* vector. The first part of this equation $X\beta$ is a fixed component that contains a full-rank matrix X and a vector β of unknown parameters. The second part represents the random disturbances that are assumed to have a zero conditional mean, is homoscedastic with finite variance, and with uncorrelated error terms.[8] The Gauss-Markov theorem (see Chipman, 2011 for a detailed description and proofs) states that for linear regression models the best linear unbiased estimate for β is obtained by minimising the sum of squared residuals. As the error is simply the difference between the observed and predicted values ($Y - X\hat{\beta}$), the least squares estimate that minimises the sum of squared residuals is the function

$$\hat{\beta} = (X'X)^{-1}X'Y$$

Finally, a column vector *c* is added to the GLM to specify a linear combination of the variables to be tested. Typically, the coefficients of the contrast vector add up to zero, they are orthogonal, and are used to test specific hypotheses between the

[8] Typically it is assumed that the error term follows a multivariate normal distribution: $e \sim N(0, \sigma^2 I_n)$ This extends to the distribution of Y as well: $Y \sim N(Xb, \sigma^2 I_n)$

means. A basic contrast vector would be $[1 \quad -1]$ which tests for a difference between two means where the first $[1]$ is greater than the second $[-1]$. This can be expanded upon by including one or more covariates in the model whilst still carrying out the same statistical test; $[1 \quad -1 \quad 0]$.

This model can be fitted at each voxel to explain the signal Y in terms of the weighted sum of the variables of interest $X\beta$ corresponding to the hypothesised effect c. The null hypothesis on the other hand can be defined as the model where $c'\beta$ is equal to zero. A t-statistic can then be computed as the null hypothesis divided by the standard error of the null hypothesis. Using the associated degrees of freedom it is possible to convert the t-value to a probability value p to assess the statistical significance. Because this process is carried out at each voxel, the output will be a statistical parametric map of over 100,000 separate observations each with its own probability. To account for the mass-univariate approach, the statistical threshold is adjusted to account for the number of statistical tests that are being carried out. Multiple comparisons correction is done using Gaussian Random Field Theory, which essentially states takes correlations in signal between neighbouring spatial locations into account when calculating error probabilities rather than assume each voxel signal is independent (Friston et al., 1996; Worsley et al., 1996). The accepted risk of error is then expressed as a family-wise error (FWE) rate and represents the likelihood that the signal in a family, or cluster, of voxels is due to chance. In this study we employ a threshold of $p < 0.05$ FWE corrected.

In fMRI analyses, modelling is further broken down into a within-subject stage (1st level analysis) followed by a between-subject stage (2nd level analysis). In first level analysis, a participant's BOLD signal time course at a given voxel is the observed data[9] and each contrast is modelled as a separate regressor where the variance only represents the variance within that participant's fMRI time-series in that specific

[9] In this case the observed data is actually the haemodynamic response function convolved with the task onset parameters.

voxel. These parameter estimates are then used instead of the BOLD signal time course in the second level analysis. Here the variance is now a combination of between- and within-subject variance and contrasts are typically used to model group membership. In our study we modelled the average response to each condition on an n-back task (1-back, 2-back, and 3-back) relative to a baseline task (0-back; is it "X"?) at first level and used these parameter estimates in our second level analysis contrasting the three groups to test for differences in BOLD response in relation to working memory load on each condition.

Chapter 3

Functional Investigation of Working Memory and Psychotic Experiences in the Developing Brain[10]

A number of psychiatric disorders first emerge during adolescence (Silva, 1990; Paus et al., 2008) and are presumed to relate to the substantial social, cognitive and physiological changes occurring during this period (Blakemore, 2008). Psychiatric disorders with onset in childhood or adolescence further disrupt cognitive and social development and there have been calls for new research into the underlying neurocognitive risk mechanisms during this period as well as the development of early and age-appropriate intervention approaches (Beddington et al., 2008).

Psychotic experiences, such as delusions, hallucinations or thought interference, show associations with later psychiatric disorder (van Os et al., 2000) yet are also prevalent among the general population (van Os et al., 2009). The incidence of psychotic experiences (PEs) is reportedly higher among children and adolescents than in adults (Cougnard et al., 2007; Kelleher et al., 2012a) and persistence of PEs is a strong indicator of increased risk for later disorder, including psychosis (Kaymaz et al., 2012). Also, the mere presence of PEs has been linked with poor psychosocial outcomes, general psychopathology, self-harm, and cognitive impairment, even in the absence of a transition to psychosis (Nishida et al., 2010; Polanczyk et al., 2010; Barnett et al., 2012; Downs et al., 2013).

Impaired cognition is of particular interest, since lower childhood cognitive ability has been found to be predictive of PEs (Barnett et al., 2012; Niarchou et al., 2013). Furthermore, neurocognitive deficits present in adults, often in the domains of executive function, processing speed and working memory (Simon et al., 2007; Fusar-

[10] The work described in this chapter has been published as a scientific paper in Cerebral Cortex, 2015, 25(12), 4828 – 4838.

Poli et al., 2012b; Valli et al., 2012), increase in severity through prodromal phases towards clinical psychosis (Simon et al., 2007; Meier et al., 2014) and greater deficits are found in those who transition (de Herdt et al., 2013). Perhaps unsurprisingly, neuroimaging studies have extended the profile of frontal lobe dysfunction to prodromal populations both in terms of elicited activation (Fusar-Poli et al., 2007; Corlett & Fletcher, 2012; Dutt et al., 2015) as well as the connectivity of underlying networks (Whalley et al., 2005; Allen et al., 2012; Jung et al., 2012; Diederen et al., 2013; Fryer et al., 2013; Schmidt et al., 2013; Orr et al., 2014; Schmidt et al., 2014b; van Lutterveld et al., 2014).

In the developing brain, prefrontal cortices are the last to reach structural maturity (Casey et al., 2005), a prolonged trajectory that is reflected in slowly developing executive functions and particularly working memory abilities (Casey et al., 2005; Blakemore, 2008; Dumontheil & Klingberg, 2012). Most studies of working memory have shown that during typical development from childhood to adulthood, memory capacity increases whilst brain activity becomes increasingly localised to a predominantly frontoparietal network (Casey et al., 2005; Klingberg, 2006; Conklin et al., 2007). Advanced analysis techniques, such as dynamic causal modelling (DCM; Friston et al. 2003), have provided insights into the underlying dynamics of this network, showing that parietal regions are involved at an earlier stage of processing than frontal regions and increasing memory load modulates parietal-to-frontal connectivity (Ma et al., 2012; Dima et al., 2014). This network shows aberrant connectivity in individuals with psychosis and, to a lesser extent, those at high risk for psychosis (see Schmidt, Diwadkar, et al. 2014 for review). Interestingly, this same pattern has been reported with regards to frontotemporal connectivity (Lawrie et al., 2008; Crossley et al., 2009; Allen et al., 2010).

Though limited, the current literature on PEs has also pointed to changes predominantly in frontal and temporal regions in terms of fMRI BOLD response (Jacobson et al., 2010; Corlett & Fletcher, 2012), functional connectivity (Diederen et

al., 2013; Orr et al., 2014; van Lutterveld et al., 2014), grey matter volume (Jacobson et al., 2010; Modinos et al., 2010a; Cullen et al., 2013), and white matter microstructure (Jacobson et al., 2010). However, to date only one small study has employed a simple multi-modal approach (Jacobson et al., 2010) and more studies are needed to capture both the structure of the brain as well as the underlying neural dynamics.

The aim of this study was to shed light on the neuropsychological profile of those with PEs by administering a working memory task in combination with functional and structural brain imaging. We hypothesized that PEs during late adolescence affect neurodevelopmental trajectories and we would be able to measure an impact on brain function in those with PEs in terms of 1) reductions in BOLD response within a working memory network and 2) differences in frontoparietal network configuration, or modulatory connections, similar to those found in individuals at high-risk for psychosis (Schmidt et al., 2013, 2014b). Furthermore, persistence of PEs from late adolescence in to adulthood would have a more profound impact and we hypothesized this would be demonstrable in terms of working memory performance and BOLD signal reductions. Finally, we undertook to examine regional grey matter volume as a potentially confounding factor in relation to brain function.

3.2 Methods

3.2.1 Participants

All participants were part of the Avon Longitudinal Study of Parents and Children (ALSPAC; http://www.bristol.ac.uk/alspac/). A total of 4,724 young adults, out of an initial cohort of around 14,000 births, were assessed with the Psychosis-Like Symptom interview (PLIKSi) at age 18 and 433 (9.2%) individuals were rated as having suspected or definite psychotic experiences (PEs) (Horwood et al., 2008; Zammit et al., 2013b). From this sample, 165 participants (93 controls and 72 with suspected or

definite PEs) were reassessed using the PLIKSi and underwent functional and structural MRI at age 20. Participants' informed consent was obtained before imaging and ethical approval was given by the Cardiff University School of Psychology Ethics Committee and the ALSPAC Ethics and Law Committee.

A total of 16 participants were excluded from analyses due to missing PLIKSi data at both time-points, task performance at or below chance level or technical issues with fMRI data preprocessing. Participants were divided into three groups based on PLIKSi rating at both time-points. Those who were rated as having PEs at both age 18 and age 20 were considered persistent PEs, those with PEs at either age 18 or age 20 were considered transient PEs, and those rated as not having PEs at either time point as healthy controls (HC). In total, there were 35 participants with persistent PEs, 36 with transient PEs and 78 HC. Out of the 36 with transient PEs, only 9 participants (25%) had been rated as having PEs at age 20 and the other 27 participants (75%) were only rated as having PEs at age 18.

Missing values were estimated using a regression imputation method (Buck 1960) across the entire ALSPAC cohort (n = 13,971). Groups differed in childhood IQ ,taken at age 8 using the Wechsler Intelligence Scale for Children (Wechsler et al., 1992), which was driven by differences between persistent PEs and HC, but were similarly distributed in terms of reported dominant hand. See table 3.

Table 3. Description of sample: demographics, childhood IQ and handedness. Age and IQ are given in median (interquartile range), gender and handedness are given as frequency (percentage).

	Controls	Transient PEs	Persistent PEs	Test Statistic
Sample Size	78	36	35	
Age	20 (1)	20 (0)	20 (1)	
Gender				χ^2 = 6.092, p = 0.048
Male	31 (40%)	7 (19%)	8 (23%)	
Female	47 (60%)	29 (81%)	27 (77%)	
Handedness				
Right	61 (78%)	27 (75%)	29 (83%)	
Left	14 (18%)	7 (19%)	5 (14%)	
No dominant hand	3 (4%)	2 (6%)	1 (3%)	
IQ at age 8	114.5 (22)	107.5 (15)	105.0 (15)	χ^2 =10.769, p = 0.005

3.2.2 Psychotic Experiences (PEs)

PEs were assessed using the PLIKSi, a semi-structured interview covering the occurrence of visual hallucinations, auditory hallucinations, delusions (being spied on, persecution, thoughts being read, reference, control, grandiose ability, other unspecified delusions) and thought interference (thought broadcasting, insertion, withdrawal) in the past 6 months and was administered at ages 18 and 20. Respondents were asked 12 core questions, 7 were derived from the Diagnostic Interview Schedule for Children, Version IV (DISC-IV; Shaffer et al. 2000) and 5 from

the Schedules for Clinical Assessment in Neuropsychiatry (SCAN; Wing et al. 1990), version 2, and clinical cross-questioning and probing was used to establish the presence or absence of any experiences. Interviewers rated experiences as definitely present, suspected to be present or absent and unless a credible example was given responses were rated down to suspected instead of definitely present. An overview of the reported PEs in each group at ages 18 and 20 is given in Appendix A, section A.1.

3.2.3 N-back Task

A letter variant of the *n*-back task was used. Participants were instructed to press a button with their index finger when the letter that was presented on the screen was identical to the one they saw *n* trials earlier, where *n* can be 1, 2 or 3. During 0-back testing, participants were instructed to press the button whenever the letter X was presented on the screen. Each condition was presented 3 times in a pseudorandom order in blocks of 14 items; each item lasted 2 seconds, and was preceded by a 3 second written instruction on the screen. During each block there were 3 correct combinations, giving a maximum of 9 correct responses per condition. Including the instruction, each block was 31 seconds long making the total duration of the n-back task 372 seconds. Task performance was measured in terms of reaction time and by the sensitivity index d', computed as $d' = Z_{HIT} - Z_{FA}$, where FA reflects false alarms. Hit and false alarm rates of 0 or 1 were adjusted as described in Haatveit et al. (2010). The highest possible d' score was 3.85 and the lowest was -3.85. Due to non-normality of the data, the Kruskal-Wallis test was used to test for group differences and pairwise post-hoc comparisons were performed using Dunn-Bonferroni correction. To test for any group-by-gender interaction effects, an adjusted rank transformation (ART) was applied as described in Leys and Schumann (2010). In short, this approach subtracts the marginal means from each individual's score and assigns a rank to the adjusted score. A factorial ANOVA is then performed on the ranked data to test for interaction effects.

3.2.4 MRI acquisition

Imaging data were acquired at the Cardiff University Brain Imaging Centre (CUBRIC) on a 3 Tesla General Electric SIGNA HDx (GE Medical Systems, Milwaukee, Wisconsin) using an 8-channel head coil for radio frequency reception.

Changes in blood-oxygenation–level dependent (BOLD) were measured using T_2*-weighted gradient echo echo-planar images (GE EPI) along the axial plane parallel to the anterior commissure — posterior commissure (AC-PC) line (repetition time = 2000ms, echo time = 30ms, flip angle = 75^0, field of view = 240x240mm , resolution = 3.75mm x 3.75mm x 3.5mm).

A high-resolution fast-spoiled gradient echo (FSPGR) T_1-weighted isotropic image was acquired with slices parallel to the AC-PC line (TR = 7808ms, TE = 2988ms, inversion time = 450ms, flip angle = 20^0, field of view = 256x256mm, resolution = $1mm^3$) to improve functional image registration to standard space and for investigation of grey matter.

3.2.5 Preprocessing

Statistical parametric mapping (SPM) was performed using SPM8 (www.fil.ion.ucl.ac.uk/spm). Functional imaging data were realigned and resliced using the first image as a reference. Slice timing correction was applied and each individual's fMRI time-series was coregistered to a T_1-weighted structural image using the mean image as the reference and normalised mutual information as the cost-function. All T_1-weighted images were segmented using default tissue probability maps of grey and white matter before importing the segmentation parameters in DARTEL (Ashburner, 2007) and producing rigidly aligned grey matter images. A study-specific mean image template was reiteratively created and the final template was affine transformed to the template defined by the Montreal Neurological Institute (MNI). Resulting deformations were applied to transform the

segmented grey matter images and fMRI time-series to the MNI template, and an 8mm full-width half-maximum Gaussian smoothing kernel was applied.

3.2.6 fMRI analysis

At first level, with the exception of 0-back which was used as an implicit baseline, the onsets of each condition were convolved with a canonical haemodynamic response function and serial correlations were modelled as an autoregressive process. Six movement parameters were added as nuisance covariates. A main effect for each explicit condition (1-back, 2-back, and 3-back) was modelled and entered in to a random effects analysis at the second level. A main effect of task was computed by collapsing groups and conditions and the increase in BOLD response was used as an activation mask at second level. Linear and quadratic trends in BOLD response with increasing task complexity were tested across groups. The three groups were then compared on each condition using one-way ANCOVA's, controlling for gender, premorbid IQ and their performance (d'). Finally, a group x task interaction analysis was performed. Statistical significance was inferred at a threshold of $p<0.05$ after family-wise error (FWE) correction.

3.2.7 VBM analysis

Voxel-wise comparison of modulated T_1-weighted segmented grey matter images of the three groups was performed using a one-way ANCOVA, controlling for gender, and premorbid IQ. As with fMRI, a threshold of $p<0.05$ FWE corrected was used to assess statistical significance.

3.2.8 DCM analysis

Underlying dynamics of frontoparietal connectivity were analysed using Dynamic Causal Modelling (Friston et al., 2003), version 10. First, regional time series derived from first-level general linear modelling were extracted from spherical volumes of interest, 6mm in diameter, from the nearest subject-specific local maxima near the peak of activation overlap (see table 3) in the bilateral middle frontal gyrus and

posterior parietal lobules (as depicted in figure 4) using the first eigenvariate of voxels above a subject-specific threshold of $p < 0.05$ uncorrected. Second, all models were specified using the same intrinsic connections, allowing reciprocal frontoparietal connections within each hemisphere and interhemispheric connections between frontal, and parietal regions. Visual input was specified as reaching the parietal lobules bilaterally first after initial cortical reception. Specification of model configuration, matched with previous literature (Schmidt et al., 2013, 2014b), was based on three possible directions of modulation from the input and could be forward parietal-to-frontal, backward frontal-to-parietal, or both. In each of these directions there were four possible configurations by taking interhemispheric modulation into account; a lack of interhemispheric modulation, only frontal interhemispheric modulation, only parietal interhemispheric modulation, or both frontal and parietal interhemispheric modulation. In total this leads to 12 different models that test different modulatory effects and cover all physiologically possible connections. These models were fit to the 2-back and the 3-back, respectively, compared to the 0-back baseline. Bayesian model selection (BMS) was used to compute both the exceedance and expected posterior probabilities at the group level (Stephan et al., 2009). The exceedance probability, i.e., the probability that a certain model is more likely than the others, was used to infer the best model fit in each group.

3.3 Results

3.3.1 N-back performance

Groups differed significantly in performance, as measured using the sensitivity index d', on the 1-back and the 2-back. Performance was poorer in persistent PE compared to HC, with transient PE not being significantly different from either group. Using the adjusted rank transformation (ART), a group*gender interaction effect was found on

the 0-back and the 3-back. Splitting the dataset by gender revealed a difference between males with persistent PEs compared to male controls on the 0-back, but no other differences were found. Average performance on each condition per gender in each group is presented in Appendix A, section A.2. Those with persistent PE had a faster reaction time on the 3-back compared to HC with neither group differing from transient PE. No other group differences were present and there was no indication of a group-by-gender interaction effect on reaction time. Performance measures are summarised in table 4.

Table 4. Performance summary for each group given as median (interquartile range)

	Controls	Transient PEs	Persistent PEs	Test Statistic	Group-by-Gender Interaction
d' (Range -3.85 to 3.85)					
0-Back	3.85 (0.00)	3.85 (0.38)	3.85 (0.37)	$\chi^2_{(2, 149)} = 7.97$, $p = 0.019$	$F_{(2,143)} = 23.07$, $p < 0.001$
1-Back	3.85 (0.00)	3.85 (0.37)	3.48 (0.37) [a]	$\chi^2_{(2, 149)} = 10.78$, $p = 0.005$	
2-Back	3.48 (0.77)	3.48 (1.16)	3.10 (1.54) [a]	$\chi^2_{(2, 149)} = 8.14$, $p = 0.017$	
3-Back	2.64 (1.02)	2.60 (0.62)	2.31 (1.00)		$F_{(2,143)} = 3.91$, $p < 0.022$

[a] Post-hoc test revealed significant decrease in persistent PE versus Controls

Table 4. Continued from previous page

	Controls	Transient PEs	Persistent PEs	Test Statistic	Group-by-Gender Interaction
Reaction Time $_{(ms)}$					
0-Back	470.45 (90.61)	471.83 (103.08)	424.33 (133.89)		
1-Back	532.89 (133.87)	530.67 (150.62)	512.44 (144.34)		
2-Back	622.26 (173.39)	606.50 (201.62)	575.25 (187.58)		
3-Back	722.86 (232.85)	655.18 (284.53)	655.67 (175.12) [a]	$\chi^2_{(2, 149)} = 6.66$, $p = 0.036$	

[a] Post-hoc test revealed significant decrease in persistent PE versus Controls

3.3.2 fMRI analysis

The main effect of each condition (1-back, 2-back, and 3-back) and group membership were collapsed to compute a main effect of task. This contrast revealed a consistent pattern of bilateral activation predominantly in the middle frontal gyrus and superior parietal lobule, as well as the insula and supplementary motor area extending into the anterior cingulate cortex (see figure 3). An overview of regions showing task-elicited increases in activation is given in Appendix A, section A.3.

The overall activation was used as a mask of a working memory network for further analyses. A one-way whole-brain ANOVA was performed to test if the groups recruited brain regions differently on the task. No differences in BOLD response were found between groups when collapsing conditions.

Further analyses comparing groups on each condition (1-back, 2-back and 3-back respectively) were performed utilising the working memory mask. No group differences in BOLD response were found on any condition.

Linear and quadratic trend analyses were performed on the whole sample to assess the effect of cognitive load and revealed almost identical patterns. There was a strong increase in BOLD response from 1-back to 2-back followed by a slight increase or decrease depending on the contrast weights (summarised in Appendix A, section A.3), as is illustrated in figure 3 for the bilateral middle frontal gyrus and superior parietal lobule.

A group-by-task interaction analysis did not reveal any significant interactions at $p<0.05$ FWE corrected.

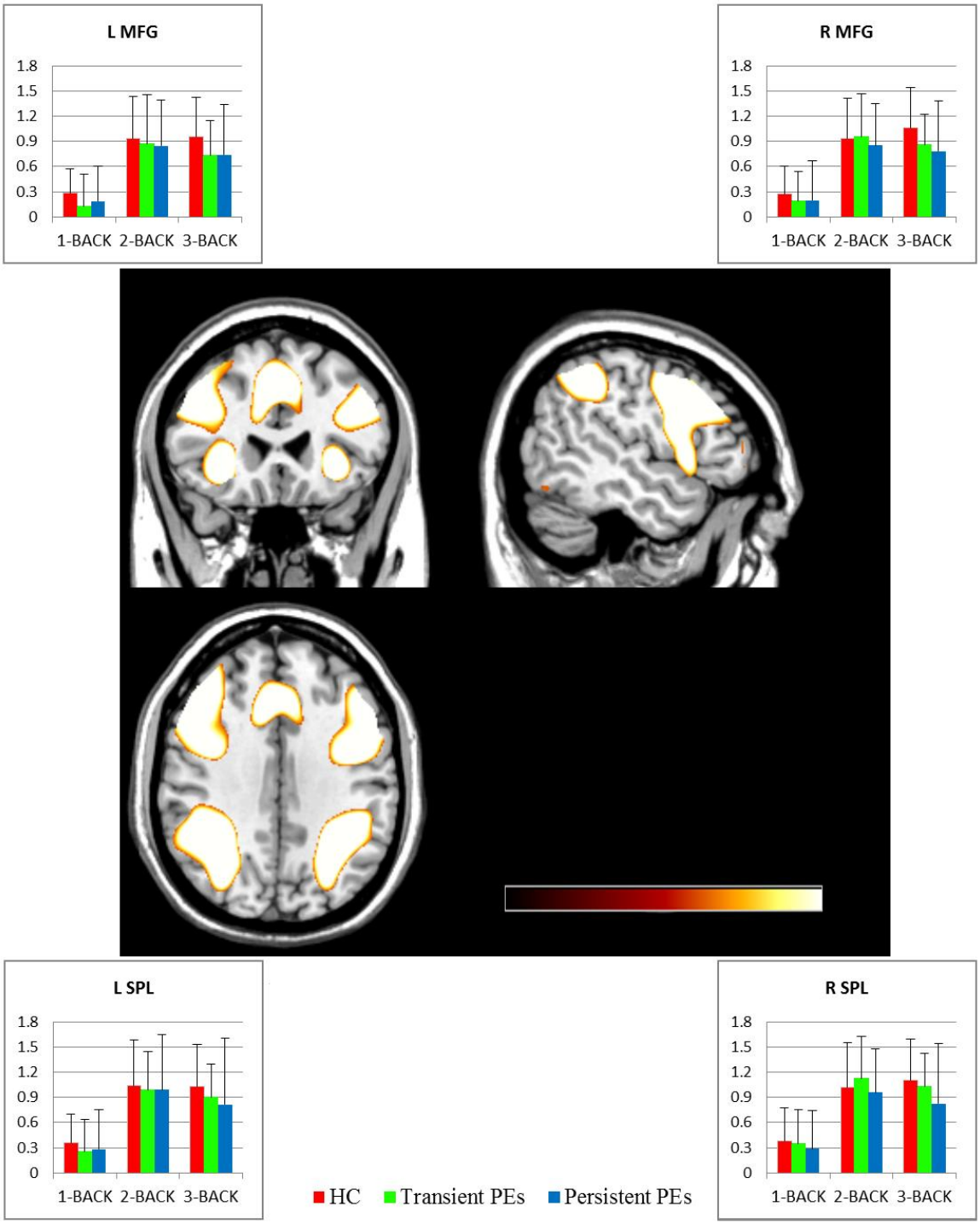

Figure 3. Increases in BOLD signal during the n-back task. Centre: Task-related increases upon collapsing both groups and conditions. The average BOLD response to each condition has been extracted and plotted for the left middle frontal gyrus (*top left*), right middle frontal gyrus (*top right*), left superior parietal lobule (*bottom left*) and right superior parietal lobule (*bottom right*).

3.3.3 Volumes of interest

Regional time series were extracted from spherical volumes centred on subject-specific local-maxima in the frontal and parietal regions of the brain as volumes of interest (VOI). Group local maxima coordinates across the task were entered as initial reference points for each VOI and are described in table 5. Deviations from these reference coordinates to subject-specific local maxima were limited to the overlap in activation between the three groups within the working memory network mask (see figure 4).

Table 5. Cluster properties of volumes of interest utilised in DCM comprised of brain regions that show an increase in BOLD signal during the task compared to the baseline and overlap across participants in all three groups in BOLD signal increases during the task

Region	Size (voxels)	MNI Coordinates			t-value	p-value (FWE corrected)
		X	Y	Z		
R Superior Parietal Lobule	15468	46	-46	47	22.46	<0.001
L Superior Parietal Lobule	12012	36	-47	38	19.70	<0.001
R Middle Frontal Gyrus	13700	30	6	54	18.31	<0.001
L Middle Frontal Gyrus	9440	-27	1	54	17.64	<0.001

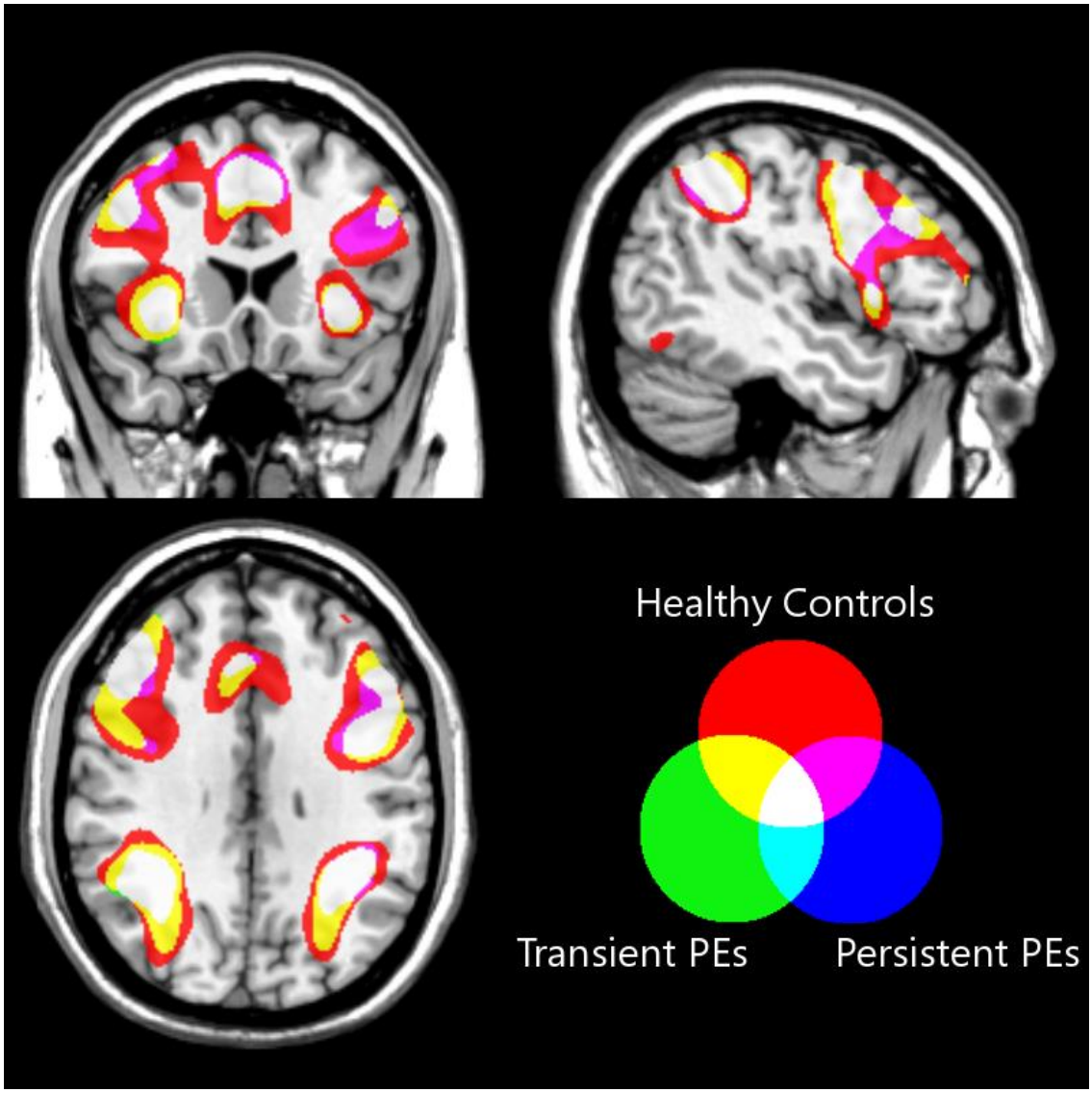

Figure 4. Overlay of increased BOLD response during the n-back task in each group. Overlap in activation across all groups is shown in white and utilised as an inclusive mask for subject-specific local maxima for volume of interest extraction.

3.3.4 VBM Analysis

Voxel-wise whole-brain analysis of local grey matter volume revealed no differences between the groups or any correlation between local grey matter volume and premorbid IQ across all participants. Limiting voxel-wise comparisons to the

functionally defined working memory network (as depicted in figure 3) did not reveal any differences in grey matter volume between the three groups either.

3.3.5 DCM Analysis

Model comparison was done using random effects Bayesian Model Selection (BMS) and was performed across all groups and within each group.

Model fit for the 2-back

Model 1 (frontal-to-parietal modulation without any interhemispheric modulation, see top left of figure 5) was the best fitting model with an exceedance probability (i.e. likelihood of that model best explaining the observed data) of 78% followed by model 9 (parietal-to-frontal modulation without any interhemispheric modulation, see bottom left of figure 5) with a probability of 22%. When looking within each group the same frontal-to-parietal modulation model was the best fit but the exceedance probability decreased from persistent PEs (82%) to transient PEs (65%) to HC (59%) whilst that of parietal-to-frontal modulation increased from persistent PEs (18%) to transient PEs (35%) to HC (41%) (see figure 5).

Model fit for the 3-back

Model 9 (parietal-to-frontal modulation without interhemispheric modulation) was the best fit to the data with an exceedance probability of 99.8%. This finding was repeated within groups for the HC (at 89%) and for transient PEs (at 98%). Though this was still the winning model in persisting PEs at 46%, the second best model 11 (parietal-to-frontal modulation with frontal interhemispheric modulation) had similar exceedance probability of 44%.

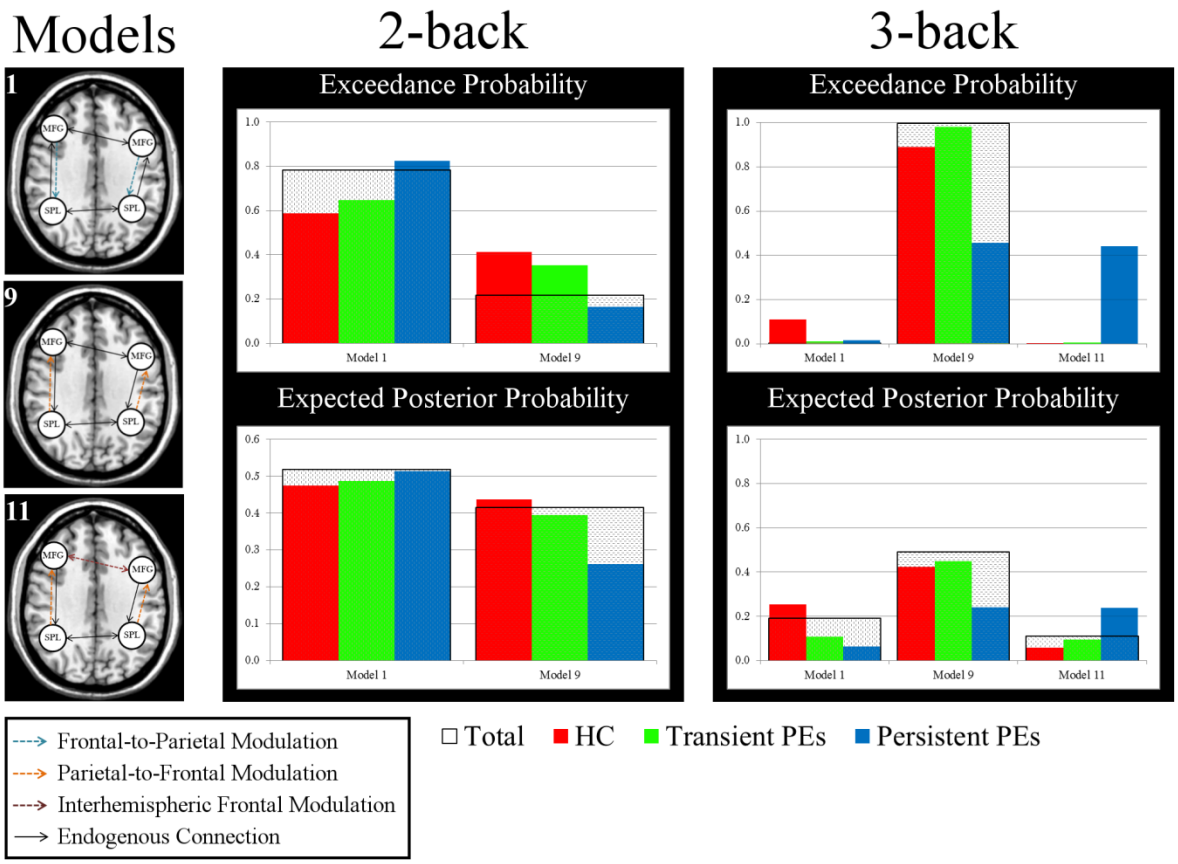

Figure 5. Illustrations of winning models (left) and the probabilities associated with these models (range 0-1) given for the total sample and for each group on both the 2-back and 3-back conditions.

3.4 Discussion

The aim of this study was to assess working memory function in individuals with psychotic experiences using functional and structural MR imaging, as well as a letter variant of the n-back task. We hypothesized that PEs during late adolescence represents a deviation from typical development and would affect working memory function. Additionally, abnormal persistence of PEs would lead to greater alterations in development and this would be demonstrable as a dose-response relationship between PEs duration and both poorer task performance and reduced BOLD signal. There was indication of differences in performance and further analysis revealed that those with persistent PEs performed worse than HC, whilst there was no evidence

that those with transient PEs differed from either group. However, there were no differences between groups in recruitment of brain regions or BOLD signal intensity in a functionally defined working memory network. Additionally, analyses of grey matter volume in the brain revealed no differences in brain structure between the groups. Further testing of effective connectivity did not support our hypotheses of qualitative differences in frontoparietal network configuration between groups. The same model of frontal-to-parietal modulation was the best fit to the data on the 2-back in all groups, but crucially, in the light of the lack of other differences between the groups, the probability dropped in a dose-response fashion from persistent PEs to transient PEs, to HC. The opposite pattern was found in terms of parietal-to-frontal modulation, which was highest in HC, lowest in persistent PEs and intermediate in the transient PEs group. On the 3-back we found a strong consistent pattern of parietal-to-frontal modulation in all groups, but in persistent PEs there was an additional presence of frontal interhemispheric modulation. Below we discuss the significance of these findings.

3.4.1 Poorer working memory performance in persistent PEs

Reduced cognitive ability has been reported in PEs (Barnett et al., 2012; Niarchou et al., 2013) and poorer performance in domains such as working memory, attention and processing speed at ages 8 to 11 has been associated with psychotic experience in the ALSPAC cohort at age 12 (Niarchou et al., 2013). However, it is unclear whether reduced cognitive ability is due to a developmental lag, or to a deviation from typical development due to PEs. The current sample of young adults at age 20 does demonstrate some reduction in working memory function but only those with persisting PEs were statistically discernible from healthy controls. Previous studies have not made distinctions regarding the duration of PEs. Additionally, there was some evidence of a group-by-gender interaction effect on working memory performance. However these findings should be interpreted with caution due to the small number of males present in both groups with PEs. Gender differences have

been described (Maric et al., 2003; Johns et al., 2004; van Os et al., 2009; Dominguez et al., 2010), but findings differ and further research on the potential effects of gender on PEs is required. It should be noted that studies using the n-back in combination with fMRI in prodromal states often do not find differences in raw performance between those deemed 'at-risk' and controls (Seidman et al., 2006; Crossley et al., 2009; Fusar-Poli et al., 2011b; Smieskova et al., 2012a). The fact that the performance of those with transient PEs lies intermediate to persistent PEs and HC lends further credence to the hypothesis that abnormal persistence of PEs is associated with a more profound and potentially pathological effect on working memory function.

3.4.2 Similar brain function in response to working memory demands

There was no indication of differences in the recruitment of brain regions involved with working memory and the groups did not differ in BOLD response on the n-back task. Previous studies of PEs that reported differences either studied children aged 9-11, without further controlling for other confounders affecting development, (Jacobson et al., 2010) or only found associations between BOLD response and magical ideation (Corlett & Fletcher, 2012). Other studies have highlighted aberrations in functional connectivity using resting-state fMRI, implicating reductions in frontotemporal connectivity (Diederen et al., 2013) and changes in connectivity between the default mode network and temporal regions (Orr et al., 2014; van Lutterveld et al., 2014). As before, it should be noted that only one of the aforementioned studies looked at PEs in general (Orr et al., 2014), whilst the others assessed functional connectivity solely only in those with auditory verbal hallucinations (Diederen et al., 2013; van Lutterveld et al., 2014) and all of these studies used very small samples. The current study focused on working memory and the frontoparietal network, but it is possible that other networks in the brain do show differences. A recent study of structural network topology in the ALSPAC neuroimaging cohort revealed changes in graph theory metrics, including a

reduction in global efficiency and density, as well as reductions in local efficiency in cingulate, parietal, occipital and frontal regions (Drakesmith et al., 2015). However, no distinction was made between durations of PEs in that study.

3.4.3 Grey matter volume in PEs

Contrary to previous studies of brain volume in PEs, which found increased temporal grey matter volume (Jacobson et al., 2010; Modinos et al., 2010a; Cullen et al., 2013), there were no differences in underlying grey matter volume in a whole-brain analysis between the groups and grey matter volume was not added as a potential confounder to our analyses. However, both Jacobson et al. (2010) and Cullen et al. (2013) examined grey matter volume in developing children and Modinos et al. (2010) reported a positive correlation between grey matter volume and higher levels of PEs assessed using self-report measures. Negative correlations between frontal and temporal cortical thickness and IQ have been found in early childhood, followed by a slower decline in cortical thinning in late childhood and adolescence (Shaw et al., 2006). The current sample with PEs showed lower childhood IQ, but grey matter volume in young adulthood showed no relation to childhood IQ. Nevertheless, we cannot rule out variations in cortical maturation during development.

3.4.4 Frontoparietal network configurations

This is the first study to investigate effective connectivity in non-clinically identified, non-help-seeking young people with PEs and the same frontoparietal network underlying working memory function was identified in all three groups. The variance in BOLD signal in this network during the 2-back condition was best explained as a feedback model where the increase in BOLD signal in the parietal lobules, which is propagated to the frontal lobes, is modulated by a backward connection from the frontal lobes to the parietal lobules. Nevertheless, the probability of this frontal-to-parietal modulation model being the best fit to the data decreased in a linear fashion from persistent PEs to HC, with transient PEs in between. In HC the variance in BOLD

signal was captured almost equally well as a signal increase in the parietal lobules that is propagated to the frontal lobes and modulates the increase in BOLD signal. The probability of this parietal-to-frontal modulation model being the best fit to the data decreased from HC to transient PEs to persistent PEs. These findings suggest a greater role for the frontal lobes in those with PEs, particularly in persistent PEs. During the 3-back there was a clear shift across all groups towards parietal-to-frontal configuration but, unlike HC and transient PEs groups, in persistent PEs the BOLD signal within this network was captured almost equally well with or without the presence of interhemispheric frontal modulation.

These differences in network configurations, in light of similar recruitment of brain regions and no differences in either BOLD signal strength or grey matter volume, reflect differences in the underlying temporal dynamics of distinct regions and highlights the importance of studying cognitive functions in terms of connectivity. Throughout adolescence and into adulthood there are ongoing changes in working memory circuitry which reflect neural maturation and further specialisation towards task-specific processing (Luna et al., 2010). These changes are associated with improvements in cognitive function and reflected in behavioural performance. Considering the minor differences in performance on the 2-back these differences in working memory dynamics could be interpreted as a subtle delay in maturation of a fully formed network whereby those with PEs show a greater dependence on top-down neural signalling from frontal areas. The 3-back condition represents a greater demand in cognitive resources and a parietal-to-frontal configuration was found to clearly best fit the data. However, in persistent PEs there was an additional role for the frontal lobes in terms of interhemispheric communication. In addition to strong convergence of network model configuration there were no differences in performance on the 3-back. Previous work by Dima et al (2014) on the n-back task in healthy volunteers has similarly found a shift towards parietal-to-frontal configurations with an increase in cognitive demands from the 1-back up to the 3-back and Ma et al (2012) also reported an enhanced connection from parietal to

frontal regions at higher digit loads. Taken together it seems that at increasing cognitive demands a parietal-to-frontal configuration is being utilised but this is less strongly the case in those with PEs, in particular persisting PEs.

Refinements in macro- and microstructure of this network occur throughout adolescence before stabilising during adulthood (Shaw et al., 2008; Østby et al., 2011) and lead to a decreased reliance on frontal areas as more specialised posterior regions become increasingly recruited (Luna et al., 2010). In our study, subtle changes can be observed at lower cognitive load in working memory circuitry and coincide with poorer performance but are less pronounced when all groups are struggling. The question arises if these differences are indicative of a developmental lag, a greater reliance on frontal top-down signalling in those with PEs that can be observed when their peers are able to perform the task adequately, or indicative of atypical wiring within this network that leads to a more prominent role for the frontal lobes. The few fMRI studies on PEs have reported greater connectivity in those with PEs than controls (Diederen et al., 2013; Orr et al., 2014), in contrast to the majority of studies in high-risk and psychosis which report a decrease in connectivity regarding the frontal lobes (Pettersson-Yeo et al., 2011). Specifically, Orr et al (2014) report hyperconnectivity between frontal and parietal areas of the brain in PEs compared to controls. In this sense, the prominent role of the frontal lobes could be considered a protective factor or resilience in response to a deviation in typical development that is associated with the manifestation of PEs (Orr et al., 2014; Johnson et al., 2015). However, due to the cross-sectional nature of the imaging data we are unable to comment on changes in these patterns over time.

3.4.5 PEs and neurodevelopmental risk factors

Whilst the current findings illustrate differences in working memory function and brain network configuration in those with persistent PEs compared to healthy controls, it is uncertain how this relates to the very phenomena that characterise these groups. More specifically, does the presence of PEs cause alterations in

working memory function or do changes in cognitive development lead to the manifestation of PEs? Though trajectories vary for specific cognitive functions, numerous studies on premorbid neuropsychological functioning have reported IQ deficits prior to the onset of schizophrenia (Woodberry et al., 2008; Reichenberg et al., 2010; Dickson et al., 2012; Meier et al., 2014), which do not seem to progress with age nor in the presence of prodromal psychotic symptoms (Woodberry et al., 2008). Neuroimaging studies also report a progressive decline in grey and white matter structures after the onset of psychosis compared to the prodromal stage (Pantelis et al., 2005; Peters & Karlsgodt, 2015). As such, it seems unlikely that the emergence of PEs is the driving force behind differences in working memory function. Instead, early neurodevelopmental risk factors, such as lower childhood IQ, may play a role in the manifestation of PEs and, in turn, psychiatric disorders.

3.4.6 Strengths and limitations

This study utilised a multi-modal approach to assess working memory function in PEs by examining the overall structure of grey matter and the regional blood flow of brain regions recruited in working memory. Additionally, DCM allowed for analysis of connectivity within this identified network to elucidate more subtle differences between groups. However, this is limited to the subject-specific regional activation and is not a measure of structural connectivity in the brain. The administration of a stringent semi-structured interview rated by trained observers, rather than a self-report measure to define PEs is one of the main strengths of this study. Overestimation of psychotic phenomena due to self-report measures limits their usefulness in aiding our etiological understanding of psychotic disorders. In the current sample, we assessed the presence of PEs over the past six months at age 18 and 20 and as such we cannot say with absolute certainty that persistent PEs are stable from age 18 to age 20. A close look at the rated PEs in this group did suggest however that the same type of symptoms are being reported at each time point, but more research on persistence of PEs is required. Similarly, the definition of transient

PEs in the current study did not differentiate between those rated as having PEs at age 18 or at age 20. Currently it is uncertain whether there is a difference between those who have recently had PEs and those who now have PEs.

The use of a well characterized, epidemiologically ascertained sample with detailed demographic and psychosocial assessments allowed for well-matched samples in terms of age, gender and handedness. Whilst the current sample includes more females than males, Zammit et al. (2013) reported that, in the ALSPAC cohort, females were more likely than males to have psychotic experiences. Similarly, other population-based studies have reported gender differences in psychotic phenomena, but overall findings have been inconsistent (Maric et al., 2003; Johns et al., 2004; van Os et al., 2009; Dominguez et al., 2010).

3.4.7 Future directions

The availability of longitudinal ratings of PEs over two years in a homogenous cohort allowed for a thorough assessment of brain function in PEs and whilst no significant differences were found in the localisation and overall strength of activation, there was a meaningful deviation from healthy controls in terms of connectivity and performance in those with persisting PEs. It is unknown what causes persistence of PEs in some whilst in others these symptoms dissipate over time. Our findings further highlight the impact of persistence and the intermediate status of those with transient PEs. What differentiates those who continue and those who cease to have PEs is of utmost importance for improving our understanding of both the phenomenology of PEs and the psychosis continuum. Having said that, as a group those with persistent PEs are at increased risk of developing a psychiatric disorder, some indeed the majority are likely to remain illness-free with other bio-psycho-social factors determining resilience, functional decline or even transition to psychosis (Bak et al., 2005; Hanssen et al., 2005; Krabbendam et al., 2005a, 2005b; Zammit et al., 2013b). This further highlights the need for longitudinal research in PEs in population-based samples, such as ALSPAC, to understand the role mediating

factors play and identify factors that are predictive of transition to psychiatric disorders. Finally, although the mere presence of PEs can be considered a deviation from typical development a closer look at the type of PE as well as frequency and severity could clarify some of the heterogeneity of outcomes within those with PEs.

Chapter 4

MRI Indices of Cortical Development in Young People with Psychotic Experiences: Influence of Genetic Risk and Symptom Persistence

Delusions and hallucinations are key psychopathological features of psychotic disorders, but these phenomena are also prevalent in the general population at levels that do not reach clinical thresholds (van Os et al., 2000; McGrath et al., 2015). Expression of such psychotic experiences (PEs) is most common during childhood and adolescence, a critical period in neurodevelopment, and typically dissipates over time. These subclinical phenomena are assumed to be part of a psychosis continuum and are reported at higher rates in the general population than psychotic disorders (van Os et al., 2009; McGrath et al., 2015). Despite the frequent transitory nature, the mere presence of PEs in an individual is associated with an elevated risk of transitioning to clinical psychosis (Zammit et al., 2013b). The manifestation of PEs can be considered part of an atypical developmental trajectory that presents a transitory vulnerability to psychosis but one that is modulated by the further presence of environmental and genetic risk factors (van Os et al., 2009). This transitory expression can become abnormally persistent in the presence of modulating risk factors and the persistence of PEs increases the already present risk of developing a psychotic disorder (Kaymaz et al., 2012). In line with the notion of a continuum, PEs similarly show familial clustering (van Os et al., 2000) and share many risk factors, including low IQ and substance use, with psychotic disorders (Polanczyk et al., 2010; Johns et al., 2004). However, the cognitive impairments associated with PEs differ from those found in psychotic disorders (Mollon et al., 2016) and PEs have also been linked to non-psychotic disorders (Yung et al., 2007; Varghese et al., 2011).

Neuroimaging techniques have been used extensively to study the prodromal phase of psychosis in an effort to map the correlates of vulnerability to psychosis and have consistently found reduced grey matter volume in individuals at high risk in prefrontal, temporal and cingulate regions (Fusar-Poli et al., 2011a, 2012c; Jung et al., 2010). More importantly, studies have found progressive changes in brain anatomy associated with transitioning to psychosis (Pantelis et al., 2005, 2007; Wood et al., 2008; Smieskova et al., 2010), supporting the idea there may be an early vulnerability to psychosis but that additional processes at a later stage in development underlie a transition to psychosis. Studies of gyrification, a neurodevelopmental measure of cortical expansion constrained by intra- and intercortical connectivity, have found widespread progressive disturbances in schizophrenia (White & Hilgetag, 2011; White & Gottesman, 2012) but hypergyria in the prefrontal lobe has been reported in individuals at high risk and unaffected siblings (Harris et al., 2004; Falkai et al., 2007; Harris et al., 2007; Stanfield et al., 2008; Palaniyappan & Liddle, 2012a; Dauvermann et al., 2012). In line with grey matter volume studies, there is a clear distinction between these groups in terms of cortical thickness across the brain (Fornito et al., 2008; Jung et al., 2011; Sprooten et al., 2013; Cannon et al., 2015) and cortical thinning has similarly been associated with subsequent onset of psychosis (Fornito et al., 2008; Cannon et al., 2015; Chung et al., 2015).

Most high risk cohorts have been defined using a combination of putative state and trait risk factors for psychosis and do not require the presence of PEs if an individual has a high genetic (familial) risk for psychosis and if a significant deterioration in functioning is present, nor if a brief intermittent psychosis episode has recently occurred (Yung et al., 1998; Phillips et al., 2000). There are few studies that have focused solely on PEs but these do implicate frontal, temporal, and cingulate brain regions. Studies on adults with PEs have reported a decrease in grey matter volume bilaterally in the orbitofrontal cortex (Pelletier-Baldelli et al., 2014), the left supramarginal gyrus and right prefrontal cortex (Drakesmith et al., 2016b), and an increase in the posterior cingulate cortex and precuneus (Modinos et al., 2010a). In

contrast, a study on children with PEs found increased grey matter volume in the right orbitofrontal cortex, left superior temporal gyrus and angular gyrus and reduced volume in the left inferior temporal gyrus (Jacobson et al., 2010). To date, only one study has looked at cortical thickness in association with PEs and reported no differences (Córdova-Palomera et al., 2014). Though there are no reported associations between gyrification and the manifestation of PEs, alterations in connectivity have been reported in the form of reduced fractional anisotropy in fronto-occipital and fronto-parietal connections (Jacobson et al., 2010; DeRosse et al., 2014; Smallman et al., 2014; O'Hanlon et al., 2015) and functional connectivity in frontal and temporal brain regions (Diederen et al., 2013; Orr et al., 2014). Unsurprisingly, reports of alterations in brain structure and connectivity seem to congregate on the frontal lobes, but there is less of an overlap with other findings.

As previously mentioned, studies have highlighted a genetic component to the brain abnormalities found in schizophrenia as well as high risk populations. Advances in genetics have allowed for the opportunity to assess the cumulative effect of multiple alleles that show small effects on risk for schizophrenia as a polygenic risk score (PGRs) that can be used to examine how genetic risk is expressed in the general population. Neuroimaging studies have used this approach and have found genetic influences on brain volume (Terwisscha van Scheltinga et al., 2013), prefrontal brain function (Walton et al., 2014; Kauppi et al., 2015; Lancaster et al., 2016), cortical thickness (French et al., 2015), hippocampal volume (Harrisberger et al., 2016), and parietal gyrification (Liu et al., 2016).

This study aimed to examine cortical morphometry and underlying white matter in relation to the manifestation of PEs as well as genetic risk for schizophrenia. Studies of brain structure in PEs have identified volumetric reductions in frontal, parietal, and temporal brain regions and we expect that, much like in psychosis, assessment of the cortical surface using structural MRI will demonstrate focal disturbances in morphometry. Firstly, we hypothesize that, disturbances in gyrification are associated

with the manifestation of PEs (H1). Furthermore, we hypothesize that the persistence of PEs represents a greater deviation from typical development and this will be demonstrable in the disparities in cortical morphometry relative to HC and transient PEs (H2). We aim to explore the relation between cortical morphometry and PGRs as not enough is currently known to devise specific hypotheses. However, transition to psychosis has been associated with greater reductions in cortical thickness and we expect individuals with abnormal persistence of PEs and high genetic risk for schizophrenia to exhibit reductions in cortical thickness (H3). Finally, white matter connectivity will be examined in relation to cortical grey matter and we hypothesise abnormalities in cortical grey matter, driven by PEs or polygenic risk for schizophrenia, will be associated with disturbances in underlying white matter (H4).

4.2 Methods

4.2.1 Participants

A total of 4724 young adults who were part of the Avon Longitudinal Study of Parent and Children (ALSPAC; http://www.bristol.ac.uk/alspac/) were assessed for the presence of psychotic experiences (PEs) at the age of 18. Based on their assessment, 126 individuals, rated as having had PEs, were recruited to undergo structural magnetic resonance imaging. Out of those with no sign of having had any PEs, 126 individuals were scanned as a control group. At the time of the scan, all participants were 19 to 20 years old and were reassessed for the presence of PEs on the day of the scan (see chapter 2 for details).

From this sample, 247 individuals had a rating for PEs at both time-points and were labelled as healthy controls, transient PEs or persistent PEs (table 6). There were 111 healthy controls with no sign of PEs at either time-point. Out of the 126 with PEs at age 18, only 70 were still rated as having had PEs at age 20 (persistent PEs). The

transient PEs were comprised of 55 individuals who were no longer rated as having had PEs at age 20 and 11 individuals who were recruited as controls but were rated as having had PEs at age 20. One individual with persistent PEs showed an enlarged left ventricle and was excluded from the study, leaving only 246 in the total sample and 69 with persistent PEs.

Table 6. Classification of participants based on PEs rating at ages 18 and 20 and allocation of participants in specific subsamples for analyses.

Assessment age 18	Assessment age 20	Label	Sample	PGRs[b] Subsample	DWI[c] Subsample
n = 252	n = 247		n = 246	n = 180	n = 178
126 HC	111 HC	HC	111	79	78 HC
	11 PEs	Transient PEs	67	52	52
126 PEs	56 HC				
	69 PEs	Persistent PEs[a]	68	49	48

[a] Out of the 69 individuals with persistent PEs, one participant was found to have an enlarged ventricle and was excluded from further analysis

[b] Only 180 out of the 247 individuals with PEs at both time-points had a polygenic risk score (PGRs) for schizophrenia available.

[c] Diffusion weighted imaging (DWI) data were not acquired for 2 individuals and so the sample size was reduced from 180 to 178.

4.2.2 Psychotic Experiences

The presence of PEs was assessed using the semi-structured Psychosis-Like Symptom Interview (Horwood et al., 2008; Zammit et al., 2013b). This instrument assesses the occurrence of hallucinations, delusions and thought interference in the past 6 months. Interviewees are asked a series of questions about experiencing PEs and further cross-questioning was carried out if a positive answer was given. PEs were rated as absent, suspected, or definitely present and a credible example was required

for PEs to be rated as definitely present (see chapter 2 for a more detailed description on PEs).

4.2.3 Genetic risk

A polygenic risk score (PGRs) had been calculated for each individual in the ALSPAC cohort with genetic data available. Scores were generated by summing the number of risk alleles present for each single nucleotide polymorphism (SNP) weighted by the logarithm of it odds ratio for schizophrenia based on the results from the second Psychiatric Genomics Consortium schizophrenia GWAS (Schizophrenia Working Group of the Psychiatric Genomics Consortium, 2014). Scores were generated from a list of SNPs with a GWAS training set ($p \leq .05$). PGRs were available for 183 individuals who were scanned. This led to a total of 180 individuals with PEs ratings at both time-points and PGRs computed. Table 1 shows a breakdown of the groups after including the PGRs.

4.2.4 Other variables

A childhood intelligence quotient (IQ), estimated at age 8 using the Wechsler Intelligence Scale for Children, was obtained from the ALSPAC database. Missing data points were estimated using regression imputation (Buck, 1960) across the entire ALSPAC dataset. Gender had been recorded for each participant and total brain volume was calculated and included as a potential confounding variable.

4.2.5 Image Acquisition

Data were acquired at Cardiff University Brain Research Imaging Centre (CUBRIC) on a 3 Tesla General Electric HDx system (GE Medical Systems, Milwaukee, Wisconsin) using an 8 channel head coil. T_1-weighted structural images with a 1mm isotropic resolution were acquired using a fast spoiled gradient echo (FSPGR) sequence (TR = 7.8ms, TE = 3.0ms, TI = 450ms, flip angle=20°, acquisition matrix = 256x192, zero-padded matrix = 256x256). High angular resolution diffusion weighted images (HARDI) were acquired with 60 gradient orientations (b = 1200 s/mm^2) and 6

unweighted scans (b = 0 s/mm^2) and a 2.4mm isotropic resolution using a spin-echo echo-planar imaging sequence (TR = cardiac-gated, TE = 87ms, acquisition matrix = 96x96, zero-padded matrix = 128x128). Following zero-padding the reconstructed image resolution for the HARDI scans was 1.8x1.8x2.4mm.

4.2.6 Surface Based Analysis

Cortical morphometry was assessed using Freesurfer version 5.3 (surfer.nmr.mgh.harvard.edu). The image processing pipeline is fully automated and has been described in greater detail in chapter 2 (or see Dale et al. 1999; Fischl et al. 1999; Fischl 2012; Schaer et al. 2012). In short, Freesurfer aims to extract the cortical grey matter by identifying the boundaries with white matter as well as the dura and/or cerebrospinal fluid and warp the cortical grey matter to a stereotactic space. In order to identify the boundary between cortical grey matter and white matter, the signal intensity of all voxels is mean centred to the white matter signal and the image is skull stripped before segmenting and binarizing this white matter volume. A surface tessellation is then used to identify the boundary between white matter and other brain tissue. This mesh of vertices is then iteratively smoothed and inflated to finally resemble a sphere and is registered to a spherical atlas (Desikan et al., 2006) based on the average folding patterns of the brain adhering to a point-to-point correspondence. Once the coordinates of each vertex are known, the surface can be represented in three dimensions again as a brain surface area. The cortical thickness (CT) can then be computed as the distance between the pial surface and the white matter boundary. The sulcal folds of the pial surface are then filled and the entire surface is binarized before creating a new surface tessellation that covers this outer hull and represents the boundary between the sulci and gyri of the pial surface. The local gyrification index (lGI) is then computed as the ratio of the amount of grey matter visible on the outer hull and the corresponding amount on the pial surface. Finally, the lGI and CT maps were smoothed using a Gaussian filter with a full-width at half maximum of 5mm and 10mm, respectively.

4.2.7 Diffusion Preprocessing and Atlas-based Tractography

Data were analysed in ExploreDTI v4.8.3 (Leemans et al. 2009; http://exploredti.com) and processing steps have been described in greater detail in chapter 2 and originally by Drakesmith et al (2015, 2016a, 2016b). Images were corrected for head motion and distortions induced by eddy currents and field inhomogeneities by registering each image volume to a synthetic T_1-weighted volume computed from a mcDESPOT processing pipeline (see Drakesmith et al., 2016a). In the presence of head rotation, the B-matrix was reoriented according to the approach described by Leemans and Jones (2009). Whole-brain tractography was carried out using a dampened Lucy-Richardson algorithm (Dell'Acqua et al., 2010) to estimate the peak in fibre orientation distribution function (fODF). Seed points were arranged in a 3x3x3 mm grid in white matter and streamlines were initiated. Streamlines continued in 1mm steps following the peak in ODF that subtended the smallest angle until the fODF amplitude fell below 0.05 or when the direction of the streamline changed at an angle greater than 45°.

Alterations in cortical morphometry were implemented as volumes of interest (VOI) for atlas-based tractography. First, clusters identified at group level were transformed to each participant's native space to produce a VOI. This volume was then dilated and eroded to fill any holes inside and trimmed using cortical ribbon masks to restrict the VOI to the cortical grey matter.

Each participant's B_0 image was registered to their T_1-weighted image (that is conformed to Freesurfer space) using a boundary-based cost function to produce a transformation matrix that describes how to get from diffusion space to Freesurfer space. The inverse of this transformation matrix was applied to the VOIs to transform these to diffusion space for atlas-based tractography. Diffusion metrics were extracted from tracts passing or ending in the VOI to assess the structural connectivity.

4.2.8 Statistical Analysis

Using a whole-brain approach, parameter estimates for vertex-wise lGI and CT were estimated using a general linear model (GLM). In studying the association with PEs, group membership and gender were treated as categorical factors and childhood IQ, total brain volume (TBV) and were included as covariates. Total brain volume was mean centred prior to inclusion as a covariate regressor. In a subsequent analysis the PGRs was also included in this model. The effect of PEs was modelled as a linear contrast (*HC ('No PEs')* > *'Persistent PEs'* with 'Transient PEs' assumed to lie intermediate) and interaction effects with TBV and PGRs were additionally examined. The association with PGRs was studied with PGRs as a continuous factor, gender as a categorical factor, and similarly included childhood IQ and TBV as covariates. In the presence of a significant effect for the linear contrast, a quadratic contrast was similarly tested to verify the assumption that Transient PEs lie intermediate (*HC* < *'Transient PEs'* > *'Persistent PEs'*). Though gender was modelled separately for each class, males and females were pooled together in statistical comparisons.

To correct for multiple comparisons, a cluster-wise correction was performed using a precomputed Monte Carlo simulation with a z-distribution (Hagler et al., 2006) with a vertex-wise threshold of $p < 0.001$ and a cluster-wise threshold of $p < 0.05$. A Bonferroni correction was applied to the cluster-wise threshold to adjust for both cerebral hemispheres.

The median value for tract length was extracted from tracts that pass through a VOI and Hartigan's dip test (Hartigan & Hartigan, 1985; Hartigan, 1985) was employed to assess the presence of a bimodal distribution that would indicate the presence of different tract classes such as, for instance, short-range association tracts and long range projection tracts. All clusters displayed a unimodal distribution, except for the precentral gyrus (Dip=0.045, $p = 0.008$). However, upon inspection of the distribution it was clear this was driven by only three participants, two HC and one transient PEs. Fractional anisotropy, mean, axial, and radial diffusivity were extracted as well as the

number of streamlines. Median diffusion metrics were entered into a general linear model (fitglm) in Matlab (The Mathworks Inc., 2016) with the same predictor variables as entered in the Freesurfer analysis, but with the addition of the cluster mean lGI as a predictor variable. The linear fit of the model was tested against the constant model and if the best fitting line had a non-zero slope the coefficients for PEs and interaction terms with TBV and lGI were assessed for significance. For VOIs that highlighted an interaction between PEs and PGRs, coefficients and interaction terms with PGRs were also assessed for significance. Thresholds for statistical significance were adjusted for multiple comparisons using a Bonferroni correction ($p<0.0071$).

4.3 Results

4.3.1 Demographics

There was no indication of a difference in gender distribution between the groups in the whole sample ($\chi^2_{(2, 246)} = 1.50$, $p = 0.47$) or in the smaller subset ($\chi^2_{(2, 180)} = 0.49$, $p = 0.78$). Both TBV and PGRs did not differ between groups, but IQ was higher in healthy controls compared to transient and persistent PEs. This finding did not change when looking at the subsample, though IQ only differed between HC and transient PEs. A summary of the demographics and statistical tests is given in table 7.

Table 7. Descriptive and inferential statistics for the 3 Psychotic Experiences Groups with Psychosis Risk Score and Brain Volume

	Healthy Controls	Transient PEs	Persistent PEs	Test Statistic
n = 246	111	67	68	
Female	68 (61.26%)	47 (70.15%)	45 (66.18%)	
Male	43 (38.74%)	20 (29.85%)	23 (33.82%)	
IQ	112.3 (14.8)	104.9 (14.0)	106.0 (14.1)	$F_{(2,243)} = 7.01$, $p = 0.001$[b]
TBV[a]	1469.9 (130.9)	1430.7 (155.6)	1457.5 (153.0)	$F_{(2,243)} = 1.55$, $p = 0.214$
n=180	79	51	50	
Female	47 (40.50%)	17 (33.33%)	19 (38.00%)	
Male	32 (59.49%)	34 (66.67%)	31 (62.00%)	
IQ	112.2 (15.1)	104.6 (15.8)	108.1 (13.3)	$F_{(2,177)} = 4.22$, $p = 0.016$[c]
TBV[a]	1471.6 (125.3)	1443.4 (161.3)	1469.1 (149.6)	$F_{(2,177)} = 0.67$, $p = 0.515$
PGRs	0.06 (0.90)	-0.15 (1.25)	-0.07 (1.09)	$F_{(2,177)} = 0.62$, $p = 0.538$

[a] Total Brain Volume (TBV) is reported in cm^3

[b] Post-hoc comparisons using Bonferroni correction revealed that only HC differed from the other groups with PEs

[c] Post-hoc comparison revealed only a difference between HC and transient PEs

4.3.2 Cortical Morphometry

We sought to examine the macrostructure of the cortical grey matter surface in relation to psychotic experiences that were transient or persistent over time. Additionally, we aimed to assess the impact of a polygenic risk score by carrying out the same analyses with the addition of a score that highlighted a genetic risk for schizophrenia.

Psychotic Experiences

Our initial assessment of gyrification revealed a main effect of group in the left Middle Temporal Gyrus that showed a decrease in lGI in those with persistent PEs relative to controls. A two-way interaction was found between the effects of PEs and TBV on lGI in the left Lateral Occipital Gyrus, the left Precentral Gyrus and the right Rostral Middle Frontal Gyrus. Plotting the mean lGI against TBV shows a more moderate increase in lGI with increasing TBV in those with persistent PEs in frontal areas as well as the Lingual Gyrus, but also a sharp decrease in lGI in the left Lateral Occipital Gyrus with increasing TBV. These findings are summarised in appendix B, section B.1.

PGRs

Including the PGRs in our statistical model did not reveal abnormalities in cortical thickness or gyrification. Furthermore, exclusion of the classification of PEs in our model did not change the overall null findings.

PEs and PGRS

Including the PGRs as a confounding variable did not eliminate the associations between PEs and the lGI in occipital, precentral and middle frontal regions. Additionally, a two-way interaction was present between the effects of PEs and PGRs on lGI in the left medial orbitofrontal gyrus and the left superior parietal lobule (see table 8 for an overview of all identified clusters). The location of the clusters is depicted in figure 6 and figures 7-9 describe the effect for each cluster in terms of the lGI for each group and as a function of total brain volume or the PGRs.

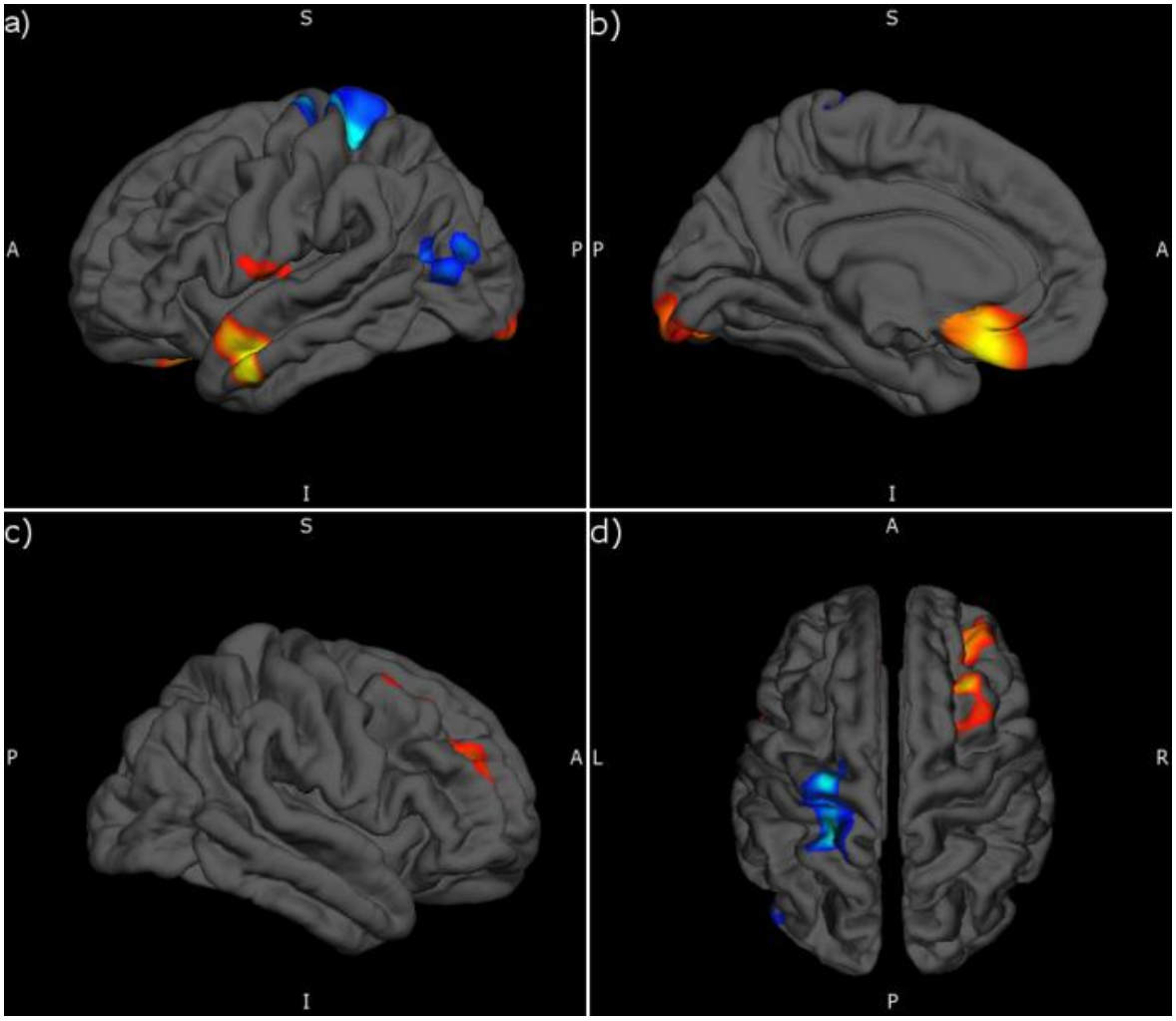

Figure 6. Regions of the cortical sheet that show deviations in lGI between groups following a linear trend and where PEs were found to interact with the PGRs and TBV on lGI. Red-yellow represents stronger reductions in persistent PEs as either an effect of group or as an interaction effect with TBV as the contrast between the 3 groups was specified as a linear decrease [1 0 -1]. Blue-light blue represents a greater decrease in lGI in transient PEs in relation to the PGRs and these are in blue as this was specified as a quadratic increase [-1 2 -1]. Please see chapter 2 for details on contrasting for general linear modelling.

Table 8. Summary of clusters where lGI is associated with PEs and PGRs. The p-value indicates the clusterwise corrected p-value and the associated z-score is derived from the p-value.

Effect (visible in figure 6 panel)	Region	Cluster Size (mm^2)	MNI Coordinates			p-value	z-score
			X	Y	Z		
PEs (a)	L Middle Temporal Gyrus	568.5	-55.1	-0.5	-27.5	0.0022	2.17
PEs x TBV (c-d)	R Rostral Middle Frontal Gyrus	834.0	29.8	40.3	20.0	0.0002	2.63
PEs x TBV (d)	R Caudal Middle Frontal Gyrus	467.0	30.0	23.5	43.9	0.0108	1.95
PEs x TBV (a-b)	L Lateral Occipital Gyrus	1319.3	-22.4	-85.1	-10.0	0.0002	2.63
PEs x TBV (a)	L Precentral Gyrus	660.7	-54.9	-5.4	8.9	0.0006	2.43
PEs x PGRS (b)	L Medial Orbito-frontal Gyrus	791.1	-5.2	24.4	-19.4	0.0002	2.63
PEs x PGRS (a, d)	L Postcentral Gyrus	1911.4	-21.5	-39.4	57.0	0.0002	2.63
PEs x PGRS (a,d)	L Inferior Parietal Gyrus	617.9	-40.6	-80.4	16.6	0.0018	2.21

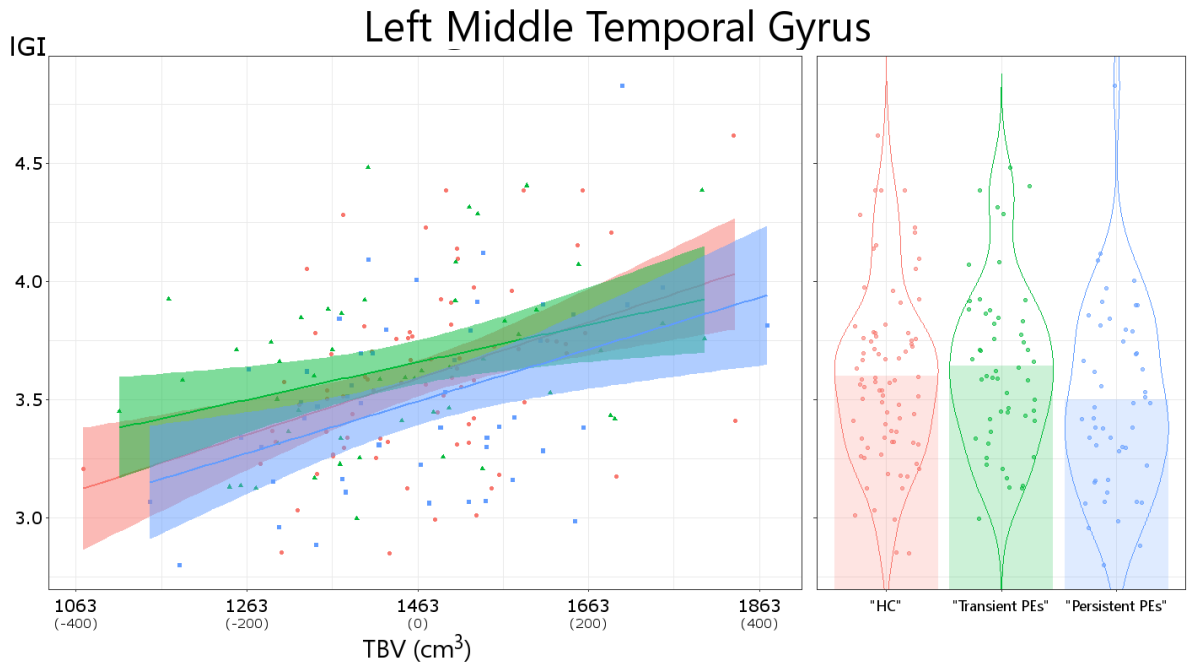

Figure 7. Reduced gyrification (lGI) in persistent PEs in the left middle temporal gyrus relative to HC (see right graph for the significant effect). The x-axis in the scatterplot denotes both the actual total brain volume (TBV) and the mean centred scores in parentheses.

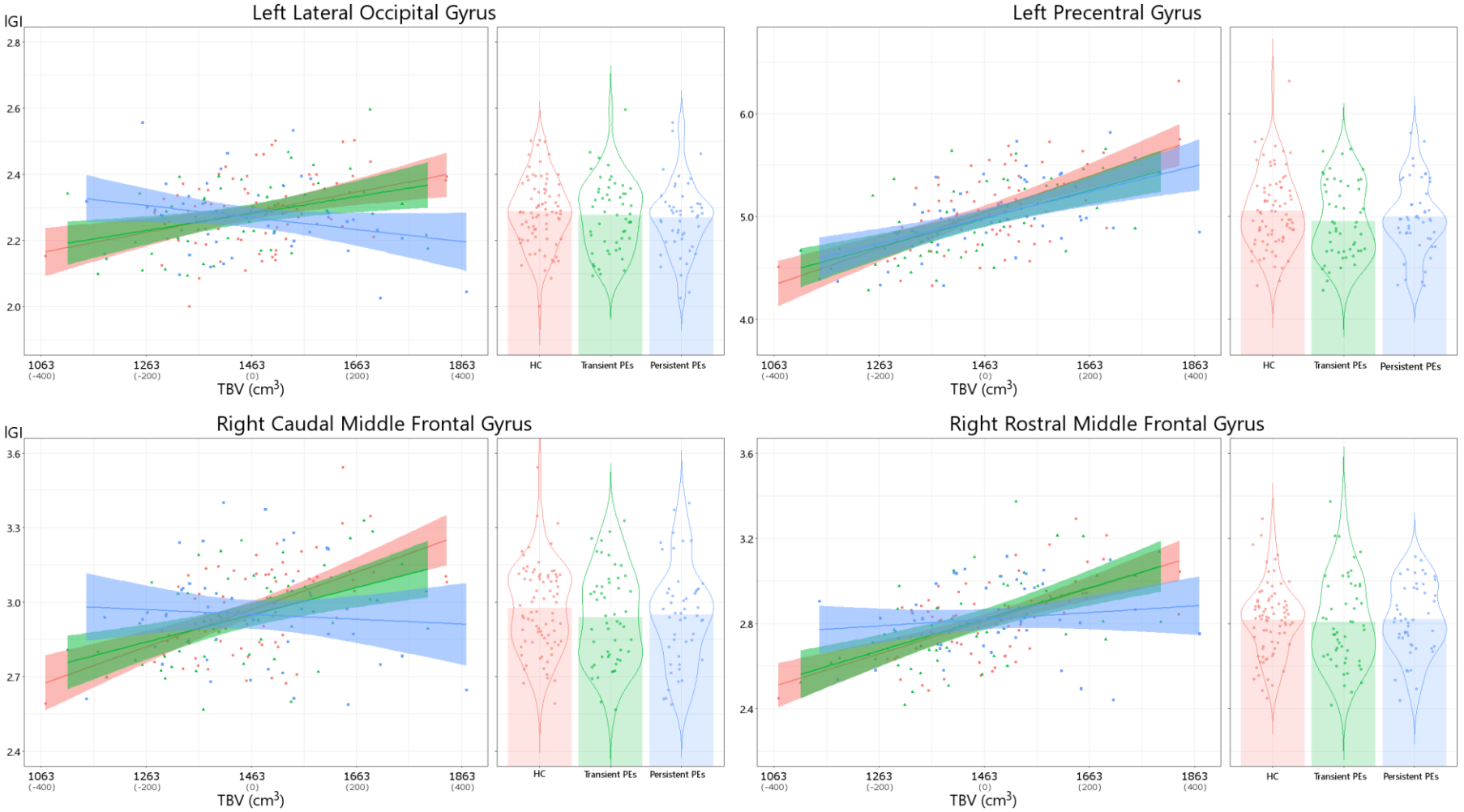

Figure 8. Group-by-TBV interaction effects on gyrification (lGI). The x-axis in the scatterplot denotes both the actual total brain volume (TBV) and the mean centred scores in parentheses.

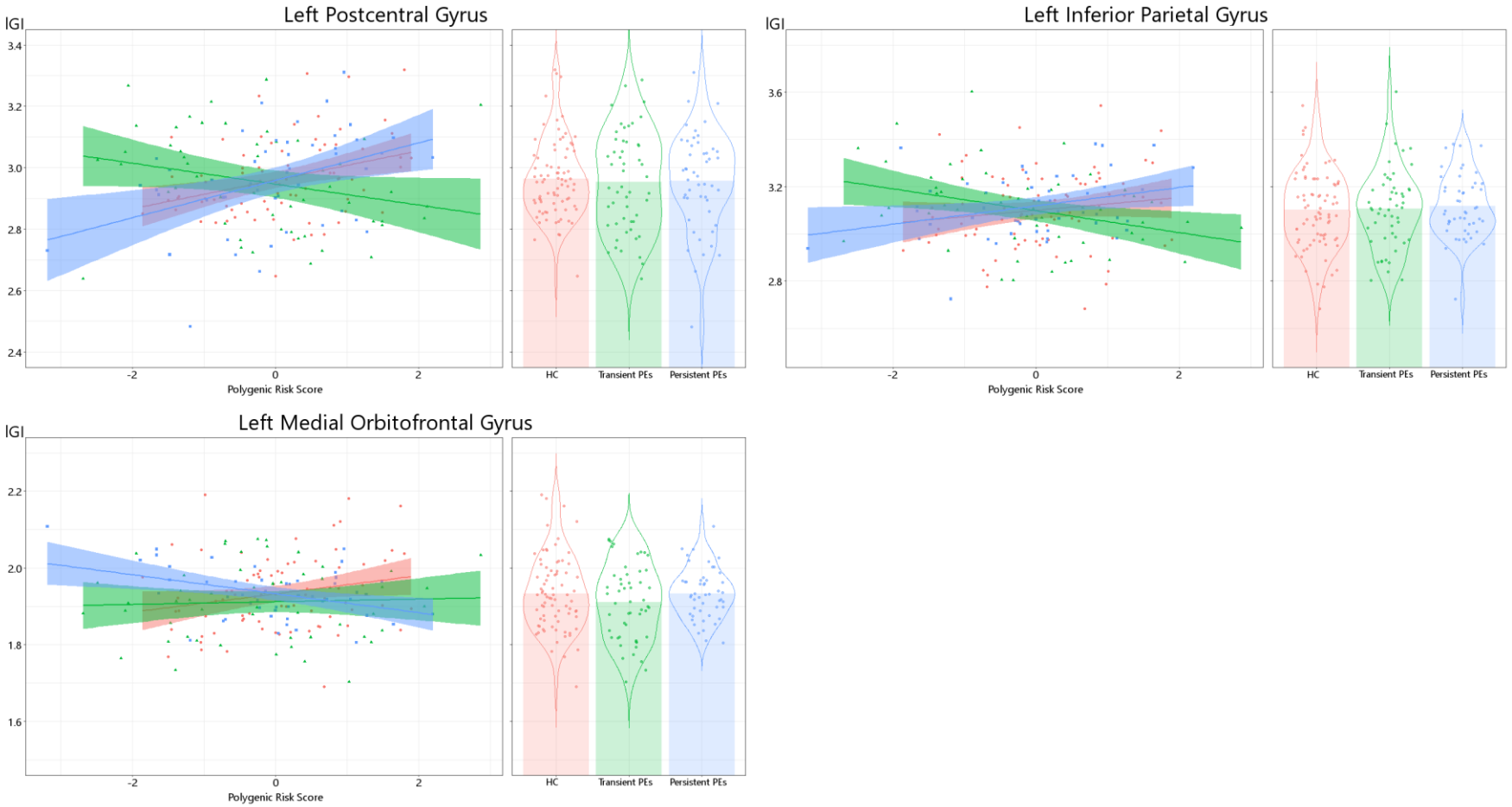

Figure 9. Group-by-PGRs interaction effects on gyrification (lGI). The top row highlights an effect for transient PEs and the bottom row for persistent PEs relative to the HC.

4.3.3 Atlas-based Tractography

All seven clusters that showed an association with PEs as well as TBV or the PGRs were used as VOIs to examine underlying white matter connectivity. There was no significant difference between groups in the size of the VOIs in native space.

Though the specified general linear model was often a better fit than the constant model (see appendix B, section B.2), in most cases there was no effect of PEs on diffusion metrics. Table 9 gives a summary of the relevant diffusion metrics for each group and the effects that were found. Persistent PEs were found to have a greater length of tracts passing through a cluster in the precentral gyrus and an interaction effect with IGI was found as well. Both transient and persistent PEs differed from controls in terms of tract volume. In the medial orbitofrontal gyrus FA was higher in those with persistent PEs. Interestingly, an effect of PGRs was found in the medial orbitofrontal gyrus as well, demonstrating a reduction in volume with a higher score. See appendix B, section B.3 for plots of the significant effect of PEs on the diffusion scalars as well as an individual example of the streamlines passing through these clusters.

Table 9. Differences in white matter tracts in transient and persistent PEs compared to healthy controls. Average and standard deviation is reported per group for each significant effect. Radial diffusivity (RD) is reported in mm^2/s^{-1}.

Volume of Interest	Metric	Healthy Controls	Transient PEs	Persistent PEs	Effects	Test Statistic
L Precentral Gyrus	Length (mm)	41.0 ±9.0	40.0 ±7.0	43.0 ±5.3	Persistent PEs	t = 2.88, p = 0.004
					Persistent PEs × lGI	t =-2.88, p = 0.005
	Volume (mm^3)	18424.2 ±6237.7	16910.0 ±5685.2	18188.1 ±4449.7	Transient PEs × lGI	t = -2.81, p = 0.006
					Persistent PEs	t = 2.93, p = 0.004
					Persistent PEs × lGI	t = -3.01, p = 0.003
R Caudal Middle Frontal Gyrus	FA ($x10^{-1}$)	2.98 ±0.38	3.02 ±0.42	2.96 ±0.49	Transient PEs	t = -2.73, p = 0.007[a]
					Transient PEs × lGI	t = 2.81, p = 0.006
L Medial Orbitofrontal Gyrus	FA ($x10^{-1}$)	2.42 ±0.46	2.46 ±0.41	2.61 ±0.35	Persistent PEs	t = 4.01, p < 0.001
	RD ($x10^{-4}$)	7.19 ±0.44	7.19 ±0.30	7.04 ±0.32	Persistent PEs	t = -2.79, p = 0.006

[a] The unrounded p-value was actually greater than the Bonferroni corrected threshold of p < 0.0071

4.4 Discussion

The principal aim of this study was to examine the properties of cortical morphometry in individuals with PEs and those at higher genetic risk of developing schizophrenia. Furthermore, we sought to link alterations in cortical grey matter to underlying white matter connectivity for a better understanding of the impact of PEs and genetic risk on cortical anatomy. We had hypothesised that the manifestation of PEs is associated with an atypical neurodevelopmental trajectory and this would be reflected in abnormalities in gyrification in areas reported to show volumetric abnormalities across studies of PEs and psychosis (H1). We expected that the persistence of PEs would highlight greater disparities in cortical morphometry (H2). Furthermore, individuals with abnormal persistence of PEs and a high genetic risk for schizophrenia (PGRs) would exhibit reductions in cortical thickness as a sign of further deterioration in progression towards psychosis (H3). Finally, we expected any deviation in gyrification to be associated with further disturbances in the underlying white matter (H4). There were several focal disturbances in gyrification, but these only highlighted differences between persistent PEs and healthy controls. Those with transient PEs did not seem to differ from controls, but there was an interaction effect between PEs and the PGRs showing a decrease in lGI with increasing PGRs in the parietal lobule in those with transient PEs. Interestingly, a similar effect was found in the orbitofrontal lobe but for those with persistent PEs instead. The combination of high genetic risk and persistence of PEs was hypothesized to be associated with reductions in cortical thickness, but no differences were observed in this study. Alterations in white matter were expected to be present alongside the focal disturbances in cortical folding but the differences in lGI and underlying white matter pathways were not as expected; FA was increased in those with persistent PEs in tracts passing through the medial orbitofrontal gyrus.

There was a reduction in lGI in the middle temporal gyrus associated with persistence of PEs. Focal aberrations in the temporal lobe are frequently reported in association

with psychosis (Honea et al., 2005; Vita et al., 2012), and a few studies have reported on reduced gyral complexity (Cachia et al., 2008; Nesvåg et al., 2014; Palaniyappan & Liddle, 2012b). We expected to find alterations in cortical folding patterns in the prefrontal lobe and this proved to be somewhat correct as the association between total brain volume and gyrification revealed a relatively lower lGI for those with persistent PEs with greater brain volume in the middle frontal gyrus, extending into the superior frontal gyrus. A reduction in cortical folding in the middle frontal gyrus has been reported in schizophrenia (Palaniyappan et al., 2011; Palaniyappan & Liddle, 2014) and seems to be present at onset of psychosis (Cachia et al., 2008; Palaniyappan et al., 2013; Gay et al., 2013). Several high risk studies have reported an opposite effect (Harris et al., 2004, 2007; Stanfield et al., 2008), but also reported on local grey matter volume differences and crucially, their findings on increased gyrification did not remain after further taking brain volume into account. We also identified an interaction effect in the precentral gyrus between lGI and brain volume in those with persistent PEs compared to controls. Reduced local gyrification in the precentral gyrus has previously been reported in schizophrenia in two independent samples (Nesvåg et al., 2014) as well as in first-episode patients (Palaniyappan et al., 2013). However, visual inspection of this relationship did not reveal a uniform effect of PEs. The lateral occipital gyrus presented a similar effect as the middle frontal gyri, where those with persistent PEs did not show a positive association between lGI and brain volume. Reduced occipital gyral complexity has previously been found in psychosis (Gay et al., 2013; Palaniyappan & Liddle, 2014), but increased curvature has also been reported (Schultz et al., 2013, 2010) hence more research is needed to clarify these complex findings. It is clear that at best these are subtle deviations in cortical folding that show some degree of overlap with regions that have been implicated in schizophrenia. Interestingly, there was no indication of deviations in lGI associated with transient PEs and this suggests that these findings are associated with the persistence rather than the manifestation of PEs. Here a similar pattern

could be discerned where a subtle early neurodevelopmental deviation is present which is exacerbated in those who transition to psychosis.

Unexpectedly, there was no overall association between the polygenic risk score for schizophrenia and cortical morphometry. There were two interaction effects between PGRs and PEs, though these did not follow a similar pattern. In the medial orbitofrontal cortex, those with persistent PEs displayed a decrease in lGI with a higher PGRs score. Gyrification was lower in the superior parietal lobule for those with transient PEs and a higher PGRs score. The association between the gyrification of the parietal lobules and a PGRs score has previously been reported on (Liu et al., 2016), though this did not include an assessment of PEs.

In terms of white matter, there were indications of differences between groups regarding tracts passing through the left precentral gyrus and medial orbitofrontal gyrus. In the precentral gyrus there was an effect of PEs on volume which was reduced in those with PEs. Additionally, there was an effect of persistent PEs and an interaction with the lGI on the median tract length and the number of reconstructed streamlines. However, there was no indication of differences in the typically reported diffusion metrics. The inclusion of tract length, number of streamlines, and tract volume was done to offer some insight to the similarity of the tracts that run through each VOI. Though these findings could reflect differences in white matter anatomy in relation to PEs, it is also possible these are simply the result of the atlas-based approach in placement of VOIs. In tractography, the best strategy for ROI or VOI placement is often dependent on the shape, size, and location of the region and it is possible that these are driven by small VOI error placements during transformation from standardised space to native space. Considering this and both the unclear interaction effect of PEs with brain volume on gyrification, we will refrain from further speculating on these findings. However, the strong differences between groups certainly merit further investigation of the implicated white matter tracts. We found increased FA in those with transient PEs in the right caudal middle frontal gyrus and

an interaction effect that highlighted the increase in FA was associated with overall brain volume. This was unexpected, but upon re-examining the initial results on the caudal middle frontal gyrus it appears that although gyrification increases with brain volume, on average transient PEs have a lesser degree of gyrification in this cluster. It is possible that reduced lGI is present in PEs in general and is more strongly affected in persistent PEs. As such, the increase in FA highlights abnormalities in microstructure alongside reduced, although not significantly, lGI in transient PEs that can be distinguished from persistent PEs. In the medial orbitofrontal gyrus, we found higher FA in those with persistent PEs in comparison to controls. The bulk of the tracts that passed through this cluster comprised the anterior portion of the cingulum and projections from the rostrum of the corpus callosum. This finding is in contrast with high risk and schizophrenia studies that have reported reduced FA in the cingulum and the corpus callosum (Canu et al., 2014; Samartzis et al., 2014), though there have equally been null findings (Peters et al., 2008, 2010). In those with PEs, reductions in FA have been reported in the cingulum (Jacobson et al., 2010; Drakesmith et al., 2016a) and frontal callosal projections (Drakesmith et al., 2016a), but other pathways have also been implicated instead (O'Hanlon et al., 2015; DeRosse et al., 2014). This could be partly explained by the dynamic changes in frontal white matter tracts during adolescence and adulthood; whilst callosal medial orbitofrontal projections show a gradual linear decrease in FA over time, there are non-linear patterns present in the non-callosal and more lateral orbitofrontal projections (Malykhin et al., 2011). As such, it is vital to isolate the implicated pathways to examine these in their respective developmental path.

Due to the cross-sectional nature of this study, it is difficult to gain deeper insight into the underlying neurodevelopmental processes. However, the combination of cortical thickness, gyrification, and diffusion metrics does allow for some conjecture. Typically, cortical folding is considered a process that begins during gestation and remains relatively stable despite the overall growth of the brain (Armstrong et al., 1995; Gautam et al., 2015). After birth there are several dynamic changes that occur

in surface curvature of the brain. From childhood to adolescence there is an increase in the cortical complexity (Dombroski et al., 2014), particularly of the prefrontal lobe (Blanton et al., 2001), but towards adulthood and onward there are age-related decreases in gyrification (Sandu et al., 2014). As such, it is uncertain if focal disturbances in gyrification in those with persistent PEs are markers of an early neurodevelopmental insult that could be considered a vulnerability factor for psychosis, or if these occur at a later stage of development that coincides with the manifestation of PEs. Changes in cortical folding from adolescence to adulthood are not independent from developmental changes in grey and white matter during this time (White et al., 2010; Mills et al., 2016) and further coincide with pronounced changes in cognition and behaviour (Razlighi et al., 2016; Blakemore, 2008). During adolescence there is a general reduction in cortical grey matter volume and this is considered to be reflective of both synaptic pruning and increased myelination (Mills et al., 2016; Giedd et al., 1999). Synaptic pruning reduces tension along neuronal fibres and this is thought to play a role in the widening of sulci with age (Kochunov et al., 2005; Klein et al., 2014). This process is particularly pronounced during adolescence and continues on in to adulthood at a slower rate (Sandu et al., 2014). If our findings on gyrification were part of a recent disturbance in development during adolescence, one possible mechanism would be a defect in synaptic pruning processes that would affect the tensile forces and this should be observable as a change in the underlying white matter. Our findings highlight many subtle differences in cortical complexity but with little evidence of any disturbances in the underlying white matter tracts. Therefore we propose that these variations in cortical folding are the result of early neurodevelopmental deviations rather than changes that take place during adolescence when the brain goes through complex reorganisation.

Our findings allude to some effects of polygenic risk for schizophrenia on both cortical grey matter and white matter pathways but the exact mechanism and how it relates to PEs is still unclear. In two clusters there was a reduction in lGI in association

with the PGRs, but this effect was found in persistent PEs and in transient PEs, respectively. Additionally, the volume of pathways passing through the medial orbitofrontal gyrus was associated with the PGRs across the sample. Previous studies have not found an association between PEs and the PGRs (Zammit et al., 2013a; Jones et al., 2016) and our findings similarly show no clear relationship. There have been genetic imaging studies that have highlighted an association between the PGRs and imaging measures (Terwisscha van Scheltinga et al., 2013; Walton et al., 2014; Kauppi et al., 2015; Lancaster et al., 2016; French et al., 2015; Harrisberger et al., 2016; Liu et al., 2016), but this is still in early stages. Cortical patterning has been found to be mediated by genetic factors (Peng et al., 2016) and more research is needed to establish the contribution of common polymorphisms associated with schizophrenia.

In this study we found differences in cortical folding patterns in those with persistent PEs with little to no evidence of differences in underlying connectivity, brain volume, and cortical thickness. Alterations in gyrification are comparable to those present in schizophrenia but were only distinguishable when further taking brain volume into account. We propose that the atypical relationship between brain volume and cortical complexity is indicative of an early neurodevelopmental insult that resulted in cortical expansion plateauing sooner in those that manifest PEs that persist. This would explain why the degree of gyrification does not increase as expected with brain volume, as the former remains relatively stable throughout life despite a vast increase in overall brain size during development (Armstrong et al., 1995). Though far from conclusive, our findings emphasize the role of early developmental deviations without evidence of progressive changes with time though these were further bound to the persistence of PEs. The focal disturbances in cortical folding could be a marker of persistence but considering the overlap with schizophrenia these could also be a precursor to transitioning. Risk of developing a psychotic disorder increases with persistence of PEs following a dose-response relation (Kaymaz et al., 2012) and it is possible that these changes are associated with the transition to psychosis. Further longitudinal studies are essential to clarify the role of persistence in the alterations

present in gyrification as either an indicator of developing psychosis or as a lingering vulnerability.

Chapter 5

Microstructural Disturbances along Commissural and Association Tracts are Associated with Psychotic Experiences

The dysconnection hypothesis was first introduced over two decades ago to describe the symptoms of schizophrenia as a failure of functional integration among brain regions (Weinberger, 1993; Friston & Frith, 1995; Friston, 1999). The notion of dysconnectivity has remained as a core feature of schizophrenia and continued advances in computational neuroimaging have produced evidence of systemic functional dysconnection between brain regions involving prefrontal, temporal and select subcortical areas (Friston et al., 2016). In functional MRI, aberrant integration can be characterised either in terms of functional or effective connectivity (Friston, 2011). Functional connectivity refers to a correlation, or coherence, over time between distinct brain regions and studies have typically reported a greater incidence of reduced functional connectivity alongside some increases in schizophrenia and seem to predominantly involve frontotemporal regions (Pettersson-Yeo et al., 2011). Effective connectivity on the other hand refers to the modulatory effect of activity in one brain region over another and is typically assessed in relation to cognitive function. Though less extensively studied, reductions in effective connectivity and disturbed modulatory control have been linked to difficulties in working memory associated with schizophrenia (Schlösser et al., 2003; Wolf et al., 2007; Crossley et al., 2009; Benetti et al., 2009; Deserno et al., 2012; Zhang et al., 2013). Though dysconnectivity is typically considered to reflect disturbances in synaptic transmission and plasticity, abnormal wiring of association fibres has also been suggested as a possible mechanism and these mechanisms are not mutually exclusive (Pettersson-Yeo et al., 2011; Stephan et al., 2006a, 2006b); the development and survival of long-range connections could be affected by early impairments in

synaptic plasticity (Bullmore et al., 1997; Stephan et al., 2006a; Fornito & Bullmore, 2014). Furthermore, patients with metachromatic leukodystrophy (MLD), a neurological disorder characterised by demyelination, show a high incidence of psychotic symptoms when the onset of MLD occurs during adolescence (Hyde, 1992).

Diffusion-weighted imaging (DWI) allows insight on the anatomical connections that mediate the transfer of information between cortical regions by inferring microstructural features of the architectural configuration of white matter. Typically, DWI studies report on fractional anisotropy (FA) which describes the anisotropy of water diffusion in white matter tissue and is modulated by, among other things, the axon diameter, density, orientation, and degree of myelination. Studies of schizophrenia have consistently reported on widespread voxel-based reductions in FA, predominantly implicating commissural and projection tracts that connect frontal and temporal brain regions, but also converge specifically on disturbances in the uncinate fasciculus, the cingulum, and the arcuate fasciculus using tractography (Pettersson-Yeo et al., 2011; Wheeler & Voineskos, 2014). As mentioned, FA is modulated by several factors but there are other sources of evidence, such as post-mortem studies and other imaging measures like magnetisation transfer ratio, that point more towards disturbances in myelination of white matter pathways in schizophrenia (Walterfang et al., 2006). More recent studies have also included additional properties of the diffusion of white matter such as radial diffusivity (RD), which is the degree to which diffusion is hindered perpendicular to the principal direction of the tract. A combination of reduced FA and increased RD can be considered a stronger indicator of disturbances in myelination than FA alone and studies of schizophrenia have reported both reduced FA and increased RD in the cingulum bundle and arcuate fasciculus (Seitz et al., 2016) as well as in the inferior longitudinal fasciculus (Ashtari et al., 2007; Seitz et al., 2016), and the corpus callosum (Whitford et al., 2010).

Myelination of white matter tracts begins during the early stages of post-natal development and the mature pattern of myelination is already present after the first year. However, myelination continues to progress across several decades of life and follows the typical posterior to anterior pattern of maturation (Lenroot & Giedd, 2006). Onset of psychosis typically occurs during adolescence, a time of complex reorganisation of the brain, and it is uncertain if the observed changes in white matter connectivity arise during this period or if there is a consistent disruption present throughout neurodevelopment. Diffusion imaging studies of first-episode (FEP) and recent-onset psychosis show high variability in the location of alterations as well as the direction of any differences (Peters & Karlsgodt, 2015), most likely confounded by differing definitions of FEP (Breitborde et al., 2009) as well as underpowered sample sizes (Melicher et al., 2015), making it unclear if disruptions in myelination could already be present. Given the current theoretical framework of schizophrenia that proposes progressive changes in brain structure and function leading up to the onset of psychosis, abnormalities should be observable in those considered at elevated risk of developing psychosis. Studies of high risk have repeatedly reported on reductions in FA converging on frontal regions with limited evidence of parietal and temporal disturbances (Peters & Karlsgodt, 2015; Vijayakumar et al., 2016). However, most studies have looked at measures such as FA using voxel-based assessments rather than isolate the implicated white matter tract. Two studies have specifically looked at the corpus callosum, the cingulum, and the arcuate and uncinate fasciculi but found no differences in those at high risk (Peters et al., 2008, 2010). More recently, population-based studies have examined white matter in individuals with psychotic experiences (PEs); a collective term for subclinical manifestations of psychosis-like symptoms such as hallucinations, delusions, and thought interference. PEs have been considered to lie along a continuum of psychotic expression (van Os et al., 2000) and provide a unique opportunity to assess white matter microstructure in relation to dysconnectivity in psychosis. As mentioned, individuals with demyelination due to MLD during adolescence are more

prone to exhibiting psychotic symptoms (Hyde, 1992) whereas PEs are most frequently reported during adolescence (Kelleher et al., 2012a) and are associated with an elevated risk for psychosis that further increases with abnormal persistence of symptoms (Kaymaz et al., 2012).

An early study on schoolchildren highlighted reductions in FA in those with PEs across parahippocampal, temporal, and occipital regions and suggested disturbances in the cingulum bundle (CB), inferior fronto-occipital fasciculus (IFOF), and inferior longitudinal fasciculus (ILF) (Jacobson et al., 2010). A more recent study, also of schoolchildren with PEs, found more widespread alterations in FA as well as other diffusion scalars implicating the IFOF, as well as the uncinate and superior longitudinal fasciculi (O'Hanlon et al., 2015). Interestingly, this study reported both increased and decreased FA in different clusters that are in areas that cover these tracts. Furthermore, clusters covering sections of the IFOF were also found to display increased and decreased axial diffusivity and there were reductions in mean diffusivity covering the SLF and reduced radial diffusivity in the IFOF and UF. To account for these conflicting findings, the authors extracted the underlying tracts and assessed the microstructure along these tracts. In the UF, there was a bilateral increase in FA and reduction in RD those with PEs. This pattern was also found in the frontal section of the right IFOF and along-tract statistics further revealed that this difference originated at the terminal sections of the tract. To date, one study from our group has examined white matter in young adults with PEs and identified reduced FA in those with PEs in a frontomedial cluster that predominantly capture portions of the corpus callosum and corona radiata (Drakesmith et al., 2016a). More interestingly, this pattern was further expanded upon when further taking into account the severity of PEs. Using an ordinal model of PEs, the authors found both reduced FA and increased RD in clusters encompassing the corpus callosum, corona radiata, internal capsule, SLF, IFOF and CB. It is important to note the key difference in age between this study and the prior studies which reported on both reduced and increased FA. Furthermore, the study by O'Hanlon et al. (2015) is the only so far that

has assessed the actual tracts rather than carry out voxel-based assessments. Further evidence towards dysconnectivity in PEs comes from functional imaging studies as altered connectivity has been reported before in terms of reduced functional coupling (Modinos et al., 2010b; Orr et al., 2014; Satterthwaite et al., 2015). However, it is uncertain if these are indicators of disturbances specific to myelination in PEs. One important study from our group has assessed cortical myelination in relation to PEs, looking at the longitudinal relaxation rate R_1 ($1/T_1$) using quantitative MRI, and found reductions in R_1 in frontal and parietal areas in the left hemisphere (Drakesmith et al., 2016b) though only when taking into account the severity of PEs. Another caveat to keep in mind is that R_1 is reportedly sensitive to differences in macromolecular composition and iron content as well (Rooney et al., 2007).

Though voxel-based assessments allow for thorough examination of white matter across the brain, it is unable to pick up on subtle changes in a specific tract and frequently identifies clusters that envelop sections of several tracts. The merits of manual tractography have always been clear, but accurate segmentation requires good anatomical knowledge, experience in segmentation, and can often be very time demanding. Furthermore, segmentation is typically carried out by several operators and results can vary between individuals due to the subjective nature of the task (Wakana et al., 2007).

The aim of this study is to examine the microstructure of three major white matter pathways that were identified in studies of PEs and that have frequently been implicated in schizophrenia and high risk for psychosis. Additionally, we aim to assess the feasibility of a novel automated segmentation approach using tract shape modelling for the extraction of the tracts of interest (Parker, 2014). The corpus callosum (CC) is a white matter structure that is vital for the integration of cognitive and sensory information between brain hemispheres (Raybaud, 2010; van der Knaap & van der Ham, 2011) and reductions in FA have consistently been reported in studies of schizophrenia and high risk for psychosis (Whitford et al., 2010;

Pettersson-Yeo et al., 2011; Peters & Karlsgodt, 2015; Vijayakumar et al., 2016). Two prominent long association tracts were also selected; the inferior fronto-occipital fasciculus (IFOF) and the superior longitudinal fasciculus (SLF). The IFOF connects the orbitofrontal and occipital lobes and is considered to play a role in the semantic network (Martino et al., 2010). This tract is known to be affected in schizophrenia (Pettersson-Yeo et al., 2011; Peters & Karlsgodt, 2015), with stronger disturbances associated with poorer outcome (Mitelman et al., 2007), and has been reported in high risk studies as well (Vijayakumar et al., 2016). The same holds true for the SLF, which connects the frontoparietal network which has been found to be vulnerable to the emergence of psychosis as both functional and structural connectivity of this pathway is often progressively reduced from individuals at high risk to patients with psychosis with first-episode patients intermediate (Schmidt et al., 2014a).

We propose that structural dysconnectivity is part of the extended phenotype of psychosis and that this is observable in those who lie along the continuum but do not meet the requirements for a psychotic disorder. Specifically, we expect that an increase in radial diffusivity along with a reduction in fractional anisotropy will be observable in those with PEs. We hypothesise that in the CC there are primarily disturbances in anterior sections; imaging studies of the midline surface area and tractography of the CC in psychosis have both highlighted abnormalities in predominantly frontal connections (Walterfang et al., 2008b, 2008a; Whitford et al., 2010) and a previous voxel-based study on PEs from our group similarly implicated frontomedial pathways (Drakesmith et al., 2016a). The anterior part of the IFOF has previously been implicated in PEs (O'Hanlon et al., 2015; Drakesmith et al., 2016a), but maturation of the IFOF has also been linked to age-related improvements in processing speed (Peters et al., 2014) which has been suggested to be impaired in PEs (Mollon et al., 2016). Therefore we hypothesise that the IFOF will be affected in those with PEs and we further expect anterior sections to show stronger reductions in FA alongside increased RD. Structural and functional MRI studies of fronto-parietal circuitry have predominantly reported reductions in prodromal and clinical psychosis

(Schmidt et al., 2014a) and we hypothesise that the SLF will similarly be affected in terms of FA and RD. Given the fact that studies of grey matter report less frequent on abnormalities in parietal structures (Honea et al., 2005; Fusar-Poli et al., 2011a, 2012c; Wheeler & Voineskos, 2014), we further expect alterations to be situated in more anterior parts of the SLF. Finally, as abnormal persistence is associated with a greater risk of transitioning, we expect to find stronger evidence of abnormalities in FA and RD in those with persistent PEs.

5.2 Methods

5.2.1 Participants

All participants were part of the Avon Longitudinal Study of Parents and Children (ALSPAC) and individuals were recruited based on the presence of psychotic experiences (PEs) at age 18. A total of 126 individuals were recruited who were rated as having had PEs in the past 6 months and a matched control group was recruited who were rated as never having had any PEs. All participants underwent magnetic resonance imaging and were reassessed for the presence of PEs on the day of the scan. All participants were 19 to 20 years old at the time of the study. Written consent was obtained prior to both assessments at age 18 and at age 20 and ethical approval for the study was provided by the ALSPAC Law and Ethics Committee, the Cardiff University School of Psychology Ethics Committee, and local research ethics committees.

The presence of PEs was assessed using the Psychosis-Like Symptoms Interview (PLIKSi; Horwood et al. 2008) to evaluate the occurrence of delusions, hallucinations, or thought interference in the interviewee over the past 6 months. The rating given at both age 18 and at age 20 was used to allocate each participant to one of three groups. Those who were rated as never having had any PEs were considered healthy

controls (HC), those who were rated as having had PEs in the past 6 months at both assessments were rated as persistent PEs. The remainder, those who were rated as having had PEs at either age 18 or at age 20 were labelled transient PEs.

In total, 247 individuals had a rating for PEs at both assessments; however diffusion imaging data was available for only 243 individuals. One participant was excluded from the study due to an atypically large ventricle. Participant demographics are given in table 10.

Table 10. Descriptive statistics for the study sample by group

	HC	Transient PEs	Persistent PEs	Test Statistic
n = 242	110	66	66	
Male	43 (39.1%)	20 (30.3%)	21 (31.8%)	
Female	67 (60.9)	46 (69.7%)	45 (68.2%)	
Childhood IQ	112.4 (14.9)	105.10 (14.2)	105.8 (14.0)	$F_{(2,239)} = 6.83$, $p = 0.001$[a]
Total Brain Volume (cm^3)	1471.4 (130.5)	1433.8 (154.7)	1454.2 (154.1)	$F_{(2,239)} = 1.41$, $p = 0.245$

[a] Post-hoc comparisons revealed both transient and persistent PEs differed from healthy controls ($p < 0.05$).

5.2.2 Magnetic Resonance Imaging

High angular resolution diffusion weighted images (HARDI) were acquired at Cardiff University Brain Research Imaging Centre (CUBRIC) on a 3 Tesla General Electric HDx (GE Medical Systems, Milwaukee, Wisconsin) using an 8 channel head coil. Images

were obtained using a spin-echo echo-planar imaging sequence (TR = cardiac-gated , TE = 87ms, acquisition matrix = 96x96, image resolution = 2.4mm^3) with 60 gradient orientations (b = 1200 s/mm^2) and 6 unweighted scans (b = 0 s/mm^2). Acquisition matrix was zero-padded (128x128) and final image resolution was 1.8x1.8x2.4mm.

Diffusion data were corrected for head motion, eddy currents and field inhomogeneities using ExploreDTI 4.8.3 (Leemans et al., 2009). Each diffusion image was corrected for head motion and registered to a T_1-weighted volume to correct for B_0 field inhomogeneities and eddy current distortions. When realigning images, the B-matrix was rotated accordingly to preserve orientational information (Leemans & Jones, 2009). Deterministic tractography was carried out using a damped Lucy-Richardson (dRL) algorithm to retrieve the fibre orientation distribution function (fODF) across a 3x3x3 mm grid (stepsize = 1mm, fODF threshold = 0.05, angular threshold = 45°, streamline lengths = 30 – 300mm).

5.2.3 Automated Segmentation

Typically, segmentation of streamlines is carried out by placing Boolean gates at strategic locations in order to isolate those that pass, or don't pass, through specific regions of interest in the brain. For instance, to extract the corpus callosum it is necessary to include streamlines that pass from one hemisphere to the other. Segmentation is done per subject as the exact positioning of gates can differ between individuals due to anatomical variability, errors in co-registration, and image noise can affect the streamline trajectories (Lori et al 2002). Additionally, the identification of anatomical landmarks for optimal gate positioning requires expert anatomical knowledge on the part of the operator and results can vary distinctively between operators due to the subjective nature of the task (Wakana et al 2007).

Several methods of automated segmentation have been proposed and the current approach uses the shape, location, and orientational information. This approach is introduced and described in great detail in the doctoral thesis of Parker (2014) and a

condensed version has been presented (Parker et al., 2013). First, a subsample of the dataset is used to create a set of training data which captures the tract of interest. Second, the training data is used to define the feature space that captures the streamline shapes. The third step in this approach would be the segmentation of new data by normalising and projecting candidate streamlines into the feature space and assigning streamlines to similarly shaped bundles. However, we tested several parameters of the final step prior to applying the optimal configuration. For each model, we carried out a voxel-based comparison of the recovered streamlines using the automated and manual tract segmentation and examined the precision and recall statistics.[11] The optimal combination of precision and recall was selected for each tract and automated segmentation of the dataset was carried out using these parameters.

5.2.4 Manual Tract Segmentation

In this study, we sought to examine the superior longitudinal fasciculus (SLF), the corpus callosum (CC), and the inferior fronto-occipital fasciculus (IFOF) in each hemisphere. Existing protocols for manual segmentation were available and were adapted for this study.

For the CC, we isolated streamlines based on their projections to different areas of the brain (Huang et al., 2005). This divided the CC in to subcomponents that represent interhemispheric orbitofrontal, prefrontal, parietal, occipital, and temporal connections. The prefrontal connections were further divided into connections that project anterior, superior or lateral. Unlike the original protocol described in Huang et al. (2005), we did not distinguish between superior and posterior parietal projections due to inconsistencies in tract architecture that did not agree with the notion of distinct superior and posterior projections. Segmentation of anterior

[11] Precision was computed by looking at the number of true (t_p) and false (f_p) positives: $precision = \frac{t_p}{t_p+f_p}$

The recall is computed by looking at the number of true positives (t_p) and false negatives (f_n): $recall = \frac{t_p}{t_p+f_n}$

projections was carried out by placing Boolean AND gates in the coronal plane anterior to the genu of the corpus callosum and inferior projections to the orbitofrontal cortex were separated from other streamlines. Frontal lateral streamlines were identified by placing AND gates lateral to the corona radiata in the sagittal plane. Superior frontal projections were isolated by placing AND gates in the axial plane anterior to the central sulcus and parietal superior projections were segmented by placing AND gates posterior to the central sulcus. Posterior streamlines projecting to the occipital and parietal regions were segmented by identifying the parieto-occipital fissure in the sagittal plane and then delineating each region in the coronal plane. Temporal projections were segmented by placing AND gates on the tapetum in the coronal slice midway through the splenium.

Segmentation of the IFOF was carried out by placing Boolean AND gates in the coronal plane. The occipital lobe was isolated by extrapolating the parieto-occipital sulcus in the sagittal plane and placing an AND gate in the coronal plane that delineates the occipital from the parietal lobe. The frontal lobe was delineated by selecting a coronal slice anterior to the genu of the corpus callosum. The protocol for segmentation was originally described in Wakana et al. (2007).

To isolate the SLF, Boolean AND gates were positioned anterior to the precentral sulcus and posterior to the postcentral sulcus respectively. A NOT gate was positioned in the temporal lobe to exclude the streamlines of the arcuate fasciculus. In the original protocol (de Schotten et al., 2011), the SLF is divided into three components by delineating three AND gates around the superior, middle, and inferior frontal gyri. However, streamlines that make up the SLF 1, which connects the parietal lobule to the superior frontal gyrus, frequently ended prematurely. As such, we segmented the SLF as a whole to evaluate the reconstruction of all the SLF components using the most amount of information.

5.2.5 Automated Shape Modelling

Following manual segmentation, streamlines are reordered according to an external reference point, filtered by length, and interpolated to a fixed 30 point representation. Streamlines are reordered based on the distance from the external reference to make use of the directional information; a three dimensional representation may travel in different directions despite describing the same shape. Each streamline is then translated to the mean shape through centre of mass subtraction and a generalised Procrustes analysis (Gower, 1975) is carried out until convergence is reached.[12] The coordinates are then concatenated to form a feature space of 90 descriptors (30 knot-points in 3 dimensions) and are combined into an observation matrix. Principal component analysis is carried out to reduce the dimensionality of the feature space by calculating the cumulative sum of the resulting eigenvalues and truncating the set of eigenvectors to a smaller set at which the cumulative sum exceeds 98% of the total. Shapes are clustered in feature space using a k-means clustering of the training data coordinates whereby different cluster centroids incorporate different shapes and each streamline is assigned to the nearest cluster.

The application of tract shape modelling to novel data then requires the same normalisation of the streamlines before projecting them into the feature space that was defined by the training data. Each streamline is then assigned a label according to the nearest cluster centroid.

5.2.6 Model Selection

Several parameters of automated tract extraction were iteratively modified to optimise agreement between manual and automated segmentation. A total of 27

[12] First, a single streamline is selected as a template and all other streamlines are warped onto the template using a Procrustes transformation which alters the size, position, and orientation but not the shape. The mean of the superimposed streamlines is then used as the template and if the difference in the positions of the template with the prior template is below a chosen threshold, convergence is reached. If not, then the process is repeated warping the streamlines onto the new template until convergence is achieved.

different models were tested with stepwise increments in parameter settings to identify the optimal arrangement for each tract of interest. Results from this process are noted in appendix C, section C.1. Once an optimal model configuration had been selected, based on the precision and recall statistics, automated tract segmentation was carried out using these parameters.

5.2.7 Along-Tract Statistics

Following segmentation, all tracts were uniformly resampled to *k* number of points, where *k* is computed as the average length of the tract divided by the voxel size rounded up to the nearest integer. All streamlines are reoriented to originate from the same point and are re-parameterized using cubic B-splines curves and are then resampled to allow for averaging of diffusion scalars at *k* number of cross-sections along the tract. This process is semi-automated in ExploreDTI and is based on the work by Colby et al. (2012).

5.2.8 Statistical Analysis

To avoid carrying out *k* number of statistical comparisons per diffusion scalar for each tract, non-linear mixed-effects models were fitted to the data (Bates et al., 1998; Pinheiro et al., 2016) using R version 3.3.1 (R Core Team, 2016). In all models a subject-level random-effect term was added to account for the repeated measures design. Both group and group-by-position interaction effects were included as fixed effects alongside gender, childhood IQ and total brain volume as potential confounders.

A Bonferroni correction was applied by dividing the p-threshold by the number of extracted indices of diffusion (FA, MD, AD, and RD). To further elucidate the nature of any interaction effect, post-hoc model comparisons were carried out by comparing each group with PEs to HC separately to assess if the interaction was still present. A further correction was applied to the thresholded p-value to account for the further comparisons being made.

5.3 Results

5.3.1 Model Selection

Optimal parameter configuration for automated segmentation was carried out by selecting the model configuration that was found to optimally agree with the manual segmentation of the training data (see appendix C, section C.1 for full details and results). Figure 10 provides an illustration of the automated and manual segmentation for each of the segmentations for a single participant. Precision and recall statistics were calculated for the voxel-based agreement between the manual and automated method and are summarised in table 11.

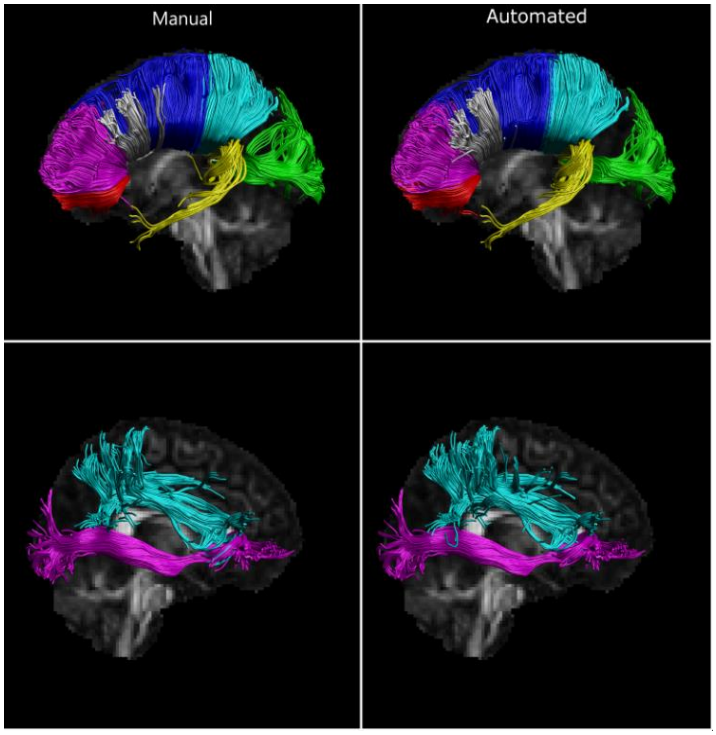

Figure 10. Comparison of manual (left) and automated (right) segmentation methods for a single individual. The top row compares the corpus callosum divided into orbitofrontal (*red*), the frontal anterior (*purple*), superior (dark blue), and lateral (*white*), the parietal (*light blue*), occipital (*green*), and temporal (*yellow*) projections. The bottom row compares the right superior longitudinal fasciculus (*light blue*) and the right inferior fronto-occipital fasciculus (*purple*).

Table 11. Mean (standard deviation) for the precision and recall statistics for each optimal model configuration per tract

Tract Name	Specific pathway	Precision	Recall
Corpus Callosum	Orbital Projections	0.65 (0.06)	0.69 (0.08)
	Frontal Anterior Projections	0.71 (0.10)	0.74 (0.06)
	Frontal Superior Projections	0.71 (0.04)	0.77 (0.02)
	Frontal Lateral Projections	0.46 (0.13)	0.46 (0.13)
	Parietal Projections	0.71 (0.08)	0.71 (0.07)
	Occipital Projections	0.66 (0.08)	0.73 (0.06)
	Temporal Projections	0.46 (0.11)	0.69 (0.08)
Inferior Fronto-occipital Fasciculus	Left IFOF	0.68 (0.04)	0.51 (0.10)
	Right IFOF	0.73 (0.03)	0.61 (0.06)
Superior Longitudinal Fasciculus	Left SLF	0.55 (0.07)	0.60 (0.03)
	Right SLF	0.53 (0.07)	0.69 (0.04)

5.3.2 Averaged Tract Statistics

Diffusion scalars as well as the number of streamlines, tract length and volume were averaged for each tract and extracted. Average tract descriptors are provided for the callosal projections in table 12 and for the association tracts, the SLF and IFOF, in tables 13 and 14 respectively.

Table 12. Average statistics for the projections of the Corpus Callosum. Mean and standard deviation are reported for each diffusion scalar (FA, MD, AD, RD) as well as length, volume, and number of streamlines per group.

Callosal Projections	Metric	HC	Transient PEs	Persistent PEs
Orbitofrontal	FA ($x10^{-1}$)	4.78±0.30	4.68±0.37	4.74±0.27
	MD ($x10^{-4}$ mm^2/s^{-1})	8.62±0.41	8.72±0.63	8.71±0.41
	AD ($x10^{-4}$ mm^2/s^{-1})	13.69±0.46	13.69±0.71	13.78±0.45
	RD ($x10^{-4}$ mm^2/s^{-1})	6.08±0.47	6.24±0.68	6.17±0.47
	Length (mm)	102.1±6.7	100.5±8.5	100.1±5.9
	Volume (cm^3)	6.8±1.4	6.3.74±1.8	6.6±1.4
	Streamlines	200.3±61.8	177.7±65.9	198.1±64.3
Frontal Anterior	FA ($x10^{-1}$)	4.88±0.23	4.84±0.27	4.86±0.24
	MD ($x10^{-4}$ mm^2/s^{-1})	8.77±0.39	8.75±0.43	8.80±0.42
	AD ($x10^{-4}$ mm^2/s^{-1})	14.00±0.47	13.92±0.54	13.99±0.45
	RD ($x10^{-4}$ mm^2/s^{-1})	6.16±0.42	6.17±0.46	6.20±0.46
	Length (mm)	105.5±4.9	102.8±5.6	104.4±5.5
	Volume (cm^3)	31.5±4.8	30.0±5.7	30.9±4.7
	Streamlines	1194.7±260.0	1139.2±287.5	1168.8±253.9
Frontal Superior	FA ($x10^{-1}$)	4.28±0.22	4.27±0.28	4.26±0.25
	MD ($x10^{-4}$ mm^2/s^{-1})	9.40±0.50	9.32±0.59	9.40±0.56
	AD ($x10^{-4}$ mm^2/s^{-1})	13.98±0.48	13.89±0.51	14.04±0.56
	RD ($x10^{-4}$ mm^2/s^{-1})	7.11±0.54	7.04±0.67	7.18±0.67
	Length (mm)	117.0±5.3	114.8±4.7	116.0±5.3
	Volume (cm^3)	53.1±9.1	51.1±11.4	51.5±8.4
	Streamlines	1686.3±404.4	1639.5±450.0	1641.2±350.9

Table 12. Continued from previous page

Callosal Projections	Metric	HC	Transient PEs	Persistent PEs
Frontal Lateral[a]	FA ($x10^{-1}$)	3.53±0.44	3.40±0.38	3.49±0.42
	MD ($x10^{-4}$ mm^2/s^{-1})	10.95±1.04	11.0±1.35	11.0±1.24
	AD ($x10^{-4}$ mm^2/s^{-1})	15.30±0.18	15.22±0.14	15.33±0.14
	RD ($x10^{-4}$ mm^2/s^{-1})	8.78±1.09	8.94±1.36	8.87±1.25
	Length (mm)	76.0±9.9	77.6±10.7	77.4±11.2
	Volume (cm^3)	8.17±3.5	7.5±4.5	7.3±3.5
	Streamlines	181.8±100.2	164.6±133.6	158.2±95.8
Parietal	FA ($x10^{-1}$)	4.49±0.22	4.45±0.27	4.43±0.25
	MD ($x10^{-4}$ mm^2/s^{-1})	8.60±0.40	8.57±0.48	8.66±0.46
	AD ($x10^{-4}$ mm^2/s^{-1})	13.23±0.41	13.15±0.46	13.23±0.43
	RD ($x10^{-4}$ mm^2/s^{-1})	6.28±0.45	6.27±0.55	6.37±0.51
	Length (mm)	131.1±5.2	129.2±5.6	130.1±6.5
	Volume (cm^3)	41.9±10.2	41.2±10.9	38.9±9.8
	Streamlines	1355.2±442.5	1329.7±479.2	1238.6±424.1
Occipital	FA ($x10^{-1}$)	5.17±0.34	5.13±0.38	5.09±0.30
	MD ($x10^{-4}$ mm^2/s^{-1})	8.99±0.63	9.23±1.02	9.20±0.79
	AD ($x10^{-4}$ mm^2/s^{-1})	14.85±0.69	15.11±0.11	15.0±0.85
	RD ($x10^{-4}$ mm^2/s^{-1})	6.01±0.67	6.29±1.01	6.29±0.80
	Length (mm)	157.0±9.3	154.5±8.9	156.5±9.3
	Volume (cm^3)	18.6±4.4	17.6±4.6	18.8±3.8
	Streamlines	567.3±206.8	539.9±201.2	567.0±174.7

[a] Average Tract Statistics are based on 239 individuals instead of 242 as the automated approach was unable to segment any streamlines for 3 individuals

Table 12. Continued from previous pages

Callosal Projections	Metric	HC	Transient PEs	Persistent PEs
Temporal[b]	FA ($x10^{-1}$)	4.03±0.64	3.94±0.74	4.01±0.68
	MD ($x10^{-4}$ mm^2/s^{-1})	11.89±1.52	12.23±1.76	11.98±1.49
	AD ($x10^{-4}$ mm^2/s^{-1})	17.18±1.42	17.50±1.60	17.26±1.30
	RD ($x10^{-4}$ mm^2/s^{-1})	9.24±1.64	9.60±1.90	9.34±1.64
	Length (mm)	147.3±26.3	142.2±26.19	147.62±26.18
	Volume (cm^3)	6.1±2.7	5.6±2.6	6.3±2.6
	Streamlines	77.1±53.4	73.0±52.9	83.1±50.6

[b] The statistics are calculated based on 239 individuals. However, these were not the same 3 individuals as for the Frontal Lateral projections (under [a] in previous section of table 12).

Table 13. Average statistics for the Inferior Fronto-Occipital Fasciculus (IFOF) for each diffusion scalar (FA, MD, AD, RD) and length, volume, and number of streamlines per group. Mean and standard deviation is reported.

	Metric	HC	Transient PEs	Persistent PEs
Left IFOF	FA ($x10^{-1}$)	4.52±0.23	4.48±0.22	4.48±0.28
	MD ($x10^{-4}$ mm^2/s^{-1})	8.21±0.25	8.29±0.30	8.30±0.42
	AD ($x10^{-4}$ mm^2/s^{-1})	12.69±0.37	12.75±0.47	12.77±0.54
	RD ($x10^{-4}$ mm^2/s^{-1})	5.96±0.30	6.05±0.31	6.07±0.44
	Length (mm)	162.0±8.7	159.3±9.7	160.1±8.4
	Volume (cm^3)	8.4±3.5	8.7±3.1	8.6±3.2
	Streamlines	119.3±85.9	120.9±70.1	126.7±78.1
Right IFOF[a]	FA ($x10^{-1}$)	4.48±0.21	4.46±0.24	4.46±0.20
	MD ($x10^{-4}$ mm^2/s^{-1})	8.16±0.29	8.19±0.29	8.17±0.28
	AD ($x10^{-4}$ mm^2/s^{-1})	12.56±0.43	12.57±0.41	12.54±0.39
	RD ($x10^{-4}$ mm^2/s^{-1})	5.97±0.29	6.00±0.32	5.98±0.29
	Length (mm)	159.9±9.1	157.9±8.5	159.6±10.0
	Volume (cm^3)	10.5±3.6	10.1±3.4	10.7±3.1
	Streamlines	193.5±103.0	175.7±110.1	195.9±95.6

[a] Average Tract Statistics are based on 241 individuals instead of the total sample of 242 as the automated approach was unable to segment any streamlines for 1 individual

Table 14. Average statistics of the Superior Longitudinal Fasciculus (SLF) for each diffusion scalar (FA, MD, AD, RD) and length, volume, and number of streamlines per group. Metrics are reported as mean and standard deviation.

	Metric	HC	Transient PEs	Persistent PEs
Left SLF	FA ($x10^{-1}$)	3.53±0.23	3.49±0.25	3.56±0.22
	MD ($x10^{-4}$ mm^2/s^{-1})	7.95±0.29	7.96±0.39	7.93±0.33
	AD ($x10^{-4}$ mm^2/s^{-1})	10.94±0.32	10.90±0.36	10.93±0.38
	RD ($x10^{-4}$ mm^2/s^{-1})	6.46±0.32	6.49±0.44	6.43±0.36
	Length (mm)	63.0±9.0	60.9±8.4	60.3±8.5
	Volume (cm^3)	14.0±4.1	13.5±4.7	13.8±5.3
	Streamlines	339.1±128.4	347.7±161.1	342.6±164.2
Right SLF	FA ($x10^{-1}$)	3.75±0.22	3.66±0.24	3.71±0.20
	MD ($x10^{-4}$ mm^2/s^{-1})	7.79±0.27	7.90±0.42	7.83±0.31
	AD ($x10^{-4}$ mm^2/s^{-1})	10.91±0.28	10.96±0.41	10.93±0.36
	RD ($x10^{-4}$ mm^2/s^{-1})	6.23±0.30	6.36±0.46	6.28±0.32
	Length(mm)	67.0±7.9	66.9±8.4	66.1±8.6
	Volume(cm^3)	21.9±5.1	21.2±6.1	21.5±5.5
	Streamlines	645.8±193.3	628.9±238.6	624.1±192.5

5.3.3 Along-Tract Statistics

Diffusion scalars were computed for points along the tract and assessed using non-linear mixed-effects models. There was no indication of a main effect of PEs but significant group-by-position effects were present in all major tracts. The full statistical output is reported in appendix C, section C.2. The significant findings are summarised in table 15 below.

Table 15. Identified group-by-position effects for each investigated tract

		Group x Position Interaction[a]	Transient PEs vs. HC[b]	Persistent PEs vs. HC[b]
CC Frontal Superior	FA	$F_{(136, 16252)} = 1.45$, $p = 0.0005$	$F_{(68, 11832)} = 1.14$, $p = 0.2051$	$F_{(68, 11832)} = 2.04$, $p < 0.0001$
CC Occipital	FA	$F_{(182, 21749)} = 1.35$, $p = 0.0012$	$F_{(91, 15834)} = 2.21$, $p < 0.0001$	$F_{(91, 15834)} = 0.70$, $p = 0.9863$
	MD	$F_{(182, 21749)} = 1.30$, $p = 0.0043$	$F_{(91, 15834)} = 2.21$, $p < 0.0001$	$F_{(91, 15834)} = 0.97$, $p = 0.5764$
	RD	$F_{(182, 21749)} = 1.34$, $p = 0.0014$	$F_{(91, 15834)} = 2.35$ $p < 0.0001$	$F_{(91, 15834)} = 0.91$, $p = 0.7260$
L IFOF	FA	$F_{(188, 22466)} = 1.26$, $p = 0.0099$	$F_{(94, 16356)} = 0.40$ $p = 1.0000$	$F_{(94, 16356)} = 2.09$, $p < 0.0001$
	RD	$F_{(188, 22466)} = 1.39$, $p = 0.0003$	$F_{(94, 16356)} = 0.79$, $p = 0.9355$	$F_{(94, 16356)} = 2.16$, $p < 0.0001$
L SLF	FA	$F_{(78, 9321)} = 1.60$, $p = 0.0006$	$F_{(39, 6786)} = 1.34$, $p = 0.0768$	$F_{(39, 6786)} = 1.98$, $p = 0.0003$
	RD	$F_{(78, 9321)} = 1.41$, $p = 0.0102$	$F_{(39, 6786)} = 1.46$, $p = 0.0333$	$F_{(39, 6786)} = 0.90$, $p = 0.6576$
R SLF	MD	$F_{(78, 9321)} = 1.59$, $p = 0.0008$	$F_{(39, 6786)} = 2.03$, $p = 0.0002$	$F_{(39, 6786)} = 0.45$, $p = 0.9989$
	AD	$F_{(78, 9321)} = 1.48$, $p = 0.0039$	$F_{(39, 6786)} = 1.89$, $p = 0.0007$	$F_{(39, 6786)} = 0.47$, $p = 0.9978$
	RD	$F_{(78, 9321)} = 1.57$, $p = 0.0011$	$F_{(39, 6786)} = 1.9$, $p = 0.0005$	$F_{(39, 6786)} = 0.52$, $p = 0.9943$

[a] Significance threshold was set to p = 0.0125 (0.05 / 4) for the initial statistical model

[b] In post-hoc testing the threshold was further reduced to 0.0063

Interaction effects were present in the left IFOF and SLF bilaterally and in the occipital and frontal-superior projections of the CC. Modalities of tracts that showed interaction effects were re-examined by limiting the model comparisons to HC versus transient PEs and HC versus persistent PEs respectively (see table 15). Post-hoc comparisons revealed differences in FA, MD, and RD between transient PEs and HC in

the occipital projections of the CC. In the frontal-anterior projections of the CC those with persistent PEs differed from HC. Models of significant callosal projections are plotted in figure 11. In the left IFOF there was no indication of an interaction between transient PEs and position along the tract but effects remained for persistent PEs. In the left hemisphere, the SLF was found to differ in FA between persistent PEs and HC whereas in the right hemisphere an interaction effect was found for transient PEs in relation to HC in terms of MD, AD and RD. Figure 12 highlights the interaction effect of group-by-position for persistent PEs compared to HC in the left IFOF and SLF. The differences in the right SLF between transient PEs and HC are depicted in figure 13.

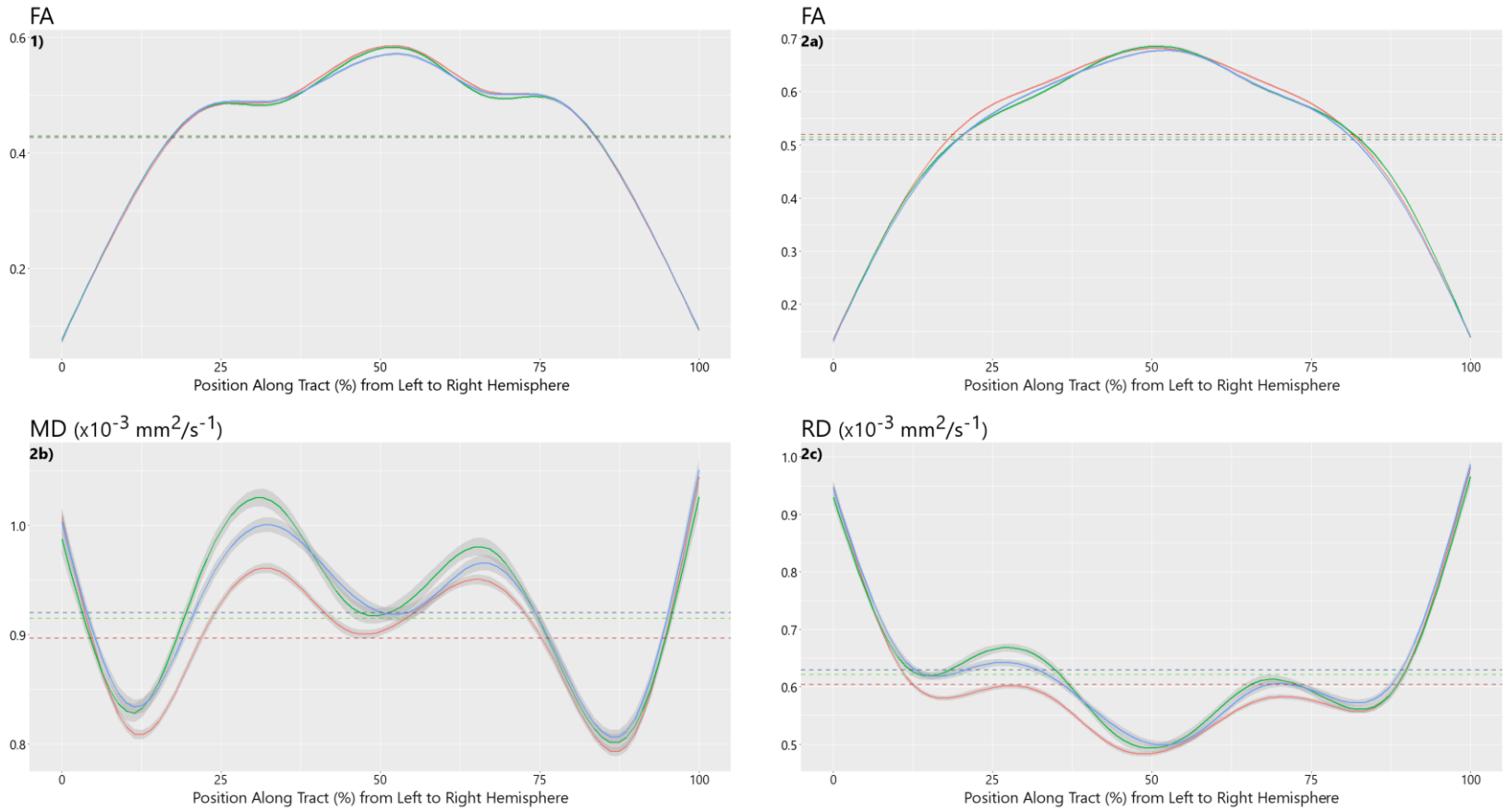

Figure 11. Group-by-position interaction effects along the length of the Corpus Callosum. Plot 1 (*top-left*) represents the FA along the frontal-superior streamlines of the Corpus Callosum. Plot 2 displays the streamlines along the occipital projections of the Corpus Callosum for FA (2a), MD (2b) and RD (2c). Dotted lines represent the average value for the tract. As before, red indicates HC, green is transient PEs, and blue is persistent PEs.

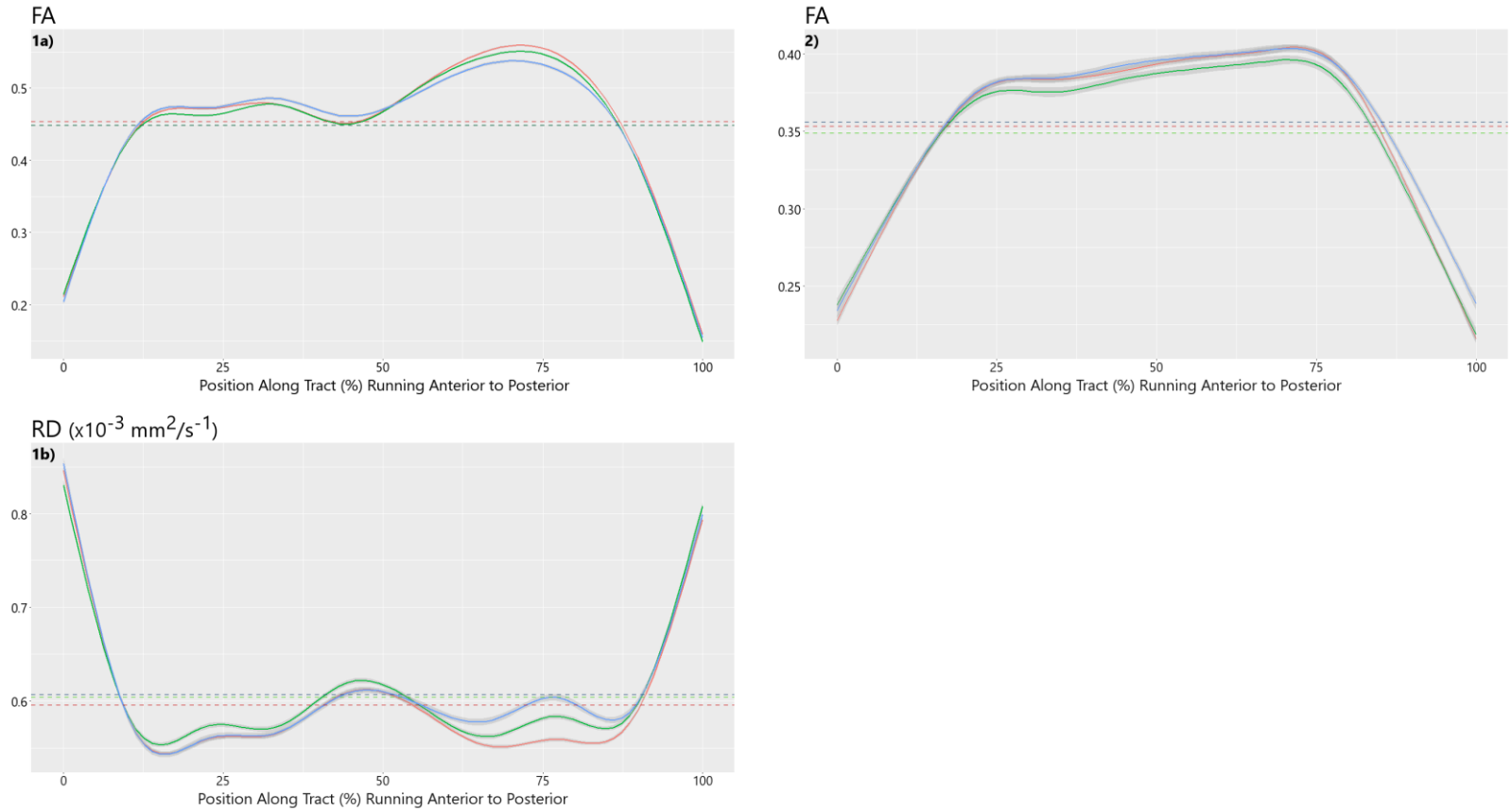

Figure 12. Indices of FA and RD along the length of the left IFOF and left SLF. In the left IFOF (left column), a group-by-interaction effect was present for those with persistent PEs in terms of FA (1a) and RD (1b). In the left SLF (2, right column), there was an interaction effect between group and position in terms of FA for persistent PEs. As before, red indicates HC, green is transient PEs, and blue is persistent PEs.

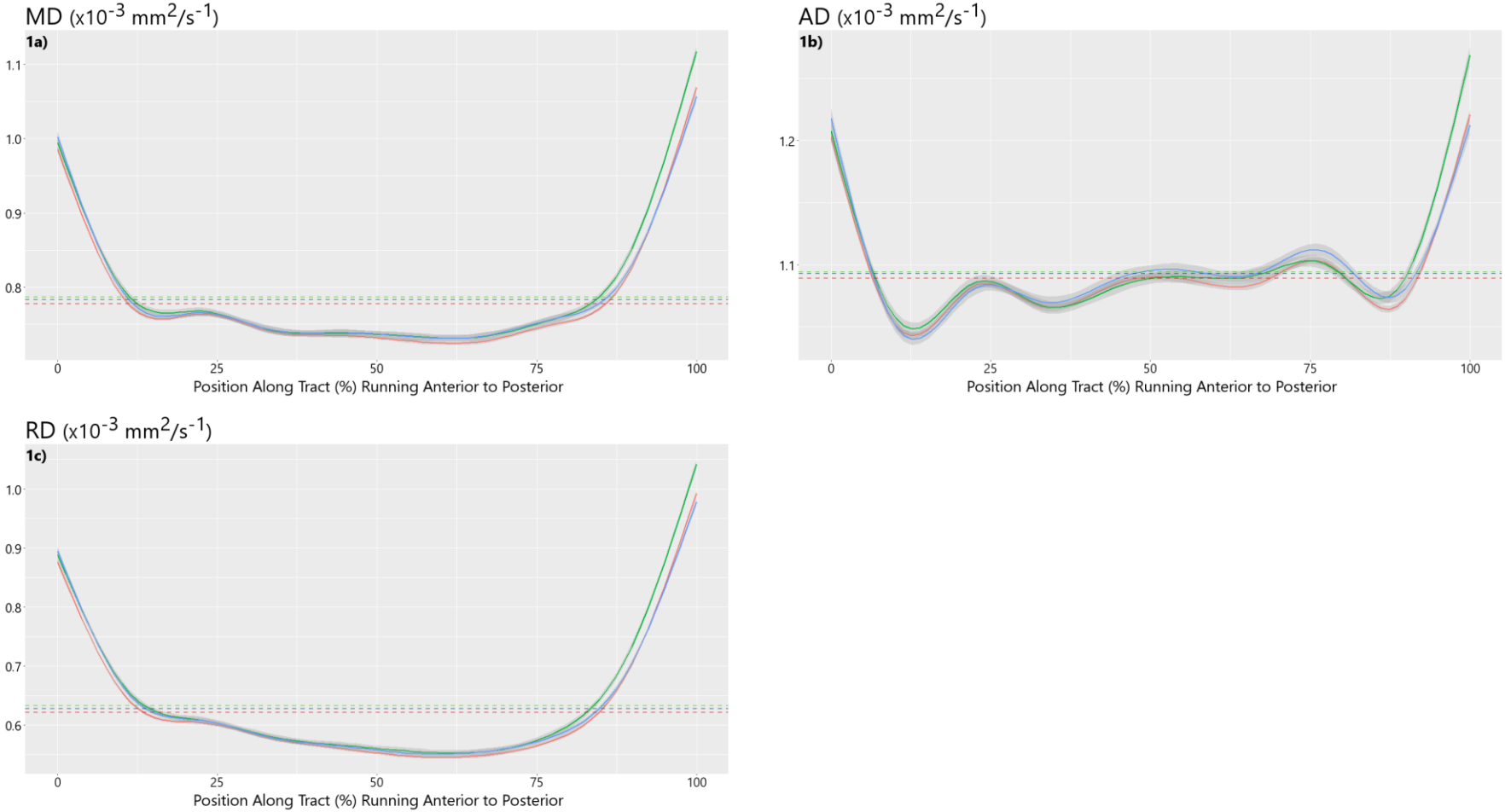

Figure 13. Diffusivity scalars plotted along the right SLF to illustrate the interaction effect of transient PEs (green) and position on MD (1a), AD (1b) and RD (1c).

5.4 Discussion

The aim of this study was to examine the microstructure of the corpus callosum, the superior longitudinal fasciculus, and the inferior fronto-occipital fasciculus. Segmentation of the tracts was carried out using automated shape modelling and diffusion scalars were extracted along an equidistant number of points per tract. We stated that as part of the extended psychosis phenotype, PEs would be associated with reductions in FA and increased RD suggestive of structural dysconnectivity as reported in prodromal and clinical psychosis (Pettersson-Yeo et al., 2011; Peters & Karlsgodt, 2015). We had hypothesised that the anterior projections of the CC would be affected and similarly stated that alterations would be more pronounced in frontal sections of the IFOF. Finally, we expected the SLF to be also associated with dysconnectivity and this would be observable in the anterior part of the tract. Furthermore, we proposed that these effects would be more pronounced in those with persisting PEs.

There was no indication of an effect of PEs on the overall tracts whilst controlling for gender, childhood IQ and total brain volume. This was unexpected, as previous studies of PEs have highlighted differences between groups using voxel-based as well as tractography approaches (Jacobson et al., 2010; O'Hanlon et al., 2015; Drakesmith et al., 2016a). The current sample is older than those in the study by O'Hanlon et al (2015). There are widespread ongoing changes in FA and MD during adolescence that carry on in to early adulthood (Lebel et al., 2008) and PEs could produce different effects depending upon when symptoms manifest during development. Though Drakesmith et al. (2016a) from our group did report on disturbances in frontomedial pathways, it is uncertain which tracts were driving these differences. Accurate tractography relies on optimal placement of Boolean AND gates to differentiate tracts whereas in voxel-based studies the individual brains are mapped to a template and averaged for statistical comparions. It is not uncommon for tractography and voxel-based studies to differ in their findings (for example, see

Peters et al., 2008, 2009) and potential differences in methodological choices and heterogeneity in samples need to be taken into consideration. Furthermore, the presence of voxel-based disturbances could be indicative of differences at specific locations of white matter tracts which would be missed in studies that examine the average tract statistics.

We identified several interactions between PEs and postion along the tract, which indicates deviations in microstructure that are present at points along the tract but are not detected when examining the average pathway. In the corpus callosum (CC), posterior streamlines that project to the occipital lobe were found to differ in transient PEs from HC and visual inspection of the tract highlighted reduced FA alongside increases in MD and RD that showed stronger deviations in the left hemisphere. We found a reduction in FA along the midline of the body of the CC in persistent PEs relative to HC in streamlines that project to the superior portions of the frontal lobe. The CC is frequently implicated in psychosis literature (Pettersson-Yeo et al., 2011; Samartzis et al., 2014; Peters & Karlsgodt, 2015), but the majority of high-risk studies have been limited to abnormalities in anterior sections whereas widespread aberrations are reported in schizophrenia proper (Vijayakumar et al., 2016). The finding of reduced FA alongside increased RD in frontal superior projections of the CC in persistent PEs could be part of a gradual deterioration prior to onset of psychosis. Disturbances in posterior sections of the CC are typically not found in those at high risk for psychosis or in first-episode patients and are thought to develop in relation to duration of illness as well as age of onset (Carpenter et al., 2009; Samartzis et al., 2014). Both the genu and splenium of the CC show rapid, early changes in FA that plateau in late childhood, but changes in MD carry on and show a protracted development in the anterior sections that stabilises during late adolescence (Lebel et al., 2008). In this regard, it seems less likely that the current deviations in FA along the body of the CC are from early developmental disturbances and could reflect a subtle deterioration towards psychosis that is exacerbated with onset of the illness.

We similarly identified deviations along the left IFOF in those with persistent PEs and highlighted reduced FA along with increased RD in more posterior sections of the tract. These findings were limited to the persistent PEs group. The IFOF has been implicated across prodromal and early stages of psychosis (Samartzis et al., 2014; Vijayakumar et al., 2016) and the IFOF has been implicated in children with PEs, but in the opposite direction and in anterior sections (O'Hanlon et al., 2015). The IFOF is assumed to play role in semantic processing (Martino et al., 2010), making it an interesting tract to study in relation to schizophrenia (Kuperberg & Heckers, 2000). However, whilst impairments in cognitive processes have been reported in PEs, it is unknown if semantic processing is affected and the overall cognitive profile of PEs seems to differ from that seen in psychotic disorders (Mollon et al., 2016). Typically, long association tracts such as the IFOF show a slower maturational trajectory and the changes seen here could be interpreted the other way round as a slower age-related increase in FA and decrease in MD (Lebel et al., 2008). However, these findings appear restricted to posterior sections of the IFOF, which involve brain regions that mature prior to more anterior portions of the brain and if this was a mere lag in maturation this would be observable in anterior regions as well. Interestingly, our findings were restricted to the left hemiphere. Longitudinal studies are required to see if these abnormalities are a causal part of a worsening prior to onset of a psychotic illness or if it is simply a slower maturation of white matter tracts.

Differences in diffusivity along the SLF were mostly found in those with transient PEs and highlighted bilateral alterations in diffusivity. In the right SLF there were marked deviations in MD, AD, and RD in the more posterior sections that could be considered the initial and terminal points of streamlines connecting fronto-parietal regions. In the left SLF there was an additional interaction effect implicating alterations in FA in persistent PEs but this was limited to the posterior portions. Imaging studies of the SLF in psychosis have frequently reported changes to connectivity but with mixed results on the direction of the effect and reduced FA is

more consistently reported in those at high risk and chronic schizophrenia (Schmidt et al., 2014a). Changes in the SLF during adolescence coincide with cognitive development and FA has been used as a predictor of cognitive abilities such as working memory (Peters et al., 2012). Higher FA has also been linked to auditory hallucinations in chronic patients (Hubl et al., 2004). It should be noted that a majority of those considered transient PEs were rated as having had hallucinations at age 18 (see chapter 2 under Participants section). However the current findings did not reveal any differences in FA in either hemisphere.

In order to assess the agreement between manual and automated segmentation, we carried out voxel-based comparisons and calculated the precision and recall of the automated method by counting the number of voxels considered false positives, false negatives, and true positives. The numbers highlighted that the agreement between these methods was low to average. This can be interpreted in two different ways. If we consider the manual segmentation by the operater the one true representation of the white matter tracts then the automated method failed to capture the actual tract. However, the automated method is designed to capture the streamline shapes that are present in a tract using a set of training data that was segmented using anatomical locations and subjective judgment when faced with ambiguous or prematurely terminated streamlines. If we then acknowledge the likely imperfection of the data, due to having a single operator, the question becomes how much weight should be placed in the comparison. As illustrated, the automated method is capable of segmenting the majority of the streamlines that make up the distinct tracts from the training data. Therefore unrecovered streamlines most likely deviate significantly from the streamlines that were recovered in either shape or location, suggesting that the automated reconstruction represent an unbiased account of the operators 'style' of segmentation. For instance, streamlines that end prematurely may represent a different shape from the actual tract but may still be included by an operator as long as it falls between the placed Boolean AND gates. In tract-based spatial statistical analysis (TBSS; Smith et al., 2006), voxelwise maps of FA

are thinned to produce a mean skeleton which represents the centres of the tracts that all groups have in common. In essence, the current approach applies the same principle to the data by using the shape and location to find streamlines that are present across groups to segment the tracts. Though our results call for further optimisation of training data and modelling, they should be regarded as reasonably reliable.

In this study we examined the microstructural properties of the corpus callosum, superior longitudinal fasciculus, and inferior fronto-occipital fasciculus in relation to PEs. Our findings highlighted subtle deviations in diffusivity along the CC and IFOF in line with our expected findings of reduced FA alongside increased RD. However, these findings were mostly limited to persistent PEs and these did not overlap with the differences found in transient PEs. In the CC there was evidence of reduced FA, MD, and RD in occipital projections in those with transient PEs and reduced FA in the superior projections along the midline of the body of the CC in persistent PEs. In the left IFOF we found lower FA and increased RD associated with persistent PEs. Transient PEs were found to show reduced diffusivity in the SLF, with bilateral reduced RD, but location of these differences did not match between hemispheres. Our findings are in partial agreement with the psychosis literature which reports widespread disturbances in FA, many of which are present prior to onset of the illness (Samartzis et al., 2014; Peters & Karlsgodt, 2015). We consider the subtle changes in FA and RD along parts of the CC and IFOF associated with the persistence of PEs to be indicative of a degeneration in white matter microstructure that worsens with abnormal persistence of symptoms and is further associated with greater risk of transition. However, further studies are needed to ascertain if there is a progressive worsening with persistence of PEs or if the presented findings highlight dynamic changes that are part of an atypical developmental trajectory that is associated with the manifestation and persistence of PEs.

Chapter 6

Final Discussion

6.1 Summary of Main Findings

The aim of this thesis was to examine the brain in individuals with psychotic experiences (PEs) using multi-modal magnetic resonance imaging. Considered a prodromal state to a frank psychotic disorder we sought to assess disturbances in brain structure, function, and organisation in those with PEs compared to healthy controls. Furthermore, we endeavoured to study the impact of persistence of PEs as well to determine if the elevated risk for psychosis is associated with more marked abnormalities. With this in mind we carried out a multi-modal imaging study that included out assessments using structural MRI, functional MRI and diffusion tensor imaging to a group of 247 individuals who were divided into controls, transient PEs or persistent PEs.

We examined the blood-oxygenation level dependent (BOLD) signal during an n-back task and additionally tested for differences in grey matter volume. Individuals with persistent PEs performed worse than healthy controls on the 0-back up to the 2-back, but there were no differences on the 3-back condition. The fMRI analyses did not reveal significant differences in BOLD signal between those with PEs and controls in any of the conditions of the n-back task. A further test of cognitive load across conditions did not reveal any abnormalities either. A voxel-based morphometry study was subsequently carried out to examine grey matter volume in this sample but there was no indication of differences in grey matter. The network configuration of the involved frontal and parietal regions of the brain during the n-back was examined using dynamic causal modelling. This identified two models that best explained the observed data on the 2-back and 3-back but we found qualitative

differences in the optimal fit of these models relating to our groups. On the 2-back we found that a frontal-to-parietal modulatory network was considered the optimal configuration, but a parietal-to-frontal modulatory network was found to be the second best fit. The likelihood of the best fitting frontal-to-parietal model was found to increase from controls to transient PEs to persistent PEs in a linear fashion whereas the opposite pattern was found in the parietal-to-frontal configuration with likelihoods of both model fits becoming relatively close to even in HC. However, on the 3-back we found clear agreement across groups that demonstrated a parietal-to-frontal configuration was more likely to fit the observed data. Our findings demonstrate poorer performance on the 2-back between groups that coincides with differences in optimal configuration of modulatory connectivity in a frontoparietal network. Interestingly, we found that the additional cognitive load during the 3-back leads to similar performance across groups and with similar modulatory configurations of the frontoparietal network.

Despite a lack of evidence for grey matter volume differences in individuals with PEs, we sought to acquire a deeper understanding of the cortical morphometry of grey matter in PEs. We examined the thickness and gyrification (lGI) of the cortical sheet and examined the relation to overall brain volume as well. There was no indication of abnormalities in cortical thickness, but persistent PEs were associated with reduced lGI in the middle temporal gyrus. More interestingly, when taking brain volume into account, those with persistent PEs were found to deviate from the typical linear increase in lGI with greater brain volume in frontal and occipital areas of the brain. We also incorporated a polygenic risk score for schizophrenia (PGRs) and identified conflicting interactions with the duration of PEs on gyrification. In transient PEs a greater PGRs was associated with reduced lGI in parietal regions but in persistent PEs this pattern was found in the orbitofrontal cortex instead. We sought to test the underlying connectivity of the implicated regions using atlas-based tractography and notably found *increased* fractional anisotropy alongside reduced radial diffusivity in persistent PEs in tracts passing through the orbitofrontal cortex. This was unexpected

as typically reductions in FA are found in schizophrenia and high risk for psychosis studies. Importantly, there was no difference between groups in FA relative to lGI. We also found increased FA in tracts passing through the middle frontal gyrus in relation to transient PEs only, and FA was found to increase with lGI in this group.

We sought to further investigate white matter microstructure in relation to PEs by segmenting the corpus callosum (CC), the inferior fronto-occipital fasciculus (IFOF), and the superior longitudinal fasciculus (SLF). To carry out segmentation on such a large sample we utilised a novel automated segmentation approach. Though the overall accuracy left room for improvement, the method did capture the overall shape of each of the tracts and an along-tract approach was carried out to examine the microstructural qualities along the tract. There was no indication of an effect of PEs on any of the diffusion scalars, but an interaction did highlight deviations in diffusivity along the tract in relation to PEs. Those with transient PEs were found to differ from HC in occipital projection of the splenium and the right SLF along these tracts. There were further deviations in diffusivity along the body of the CC and the left IFOF and SLF in relation to persistence of PEs.

6.2 Integration of Main Findings

Throughout this thesis we have identified alterations in relation to PEs that show varying degrees of spatial overlap across different imaging modalities. Our initial finding of a disturbed relationship between gyrification and brain volume in persistent PEs in the left lateral occipital gyrus gains additional support from our assessment of the left IFOF where we found evidence of microstructural alterations, in posterior portions of the tract (see figure 14). These findings highlight an aberration in relation to occipital or fronto-occipital circuitry in relation to the persistence of PEs. Within the IFOF there is branching to the frontal pole, superior and middle frontal gyri, and the orbitofrontal cortex (Sarubbo et al., 2013; Wu et al.,

2016). In the right middle frontal gyrus we had found a similar disturbance in gyrification, but no evidence of abnormalities in occipital regions or in the right IFOF. There was an interesting effect of reduced gyrification in the left medial orbitofrontal gyrus in those with persistent PEs with increasing polygenic risk for schizophrenia. Taken together this further suggests that there is evidence that disruptions are present in fronto-occipital rather than just occipital circuitry in relation to persistence of PEs. The role of high genetic risk for schizophrenia demands further research.

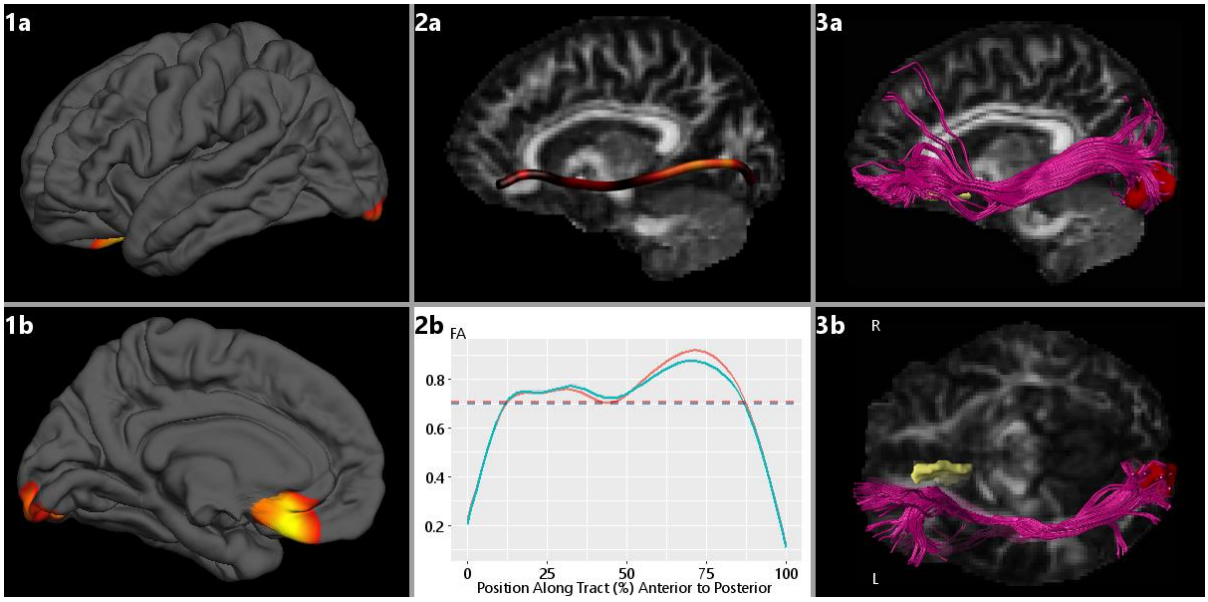

Figure 14. A summary of the disturbances found in fronto-occipital circuitry in those with persistent PEs. 1a-b: Sagittal (lateral and medial) view of disturbances in gyrification in occipital and orbitofrontal clusters. 2a: Visualisation of the magnitude of differences in fractional anisotropy (FA) between groups along the tract expressed using a 'normalised' t-statistic.[13] 2b: FA along the tract for persistent PEs (blue) and HC (red). 3a-b: Sagittal and axial overlay of the IFOF (purple) with the occipital (red) and orbitofrontal (yellow) clusters.

[13] Essentially we transformed the t-statistics for each point along the tract to a range of 0-1 in order to visualise the scores in ExploreDTI. By taking the maximum and minimum values of each t-statistic we were able to transform the scores using the following equation: $t_i = \frac{t_i - t_{min}}{t_{max} - t_{min}}$

As mentioned, the right caudal and rostral middle frontal gyrus was found to show an atypical relation between gyrification and brain volume. Though we found no evidence of disturbances in the right IFOF, we did identify reduced FA in the body of the CC. Along the anterior midline of the CC, the FA values have been suggested to closely correspond to the fibre composition (Hofer & Frahm, 2006) and reductions in FA could indicate poorer alignment or reduced density of callosal fibres (Paul, 2011). This is further reflected in the fact that reduced FA has been associated with greater hemispheric dominance (Putnam et al., 2008). Regional variations in cortical folding in the right frontal lobe could be the result of focal disturbances in fibre composition, thought to modulate the size and shape of gyri and sulci (Zilles et al., 2013).

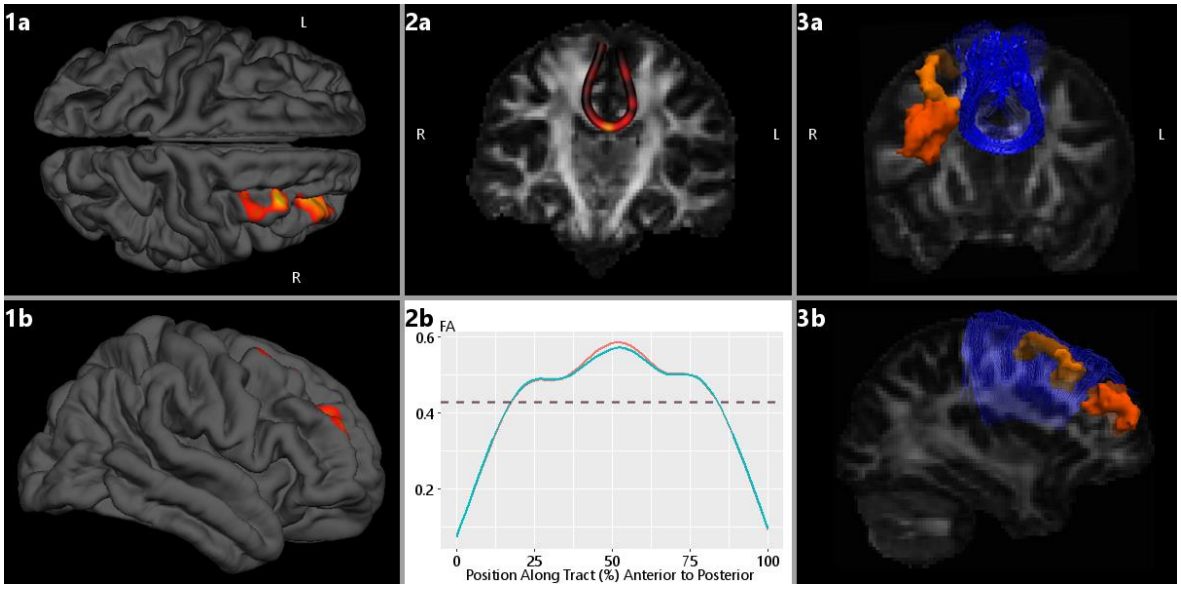

Figure 15. A summary of our findings in middle and superior frontal regions that were differed in persistent PEs. 1a-b: Axial and sagittal (lateral) view of differences in gyrification in the caudal and rostral middle frontal gyrus. 2a: Visualisation of differences between HC and persistent PEs across the frontal superior projections of the body of the CC. 2b: The FA along the tract for HC (red) and persistent PEs (blue) highlighting the differences along the midline. 3a-b: A coronal and sagittal view of our findings regarding the CC (blue) and middle frontal gyrus (orange).

However, the superior projections of the body of the CC did not appear to demonstrate a clear spatial overlap with the middle frontal aberrations in gyrification. These are collated in figure 15 to illustrate the lack of spatial agreement between findings. However, we cannot exclude possible subtle variations in cortico-cortical microstructure that link poorer interhemispheric connectivity of homologous superior frontal regions and reduced cortical folding in the middle frontal gyrus.

Though most of our findings highlight alterations in imaging-derived metrics in those with persisting PEs, there was evidence of complex effects in those with transient PEs in the parietal lobule and fronto-parietal connectivity. More specifically, we found deviations in diffusivity in the terminal sections of the right SLF in those with transient PEs but an interaction effect of reduced gyrification in the left inferior parietal lobule in those with transient PEs and a higher polygenic risk for schizophrenia. This might highlight a disturbance in fronto-parietal circuitry in relation to PEs as those with persistent PEs showed reduced FA in the left, rather than the right, SLF. Our initial assessment of fronto-parietal network configuration highlighted a greater reliance on frontal areas in those with PEs that increased with duration of PEs and fronto-parietal aberrations have frequently been implicated in psychosis (Schmidt et al., 2014a). However, disturbances in gyrification were solely present in those with transient PEs in the left hemisphere whereas white matter alterations were found in the right SLF with was no indication of accompanying alterations in cortical grey matter in the right hemisphere. It is therefore unlikely that these findings represent a disruption of fronto-parietal circuitry in relation to PEs as there is no strong converging evidence across PEs.

There are methodological considerations that need to be taken into account when interpreting the results for transient PEs. First, it is uncertain how polygenic risk for schizophrenia affects our findings. In terms of grey matter we had found conflicting results and it is uncertain if the effect should be attributed to PEs or to genetic risk. Second, our findings on the SLF seem to be isolated to the initial and terminal points

of the streamlines which show the highest degree of variance and it is important to take this into account. Third, we did not assess the role of a high genetic loading for schizophrenia on white matter tracts due the confusing interplay with PEs on grey matter macrostructure.

6.3 Implications for Psychosis

Psychotic experiences are considered part of an extended phenotype of psychosis that is expressed below clinical relevance (van Os et al., 2000). The presence of PEs is considered to be a risk factor for development of a psychotic disorder and, though typically transient in nature, abnormal persistence of PEs is associated with a further elevated risk of transitioning (Kaymaz et al., 2012). So far, imaging studies of PEs have been limited but have found some overlap with schizophrenia (DeRosse et al., 2014; Orr et al., 2014; Pelletier-Baldelli et al., 2014; Drakesmith et al., 2015, 2016a, 2016b). Typically, there are progressive changes from the high risk prodrome to first-episode and finally chronic schizophrenia in the brain. Studies of grey matter have found volume reductions during the prodromal phase predominantly in frontal, temporal, and cingulate regions that are greater in those who end up transitioning (Fusar-Poli et al., 2011a; Smieskova et al., 2012b; Bois et al., 2015). In schizophrenia, an accelerated loss of volume over time is observed that does not affect the whole brain uniformly but instead shows greater reductions in the temporal lobe and this is already present in first-episode patients (Vita et al., 2012). Progressive changes are also associated with reductions in cortical folding of the frontal lobe (White & Gottesman, 2012) and abnormalities seem to be present prior to onset (Harris et al., 2004, 2007; Stanfield et al., 2008). Functional imaging studies have highlighted aberrant functional activation predominantly in the prefrontal cortex but also implicate cingulate and parietal regions (Fusar-Poli et al., 2007; Fusar-Poli, 2012; Dutt et al., 2015), but studies of functional connectivity have linked these to alterations in

functional network coupling with parietal, temporal, and striatal regions (Shim et al., 2010; Allen et al., 2010; Dandash et al., 2014). Findings of dysconnectivity are consistent across the course of schizophrenia, albeit to varying degrees, and appear to become more widespread over time with transition (Pettersson-Yeo et al., 2011). Abnormalities in functional connectivity imply disturbances in white matter connectivity which have been found across the course of schizophrenia starting during the prodromal phase and worsening with the onset of psychosis (Pettersson-Yeo et al., 2011; Wheeler & Voineskos, 2014). The most prominent findings relate to frontal, fronto-temporal and fronto-limbic connections, that include the superior longitudinal fasciculus, the cingulum, and the uncinate fasciculus, and suggest that schizophrenia arises along with disturbances in structural connectivity in these pathways (Samartzis et al., 2014).

In the current study, we did not find any evidence of reductions in grey matter volume, but the degree of cortical folding was lower in those with persistent PEs compared to those typical controls, in the temporal lobe. In relation to brain volume, gyrification was further found to be reduced in those with persisting PEs in middle frontal and lateral occipital gyri. Furthermore, there was evidence of microstructural aberrations along the left posterior portion of the IFOF and frontal-superior projections of the body of the CC in persistent PEs which seems to implicate disturbances in frontal and fronto-occipital connectivity. These findings seem consistent with the notion of localised disturbances that implicate frontal brain regions prior to a psychotic disorder (Pantelis et al., 2009; Samartzis et al., 2014), but do not appear to occur as a result of the manifestation of PEs. In transient PEs, we were unable to find similar effects both in terms of cortical morphometry and white matter microstructure. As such the current findings do not provide compelling evidence for a similar neuroimaging profile in PEs overall to that found in high risk and schizophrenia. Having said that, these findings do highlight a profile in persistence of PEs and the subtle changes in micro- and macrostructure found could be a reflection of the notion of a dose-response relationship between the duration of

PEs and the risk of developing a psychotic disorder (Kaymaz et al., 2012). It is important for further studies to establish if these aberrations become exacerbated in transition to full-blown psychosis.

6.4 Evidence of Neurodevelopmental Deviations

Though the prevalence of PEs is greater than that of psychotic disorders, the manifestation of PEs is still an uncommon occurrence and should be considered an expression of an atypical developmental trajectory (van Os et al., 2009). The manifestation of PEs most frequently occurs during adolescence; a period of complex cortical reorganisation. In recent years, extensive longitudinal studies have been carried out to characterise the typical progression of brain maturation. Several key studies allow for an insight into the potential underlying developmental processes that could be affected in those with PEs looking at the findings presented in this thesis. First, it is important to note that on a global scale cortical grey matter volume reaches its peak during childhood and continues to decline for the next few decades whereas cerebral white matter volume increases from late childhood and stabilises during late adolescence (Mills et al., 2016). However, different age-related changes in grey matter volume occur in different regions and association cortices are slower to mature (Gogtay et al., 2004; Lenroot & Giedd, 2006). Indices of cortical morphometry show more uniform reductions in surface area but differentiate in the rate of changes in cortical thickness and gyrification (Hogstrom et al., 2013). Notably, increases in surface area are associated with cortical thinning and increased gyrification. In white matter, FA has further been found to increase with age throughout childhood in to adulthood whereas MD slowly decreases though these trajectories do not occur in unison as changes in MD typically occur later than increases in FA (Lebel et al., 2008). During late childhood the value of FA in the CC is mostly stabilised, but both the IFOF and SLF show a protracted rate of plateauing that ends during middle to late

adolescence. In terms of MD, a different pattern is present and the IFOF stabilises during early adolescence whereas in the SLF this process takes another decade of gradual decrease. The genu of the CC takes longer to plateau than the splenium by a few years and does not plateau until late instead of middle adolescence.

The complex interplay between grey and white matter development is still poorly understood, but the relative changes in cortical grey matter appear to follow different trajectories in terms of timing, magnitude and location from late childhood to early adulthood (Tamnes et al., 2010). Furthermore, the thinning and stretching of the cortical surface during adolescence appears to occur relatively independent from the changes in white matter volume and architecture (Tamnes et al., 2010; Hogstrom et al., 2013). Though the relationship of cortical thinning and surface expansion with increasing cortical complexity has been demonstrated (Hogstrom et al., 2013), the degree of cortical folding of grey matter is believed to be driven by the folding of cortical white matter which is bound by the connectivity-related tension within the white matter (Herculano-Houzel et al., 2010). This is also reflected in the observation that both myelination and gyrification advances posterior to anterior and higher-order cortical areas show a further protracted trajectory of maturation (Lebel et al., 2008; Tau & Peterson, 2010; White et al., 2010). The directionality of these changes is further reflected in the refinements in higher-order cognitive abilities and the recruitment of increasingly fine-tuned functional cortical networks (Casey et al., 2005; Luna et al., 2010).

In this thesis, we highlighted abnormalities in the macrostructure of frontal, temporal, and occipital grey matter and underlying microstructure as well as in-depth assessments along specific white matter tracts that connect fronto-parietal (SLF) and occipito-frontal (IFOF) regions as well as interhemispheric homologous structures (CC). There was evidence of coinciding abnormalities in grey and white matter in orbitofrontal and middle frontal gyri but this captured several prominent white matter structures and did not demonstrate the expected positive association

between lGI and FA. Assessments of specific tracts highlighted convincing deviations in diffusivity in occipital and frontal-superior projections of the CC, the left IFOF and bilateral SLF, and these effects overlapped in relation to the duration of PEs. Importantly, alterations in microstructure in persistent PEs relative to controls seemed to lie along posterior sections of the IFOF and SLF and only along frontal projections of the CC. If we consider PEs part of an atypical neurodevelopmental trajectory, do we find evidence of developmental deviations in the findings presented in this thesis? Disturbances in gyrification were present across regions with differing trajectories of maturation which would suggest that such alterations do not occur late in brain development. Furthermore, the occipital and middle frontal regions were found to demonstrate an abnormal relationship between brain volume and gyrification for which we provide two possible explanations. First, it is possible that gyrification in early life plateaued sooner than expected but brain volume increased in a typical fashion. On the other hand, it is also possible that during adolescence there are more pronounced changes in neuronal connectivity, presumably as a result of synaptic pruning, and a greater release of axonal tension leads to wider sulci and narrower gyri and hence a reduced gyrification index. Across imaging modalities we found evidence of abnormalities in frontal and occipital regions, but these did not match in terms of duration of PEs. In transient PEs we found alterations in pathways of the CC that project to the occipital lobe. The left IFOF was implicated in persistent PEs and the alterations were found in more posterior sections of the tract spatially overlapping with occipital abnormalities in gyrification. The reductions in FA along with increased RD in frontal projections of the body of the CC further seem to spatially match the disturbances in gyrification in the right middle frontal gyrus. The CC has been found to show maturation faster and at an earlier stage than most major white matter tracts and it is possible that these findings demonstrate an asymmetric disturbance in the CC that drives the abnormalities in cortical folding in the middle frontal gyrus. It should be noted that the deviations in the middle frontal gyri, particularly in caudal regions, extend beyond the projections of the body of the

CC and the callosal differences are present along the midline rather than in projections to the right hemisphere.

Unfortunately we did not examine the structural connectivity of fronto-temporal pathways and it is uncertain if the disturbances in gyrification are further related to abnormalities in white matter. We had identified subtle impairments in working memory and the connectivity of the underlying frontoparietal network during the task suggested a lag in maturation in relation to the duration of PEs. Though the microstructural qualities of the SLF were found to statistically differ from controls, findings were conflicting and mostly limited to the initial and terminal points of streamlines (which are subject to measurement error) rather than originating prior to that. As such we do not consider these to be convincing or part of a maturational lag in the development of working memory function. While functional and structural connectivity are intrinsically linked they do not reflect the same process and differences in configuration do not necessarily rely on different architecture of the white matter pathways. It is important to mention that neurodevelopment is an active ongoing area of research and at present our understanding of the dynamic interchanges that occur are not well understood. It is clear that PEs are associated with disturbances in macro- and microstructure of cortical grey matter and white matter, relative to healthy controls, but the underlying mechanism is not yet clear.

6.5 Limitations

There are some major limitations to the work presented in this doctoral thesis that are important when considering the implications of our findings. First, throughout this thesis we have discussed PEs as part of an atypical developmental trajectory and as a prodrome to psychosis as part of the extended psychosis phenotype (van Os et al., 2009). However despite the proposal of a continuum along which psychotic symptoms can be expressed, in practice this still means setting a threshold above

which we define a phenomenon as a *'psychotic experience'*. This obviously has implications for the assumption that PEs are associated with a subsequent psychotic disorder. Prior assessment at age 12 did not provide strong predictive value towards a psychotic disorder at age 18 (Zammit et al., 2013b) and it is uncertain if the presence of PEs at age 18 or age 20 is more strongly related to a later psychotic disorder. It should be noted that assessment by semi-structured interview does provide a more thorough evaluation and leads to more conservative ratings than those assessed using self-report measures (Horwood et al., 2008).

The reported PEs in our sample typically did not reside in a single domain but instead were mostly a combination of symptoms in the hallucinations domain with either thought interferences, delusions, or both of these domains. As such it was not possible to further examine specific PEs in relation to the imaging data. Hallucinations and delusions have been known to show strong associations (Johns & van Os, 2001), but more research is needed to gauge if PEs typically cluster across domains.

A principal assumption throughout this thesis is that those with persisting PEs would demonstrate more profound differences than those with transient PEs and of course, healthy controls without PEs. The presence of PEs was assessed when participants were around 18 years old and again 2 years later when they were 20 years old and underwent MRI scanning. Though Kaymaz et al. (2012) highlighted an increased risk of transition to a psychotic disorder in those with PEs, the dose-response relationship with persistence was based on longitudinal assessments that ranged from 3 up to 24 years. There is no clearly defined duration of symptoms that distinguish transient from persisting PEs and our labelling of persistence as *'the presence of symptoms at two independently rated assessments that were two years apart'* might have been presumptuous. Though we found evidence of abnormalities associated with the persistence of PEs, it is possible that the assumption of greater differences in those

with persistence caused us to miss overlapping variances in relation to PEs regardless of duration.

We mentioned the occurrence of non-psychotic disorders in individuals with PEs (Kelleher et al., 2012b), but the presence of other psychiatric conditions was not further investigated in this thesis. Previous studies from our group did identify general psychopathology, measured using the Clinical Interview Schedule-Revised (CIS-R; Lewis et al. 1992), as a potential confounding factor on findings regarding cortical myelination and diffusivity (Drakesmith et al., 2016a, 2016b). It is believed that the pattern of comorbidity in PEs resembles the psychopathological associations that are present in schizophrenia (Buckley et al., 2009) and as such we cannot exclude the possibility that general psychopathology confounds our findings in the same way a comorbid psychiatric disorder might confound imaging findings in schizophrenia.

We have discussed all our findings in terms of their relation to the psychosis literature as well as what is known about typical neurodevelopment. However, the cross-sectional nature of the imaging data means that much of our interpretation remains speculative and requires validation using a longitudinal design. Imaging studies of PEs are becoming more frequent and the work presented here highlights the need for repeated measurements in order to establish the direction of these changes along developmental trajectories. Throughout this thesis we have predominantly made use of linear modelling to examine the effect and interaction effects of PEs in relation to imaging measures. The use of linear modelling allows for an unambiguous fit of the imaging data in relation to the effects of PEs, but our approach may have overlooked non-linear relationships in our data. It is possible that the distinctive findings in grey and white matter are in part due to the different approaches in statistical modelling.

6.6 Future Directions

6.6.1 MRI study design considerations

Since PEs are generally considered a risk factor for psychosis and that the risk increases with persisting symptoms, longitudinal studies of PEs are obviously vital. Both the onset and duration of PEs are likely to impact neurodevelopment and continued assessments of PEs and re-imaging of the brain could help understand the disturbances associated with PEs. Furthermore, the assessment of PEs in ongoing longitudinal imaging studies would greatly benefit our understanding of the developmental deviations that occur prior to the manifestation of symptoms. Furthermore, just as it is unclear what causes the persistence of PEs we know very little about what causes PEs to be transient as well. Though it has been reported that symptoms typically dissipate over time, it is not clear if there is a 'normalisation' of aberrations that coincide with PEs or if there are lingering disturbances after symptoms have dissipated that can still be observed using MRI.

There have been no imaging studies to date that have assessed PEs in non-clinical, non-help seeking young people, in relation to high risk for psychosis, first-episode patients and chronic schizophrenia to assess the presence of gradual changes through the prodromal state and towards a psychotic disorder.

As is illustrated throughout this thesis, interpretations can differ when considering the findings across rather than within modalities and multi-modal imaging should be the recommended approach for further studies. Not all of our findings could be encompassed into a single, consistent explanatory framework hence future work should focus on assessing the relation between cortical grey matter and white matter using voxel-based approaches prior to examining specific white matter tracts. In fact, a multi-modal approach that additionally incorporates more recent myelin-specific markers, using for instance multicomponent relaxometry or quantitative

susceptibility mapping (Deoni et al., 2011; Liu et al., 2015), to allow for more meaningful inferences on myelination.

6.6.2 Unravelling genetic factors

In chapter 4 we introduced a polygenic risk score for schizophrenia (PGRs) to assess the impact of high genetic risk for schizophrenia in relation to PEs. However, there were non-specific interactions with PEs and the PGRs rather than additive effects of the PGRs on duration of PEs. The use of PGRs in imaging studies has been fairly recent and has been used across different samples in relation to schizophrenia (Terwisscha van Scheltinga et al., 2013; Walton et al., 2014; French et al., 2015; Kauppi et al., 2015; Harrisberger et al., 2016; Lancaster et al., 2016; Liu et al., 2016). It is important to establish the effect of high genetic risk both in the general population as well as in specific at-risk samples and those with a psychotic disorder. Further work taking advantage of refinements in the PGRs will perhaps lead to more definite findings in this area.

6.6.3 Mass-univariate vs. multivariate approaches

The work presented in this thesis utilised a mass-univariate approach by fitting a general linear model at each voxel to test for effects of transient and persistent PEs and to take into account potential confounding effects of brain volume, gender, handedness, and childhood IQ. This approach allowed us to make inferences about the impact of PEs at the group level in each voxel, adding to the body of knowledge that has focused on identifying focal alterations associated with psychosis. Thus, we were able to evaluate the spatial overlap of findings as well as consider similarities in the direction of estimated effects with regards to those reported in the psychosis literature.

Though this approach provides a flexible framework for many different tests and models, it fails to take full advantage of the richness of information available by treating the brain as a large number of independent data points rather than as a

complex structure. Furthermore, it does not allow us to make predictions about future individual cases. Whereas the general linear model seeks to *explain* the variance in each voxel as a linear combination of a series of predictor variables, in a multivariate analogue the goal is often to *predict* a class or outcome given the data. More specifically, a classifier can be trained on a dataset of examples to model the relationship between each outcome and a set of features. The label could be transient or persistent PEs and features could be each voxel or, more often, some derived quantiles. A trained classifier can then be applied to novel observations to assess whether the features truly contain information that can be used to determine the label. This approach has been applied in imaging studies with moderate success in classifying schizophrenia (Kambeitz et al., 2015) and is showing promise in predicting psychosis onset (Gifford et al., 2017), but classification of psychotic experiences has received little attention (Modinos et al., 2012).

As mentioned in chapter 1, one of the principal aims of studying prodromal states for psychosis is to not only identify individuals considered at risk but to prevent the development of a psychotic disorder by targeting those likely to transition for early intervention treatments. Though most individuals with PEs are unlikely to transition (Zammit et al., 2013b), the risk increases with persistence of symptoms (Kaymaz et al., 2012) and it would be of great interest to test the feasibility of predicting persistence of PEs using imaging data. However, even in the event that it is possible to train a statistical model that can make accurate predictions we would still want to obtain some estimate of the underlying mechanisms. Throughout adolescence to adulthood there are continuing complex changes occurring in brain structure and functional organisation (Luna et al., 2010; Tamnes et al., 2010; Mills et al., 2016), and as highlighted it is important to ascertain whether alterations reflect a lag in typical developmental trajectories or an accelerated degeneration towards psychosis. Naturally either effect could produce a pattern distinctive from typically developing peers. On the other hand, whilst an explanatory mass-univariate approach allows for ease of interpretation of observed differences, a predictive multivariate approach

would likely identify a far more accurate pattern of differences that best distinguish individuals with PEs from their peers.

It is clear that both methods have their own strengths but provide answers to different questions and the correct approach will always depend on the research questions being asked. Due to the novelty of the study of PEs we chose to build upon previous research that has sought to produce biomarkers for psychosis but while we continue to improve our understanding of the brain abnormalities that occur in psychosis, we are no closer to producing a clinically useful biomarker (Fusar-Poli & Meyer-Lindenberg, 2016). Incorporating machine learning techniques will most likely improve current explanatory frameworks of psychosis and, more importantly, help us ascertain the role of imaging research as a prognostic tool in our pursuit of predictive models for psychosis.

6.7 Conclusion

Using multi-modal imaging we were able to identify subtle changes in a population-based sample of young people with PEs in relation to brain structure and connectivity. Structural findings were mostly restricted to those with persisting PEs but underlying connectivity identified distinct disturbances in transient and persistent PEs respectively. There was a decent overlap of findings between imaging modalities in frontal and fronto-occipital circuitry in relation to the persistence of PEs but transient PEs were found to have some sporadic effects. The imaging profile of PEs overall did not match that of psychosis but the persistence of PEs was found to demonstrate subtle differences that were similar to those found in clinical high risk and psychosis populations. It is possible that the white matter disturbances play a causal role in the further abnormalities in cortical complexity but it is uncertain if these reflect developmental disturbances or are part of a degenerative process towards psychosis. Importantly, it is not the manifestation of PEs, but the abnormal

persistence of symptoms that seems to be associated with disturbances in cortical folding and structural connectivity that highlights frontal and fronto-occipital circuitry.

References

Allen, P., Luigjes, J., Howes, O.D., Egerton, A., Hirao, K., Valli, I., Kambeitz, J., Fusar-Poli, P., Broome, M. & McGuire, P. (2012). Transition to psychosis associated with prefrontal and subcortical dysfunction in ultra high-risk individuals. *Schizophrenia Bulletin*. 38 (6). p.pp. 1268–1276.

Allen, P., Stephan, K.E., Mechelli, A., Day, F., Ward, N., Dalton, J., Williams, S.C. & McGuire, P. (2010). Cingulate activity and fronto-temporal connectivity in people with prodromal signs of psychosis. *NeuroImage*. 49 (1). p.pp. 947–955.

Armstrong, E., Schleicher, A., Omran, H., Curtis, M. & Zilles, K. (1995). The ontogeny of human gyrification. *Cerebral Cortex*. 5 (1). p.pp. 56–63.

Ashburner, J. (2007). A fast diffeomorphic image registration algorithm. *NeuroImage*. 38 (1). p.pp. 95–113.

Ashtari, M., Cottone, J., Ardekani, B. a, Cervellione, K., Szeszko, P.R., Wu, J., Chen, S. & Kumra, S. (2007). Disruption of white matter integrity in the inferior longitudinal fasciculus in adolescents with schizophrenia as revealed by fiber tractography. *Archives of General Psychiatry*. 64 (11). p.pp. 1270–1280.

Bak, M., Myin-Germeys, I., Delespaul, P., Vollebergh, W., De Graaf, R. & Van Os, J. (2005). Do different psychotic experiences differentially predict need for care in the general population? *Comprehensive Psychiatry*. 46 (3). p.pp. 192–199.

Barnett, J.H., McDougall, F., Xu, M.K., Croudace, T.J., Richards, M. & Jones, P.B. (2012). Childhood cognitive function and adult psychopathology: associations with psychotic and non-psychotic symptoms in the general population. *British Journal of Psychiatry*. 201 (2). p.pp. 124–130.

Bates, D.M., Pinheiro, J.C. & Bates, D.M. (1998). Linear and nonlinear mixed-effects models. *Annual Conference on Applied Statistics in Agriculture*. p.pp. 0–21.

Beddington, J., Cooper, C.L., Field, J., Goswami, U., Huppert, F. a, Jenkins, R., Jones, H.S., Kirkwood, T.B.L., Sahakian, B.J. & Thomas, S.M. (2008). The mental wealth of nations. *Nature*. 455 (7216). p.pp. 1057–1060.

Benetti, S., Mechelli, A., Picchioni, M., Broome, M., Williams, S. & McGuire, P. (2009). Functional integration between the posterior hippocampus and prefrontal cortex is impaired in both first episode schizophrenia and the at risk mental state. *Brain*. 132 (9). p.pp. 2426–2436.

Blakemore, S.J. (2008). The social brain in adolescence. *Nature Reviews Neuroscience*. 9 (4). p.pp. 267–277.

Blanton, R.E., Levitt, J.G., Thompson, P.M., Narr, K.L., Capetillo-Cunliffe, L., Nobel, A., Singerman, J.D., McCracken, J.T. & Toga, A.W. (2001). Mapping cortical asymmetry and complexity patterns in normal children. *Psychiatry Research: Neuroimaging*. 107 (1). p.pp. 29–43.

Bois, C., Whalley, H., McIntosh, A. & Lawrie, S. (2015). Structural magnetic resonance imaging markers of susceptibility and transition to schizophrenia: A review of familial and clinical high risk population studies. *Journal of Psychopharmacology*. 29 (2). p.pp. 144–154.

Bora, E. & Murray, R.M. (2014). Meta-analysis of cognitive deficits in ultra-high risk to psychosis and first-episode psychosis: Do the cognitive deficits progress over, or after, the onset of psychosis? *Schizophrenia Bulletin*. 40 (4). p.pp. 744–755.

Breitborde, N.J.K., Srihari, V.H. & Woods, S.W. (2009). Review of the operational definition for first-episode psychosis. *Early Intervention in Psychiatry*. 3 (4) p.pp. 259–265.

Buck, S.F. (1960). A method of estimation of missing values in multivariate data suitable for use with an electronic computer. *Journal of the Royal Statistical Society Series B-Statistical Methodology*. 22 (2). p.pp. 302–306.

Buckley, P.F., Miller, B.J., Lehrer, D.S. & Castle, D.J. (2009). Psychiatric comorbidities and schizophrenia. *Schizophrenia Bulletin*. 35 (2). p.pp. 383–402.

Bullmore, E.T., Frangou, S. & Murray, R.M. (1997). The dysplastic net hypothesis: An integration of developmental and dysconnectivity theories of schizophrenia. *Schizophrenia Research*. 28 (2). p.pp. 143–156.

Cachia, A., Paillère-Martinot, M.L., Galinowski, A., Januel, D., de Beaurepaire, R., Bellivier, F., Artiges, E., Andoh, J., Bartrés-Faz, D., Duchesnay, E., Rivière, D., Plaze, M., Mangin, J.F. & Martinot, J.L. (2008). Cortical folding abnormalities in schizophrenia patients with resistant auditory hallucinations. *NeuroImage*. 39 (3). p.pp. 927–935.

Cannon, T.D., Chung, Y., He, G., Sun, D., Jacobson, A., van Erp, T.G.M., McEwen, S., Addington, J., Bearden, C.E., Cadenhead, K., Cornblatt, B., Mathalon, D.H., McGlashan, T., Perkins, D., Jeffries, C., Seidman, L.J., Tsuang, M., Walker, E., Woods, S.W. & Heinssen, R. (2015). Progressive Reduction in Cortical Thickness as Psychosis Develops: A Multisite Longitudinal Neuroimaging Study of Youth at Elevated Clinical Risk. *Biological Psychiatry*. 77 (2). p.pp. 147–157.

Canu, E., Agosta, F. & Filippi, M. (2014). A selective review of structural connectivity abnormalities of schizophrenic patients at different stages of the disease. *Schizophrenia Research*. 161 (1). p.pp. 19–28.

Carpenter, D.M., Tang, C.Y., Friedman, J.I., Hof, P.R., Stewart, D., Buchsbaum, M., Harvey, P.D., Gorman, J. & Davis, K.L. (2009). Temporal Characteristics of Tract-Specific Anisotropy Abnormalities in Schizophrenia. *Neuroreport*. 19 (14). p.pp. 1369–1372.

Casey, B.J., Tottenham, N., Liston, C. & Durston, S. (2005). Imaging the developing brain: What have we learned about cognitive development? *Trends in Cognitive Sciences*. 9 (3). p.pp. 104–110.

Chan, R.C.K., Di, X., McAlonan, G.M. & Gong, Q.Y. (2011). Brain anatomical abnormalities in high-risk individuals, first-episode, and chronic schizophrenia: An activation likelihood estimation meta-analysis of illness progression. *Schizophrenia Bulletin*. 37 (1). p.pp. 177–188.

Chipman, J.S. (2011). Gauss-Markov Theorem. *International Encyclopedia of Statistical Science*. p.pp. 577–582.

Chung, Y., Jacobson, A., He, G., van Erp, T.G., McEwen, S., Addington, J., Bearden, C.E., Cadenhead, K., Cornblatt, B., Mathalon, D.H., McGlashan, T., Perkins, D., Seidman, L.J., Tsuang, M., Walker, E., Woods, S.W., Heinssen, R. & Cannon, T.D. (2015). Prodromal Symptom Severity Predicts Accelerated Gray Matter Reduction and Third Ventricle Expansion Among Clinically High Risk Youth Developing Psychotic Disorders. *Molecular Neuropsychiatry*. 1 (1). p.pp. 13–22.

Colby, J.B., Soderberg, L., Lebel, C., Dinov, I.D., Thompson, P.M. & Sowell, E.R. (2012). Along-tract statistics allow for enhanced tractography analysis. *NeuroImage*. 59 (4). p.pp. 3227–3242.

Conklin, H.M., Luciana, M., Hooper, C.J. & Yarger, R.S. (2007). Working memory performance in typically developing children and adolescents: behavioral evidence of protracted frontal lobe development. *Developmental Neuropsychology*. 31 (1). p.pp. 103–128.

Córdova-Palomera, A., Alemany, S., Falcón, C., Bargalló, N., Goldberg, X., Crespo-Facorro, B., Nenadic, I. & Fañanás, L. (2014). Cortical thickness correlates of psychotic experiences: Examining the effect of season of birth using a genetically informative design. *Journal of Psychiatric Research*. 56 (1). p.pp. 144–149.

Corlett, P.R. & Fletcher, P.C. (2012). The neurobiology of schizotypy: fronto-striatal prediction error signal correlates with delusion-like beliefs in healthy people. *Neuropsychologia*. 50 (14). p.pp. 3612–3620.

Cougnard, A., Marcelis, M., Myin-Germeys, I., De Graaf, R., Vollebergh, W., Krabbendam, L., Lieb, R., Wittchen, H.-U.U., Henquet, C., Spauwen, J. & Van Os, J. (2007). Does normal developmental expression of psychosis combine with environmental risk to cause persistence of psychosis? A psychosis proneness-persistence model. *Psychological Medicine*. 37 (4). p.pp. 513–527.

Crossley, N.A., Mechelli, A., Fusar-Poli, P., Broome, M.R., Matthiasson, P., Johns, L.C., Bramon, E., Valmaggia, L., Williams, S.C.R. & McGuire, P.K. (2009). Superior temporal lobe dysfunction and frontotemporal dysconnectivity in subjects at risk of psychosis and in first-episode psychosis. *Human Brain Mapping*. 30 (12). p.pp. 4129–4137.

Crossley, N.A., Mechelli, A., Ginestet, C., Rubinov, M., Bullmore, E.T. & Mcguire, P. (2016). Altered hub functioning and compensatory activations in the connectome: A meta-analysis of functional neuroimaging studies in schizophrenia. *Schizophrenia Bulletin*. 42 (2). p.pp. 434–442.

Cullen, A.E., De Brito, S. a., Gregory, S.L., Murray, R.M., Williams, S.C.R., Hodgins, S. & Laurens, K.R. (2013). Temporal lobe volume abnormalities precede the prodrome: A study of children presenting antecedents of schizophrenia. *Schizophrenia Bulletin*. 39 (6). p.pp. 1318–1327.

Dale, A.M., Fischl, B. & Sereno, M.I. (1999). Cortical Surface-Based Analysis: I. Segmentation and Surface Reconstruction. *NeuroImage*. 9 (2). p.pp. 179–194.

Dandash, O., Fornito, A., Lee, J., Keefe, R.S.E., Chee, M.W.L., Adcock, R.A., Pantelis, C., Wood, S.J. & Harrison, B.J. (2014). Altered striatal functional connectivity in subjects with an at-risk mental state for psychosis. *Schizophrenia Bulletin*. 40 (4). p.pp. 904–913.

Dauvermann, M.R., Mukherjee, P., Moorhead, W.T., Stanfield, A.C., Fusar-Poli, P., Lawrie, S.M. & Whalley, H.C. (2012). Relationship between gyrification and functional connectivity of the prefrontal cortex in subjects at high genetic risk of schizophrenia. *Current Pharmaceutical Design*. 18 (4). p.pp. 434–442.

David, A.S. (2010). Why we need more debate on whether psychotic symptoms lie on a continuum with normality. *Psychological Medicine*. 40 (12). p.pp. 1935–1942.

Dell'Acqua, F., Scifo, P., Rizzo, G., Catani, M., Simmons, A., Scotti, G. & Fazio, F. (2010). A modified damped Richardson-Lucy algorithm to reduce isotropic background effects in spherical deconvolution. *NeuroImage*. 49 (2). p.pp. 1446–1458.

Deoni, S.C.L., Mercure, E., Blasi, A., Gasston, D., Thomson, A., Johnson, M., Williams, S.C.R. & Murphy, D.G.M. (2011). Mapping Infant Brain Myelination with Magnetic Resonance Imaging. *Journal of Neuroscience*. 31 (2). p.pp. 784–791.

DeRosse, P., Ikuta, T., Peters, B.D., Karlsgodt, K.H., Szeszko, P.R. & Malhotra, a K. (2014). Adding insult to injury: Childhood and adolescent risk factors for psychosis predict lower fractional anisotropy in the superior longitudinal fasciculus in healthy adults. *Psychiatry Research*. 224 (3). p.pp. 296–302.

Deserno, L., Sterzer, P., Wüstenberg, T., Heinz, A., Schlagenhauf, F., Wustenberg, T., Heinz, A. & Schlagenhauf, F. (2012). Reduced prefrontal-parietal effective connectivity and working memory deficits in schizophrenia. *The Journal of Neuroscience*. 32 (1). p.pp. 12–20.

Desikan, R.S., Ségonne, F., Fischl, B., Quinn, B.T., Dickerson, B.C., Blacker, D., Buckner, R.L., Dale, A.M., Maguire, R.P., Hyman, B.T., Albert, M.S. & Killiany, R.J. (2006). An automated labeling system for subdividing the human cerebral cortex on MRI scans into gyral based regions of interest. *NeuroImage*. 31 (3). p.pp. 968–980.

Dickson, H., Laurens, K.R., Cullen, a. E. & Hodgins, S. (2012). Meta-analyses of cognitive and motor function in youth aged 16 years and younger who subsequently develop schizophrenia. *Psychological Medicine*. 42 (4). p.pp. 743–755.

Diederen, K.M.J., Neggers, S.F.W., de Weijer, A.D., van Lutterveld, R., Daalman, K., Eickhoff, S.B., Clos, M., Kahn, R.S. & Sommer, I.E.C. (2013). Aberrant resting-state connectivity in non-psychotic individuals with auditory hallucinations. *Psychological Medicine*. 43 (8). p.pp. 1685–1696.

Dima, D., Jogia, J. & Frangou, S. (2014). Dynamic causal modeling of load-dependent modulation of effective connectivity within the verbal working memory network. *Human Brain Mapping*. 35 (7). p.pp. 3025–3035.

Dombroski, B., Nitzken, M., Elnakib, A., Khalifa, F., Switala, A., El-Baz, A. & Casanova, M. (2014). Cortical surface complexity in a population-based normative sample. *Translational Neuroscience*. 5 (1). p.pp. 17–24.

Dominguez, M.D.G., Saka, M.C., Lieb, R., Wittchen, H.U. & van Os, J. (2010). Early expression of negative/disorganized symptoms predicting psychotic experiences and subsequent clinical psychosis: a 10-year study. *American Journal of Psychiatry*. 167 (9). p.pp. 1075–1082.

Downs, J.M., Cullen, A.E., Barragan, M. & Laurens, K.R. (2013). Persisting psychotic-like experiences are associated with both externalising and internalising psychopathology in a longitudinal general population child cohort. *Schizophrenia Research*. 144 (1). p.pp. 99–104.

Drake, R.J., Haley, C.J., Akhtar, S. & Lewis, S.W. (2000). Causes and consequences of duration of untreated psychosis in schizophrenia. *The British Journal of Psychiatry*. 177 (6). p.pp. 511–515.

Drakesmith, M., Caeyenberghs, K., Dutt, A., Zammit, S., Evans, C.J., Reichenberg, A., Lewis, G., David, A.S. & Jones, D.K. (2015). Schizophrenia-like topological changes in the structural connectome of individuals with subclinical psychotic experiences. *Human Brain Mapping*. 36 (7). p.pp. 2629–2643.

Drakesmith, M., Dutt, A., Fonville, L., Zammit, S., Reichenberg, A., Evans, C.J., Lewis, G., Jones, D.K. & David, A.S. (2016a). Mediation of Developmental Risk Factors for Psychosis by White Matter Microstructure in Young Adults With Psychotic Experiences. *JAMA Psychiatry*. 73 (4). p.pp. 396–406.

Drakesmith, M., Dutt, A., Fonville, L., Zammit, S., Reichenberg, A., Evans, C.J., McGuire, P., Lewis, G., Jones, D.K. & David, A.S. (2016b). Volumetric, relaxometric and diffusometric correlates of psychotic experiences in a non-clinical sample of young adults. *NeuroImage: Clinical*. 12. p.pp. 550–558.

Dumontheil, I. & Klingberg, T. (2012). Brain Activity during a Visuospatial Working Memory Task Predicts Arithmetical Performance 2 Years Later. *Cerebral Cortex*. 22 (5). p.pp. 1078–1085.

Dutt, A., Tseng, H.H., Fonville, L., Drakesmith, M., Su, L., Evans, J., Zammit, S., Jones, D., Lewis, G. & David, A.S. (2015). Exploring neural dysfunction in 'clinical high risk' for psychosis: A quantitative review of fMRI studies. *Journal of Psychiatric Research*. 61. p.pp. 122–134.

Evans, A.C., Collins, D.L., Mills, S.R., Brown, E.D., Kelly, R.L. & Peters, T.M. (1993). 3D statistical neuroanatomical models from 305 MRI volumes. In: *IEEE Conference Record Nuclear Science Symposium and Medical Imaging Conference*. 1993, pp. 1813–1817.

Falkai, P., Honer, W.G., Kamer, T., Dustert, S., Vogeley, K., Schneider-Axmann, T., Dani, I., Wagner, M., Rietschel, M., Müller, D.J., Schulze, T.G., Gaebel, W., Cordes, J., Schönell, H., Schild, H.H., Block, W., Träber, F., Steinmetz, H., Maier, W. & Tepest, R. (2007). Disturbed frontal gyrification within families affected with schizophrenia. *Journal of Psychiatric Research*. 41 (10). p.pp. 805–813.

Fischl, B. (2012). FreeSurfer. *NeuroImage*. 62 (2). p.pp. 774–781.

Fischl, B., Sereno, M.I. & Dale, A.M. (1999). Cortical Surface-Based Analysis II: Inflation, Flattening, and a Surface-Based Coordinate System. *NeuroImage*. 9 (2). p.pp. 195–207.

Fornito, A. & Bullmore, E.T. (2014). Reconciling abnormalities of brain network structure and function in schizophrenia. *Current Opinion in Neurobiology*. 30. p.pp. 44–50.

Fornito, A., Yung, A.R., Wood, S.J., Phillips, L.J., Nelson, B., Cotton, S., Velakoulis, D., McGorry, P.D., Pantelis, C. & Yücel, M. (2008). Anatomic Abnormalities of the Anterior Cingulate Cortex Before Psychosis Onset: An MRI Study of Ultra-High-Risk Individuals. *Biological Psychiatry*. 64 (9). p.pp. 758–765.

French, L., Gray, C., Leonard, G., Perron, M., Pike, G.B., Richer, L., Séguin, J.R., Veillette, S., Evans, C.J., Artiges, E., Banaschewski, T., Bokde, A.W.L., Bromberg, U., Bruehl, R., Buchel, C., Cattrell, A., Conrod, P.J., Flor, H., Frouin, V., Gallinat, J., Garavan, H., Gowland, P., Heinz, A., Lemaitre, H., Martinot, J.-L., Nees, F., Orfanos, D.P., Pangelinan, M.M., Poustka, L., Rietschel, M., Smolka, M.N., Walter, H., Whelan, R., Timpson, N.J., Schumann, G., Smith, G.D., Pausova, Z. & Paus, T. (2015). Early Cannabis Use, Polygenic Risk Score for Schizophrenia and Brain Maturation in Adolescence. *JAMA Psychiatry*. 72 (10). p.pp. 1002–1011.

Friston, K., Brown, H.R., Siemerkus, J. & Stephan, K.E. (2016). The dysconnection hypothesis (2016). *Schizophrenia Research*. 176 (2) p.pp. 83–94.

Friston, K.J. (2011). Functional and effective connectivity: a review. *Brain Connectivity*. 1 (1). p.pp. 13–36.

Friston, K.J. (1999). Schizophrenia and the disconnection hypothesis. *Acta Psychiatrica Scandinavica*. 99 (s395). p.pp. 68–79.

Friston, K.J. & Frith, C.D. (1995). Schizophrenia: a disconnection syndrome? *Clinical neuroscience (New York, N.Y.)*. 3 (2) p.pp. 89–97.

Friston, K.J., Harrison, L. & Penny, W. (2003). Dynamic causal modelling. *Neuroimage*. 19 (4). p.pp. 1063–1090.

Friston, K.J., Holmes, A., Poline, J.B., Price, C.J. & Frith, C.D. (1996). Detecting activations in PET and fMRI: levels of inference and power. *NeuroImage*. 4 (3). p.pp. 223–235.

Fryer, S.L., Woods, S.W., Kiehl, K. a., Calhoun, V.D., Pearlson, G.D., Roach, B.J., Ford, J.M., Srihari, V.H., McGlashan, T.H. & Mathalon, D.H. (2013). Deficient Suppression of Default Mode Regions during Working Memory in Individuals with Early Psychosis and at Clinical High-Risk for Psychosis. *Frontiers in Psychiatry Psychiatry*. 4. p.p. 92.

Fusar-Poli, P. (2012). Voxel-wise meta-analysis of fMRI studies in patients at clinical high risk for psychosis. *The Journal of Psychiatry and Neuroscience*. 37 (2). p.pp. 106–112.

Fusar-Poli, P., Bonoldi, I., Yung, A.R., Borgwardt, S., Kempton, M.J., Valmaggia, L., Barale, F., Caverzasi, E. & Mcguire, P. (2012a). Predicting Psychosis. *Archives of General Psychiatry*. 69 (3). p.pp. 220–229.

Fusar-Poli, P., Borgwardt, S., Crescini, A., Deste, G., Kempton, M.J., Lawrie, S., Mc Guire, P. & Sacchetti, E. (2011a). Neuroanatomy of vulnerability to psychosis: A voxel-based meta-analysis. *Neuroscience and Biobehavioral Reviews*. 35 (5). p.pp. 1175–1185.

Fusar-Poli, P., Broome, M.R., Woolley, J.B., Johns, L.C., Tabraham, P., Bramon, E., Valmaggia, L., Williams, S.C. & McGuire, P. (2011b). Altered brain function directly related to structural abnormalities in people at ultra high risk of psychosis: Longitudinal VBM-fMRI study. *Journal of Psychiatric Research*. 45 (2). p.pp. 190–198.

Fusar-Poli, P., Deste, G., Smieskova, R., Barlati, S., Yung, A.R., Howes, O., Stieglitz, R.-D.D., Vita, A., McGuire, P. & Borgwardt, S. (2012b). Cognitive functioning in prodromal psychosis: a meta-analysis. *Archives of General Psychiatry*. 69 (6). p.pp. 562–571.

Fusar-Poli, P. & Meyer-Lindenberg, A. (2016). Forty years of structural imaging in psychosis: promises and truth. *Acta Psychiatrica Scandinavica*. 134 (3) p.pp. 207–224.

Fusar-Poli, P., Perez, J., Broome, M., Borgwardt, S., Placentino, A., Caverzasi, E., Cortesi, M., Veggiotti, P., Politi, P., Barale, F. & McGuire, P. (2007). Neurofunctional correlates of vulnerability to psychosis: A systematic review and meta-analysis. *Neuroscience and Biobehavioral Reviews*. 31 (4). p.pp. 465–484.

Fusar-Poli, P., Radua, J., McGuire, P. & Borgwardt, S. (2012c). Neuroanatomical maps of psychosis onset: Voxel-wise meta-analysis of antipsychotic-naive vbm studies. *Schizophrenia Bulletin*. 38 (6). p.pp. 1297–1307.

Gautam, P., Anstey, K.J., Wen, W., Sachdev, P.S. & Cherbuin, N. (2015). Cortical gyrification and its relationships with cortical volume, cortical thickness, and cognitive performance in healthy mid-life adults. *Behavioural Brain Research*. 287. p.pp. 331–339.

Gay, O., Plaze, M., Oppenheim, C., Mouchet-Mages, S., Gaillard, R., Olié, J.P., Krebs, M.O. & Cachia, A. (2013). Cortex morphology in first-episode psychosis patients with neurological soft signs. *Schizophrenia Bulletin*. 39 (4). p.pp. 820–829.

Giedd, J.N., Blumenthal, J., Jeffries, N.O., Castellanos, F.X., Liu, H., Zijdenbos, A., Paus, T., Evans, a C. & Rapoport, J.L. (1999). Brain development during childhood and adolescence: a longitudinal MRI study. *Nature Neuroscience*. 2 (10). p.pp. 861–863.

Gifford, G., Crossley, N., Fusar-Poli, P., Schnack, H.G., Kahn, R.S., Koutsouleris, N., Cannon, T.D. & McGuire, P. (2017). Using neuroimaging to help predict the onset of psychosis. *NeuroImage*. 145 (April). p.pp. 209–217.

Glahn, D.C., Ragland, J.D., Abramoff, A., Barrett, J., Laird, A.R., Bearden, C.E. & Velligan, D.I. (2005). Beyond hypofrontality: A quantitative meta-analysis of functional neuroimaging studies of working memory in schizophrenia. *Human Brain Mapping*. 25 (1). p.pp. 60–69.

Gogtay, N., Giedd, J.N., Lusk, L., Hayashi, K.M., Greenstein, D., Vaituzis, A.C., Nugent, T.F., Herman, D.H., Clasen, L.S., Toga, A.W., Rapoport, J.L. & Thompson, P.M. (2004). Dynamic mapping of human cortical development during childhood through early adulthood. *Proceedings of the National Academy of Sciences of the United States of America*. 101 (21). p.pp. 8174–8179.

Haatveit, B.C., Sundet, K., Hugdahl, K., Ueland, T., Melle, I. & Andreassen, O. a (2010). The validity of d prime as a working memory index: results from the 'Bergen n-back task'. *Journal of Clinical and Experimental Neuropsychology*. 32 (8). p.pp. 871–880.

Hagler, D.J., Saygin, A.P. & Sereno, M.I. (2006). Smoothing and cluster thresholding for cortical surface-based group analysis of fMRI data. *NeuroImage*. 33 (4). p.pp. 1093–1103.

Hanssen, M., Bak, M., Bijl, R., Vollebergh, W. & van Os, J. (2005). The incidence and outcome of subclinical psychotic experiences in the general population. *The British Journal of Clinical Psychology*. 44 (2). p.pp. 181–191.

Harris, J.M., Moorhead, T.W.J., Miller, P., McIntosh, A.M., Bonnici, H.M., Owens, D.G.C., Johnstone, E.C. & Lawrie, S.M. (2007). Increased Prefrontal Gyrification in a Large High-Risk Cohort Characterizes Those Who Develop Schizophrenia and Reflects Abnormal Prefrontal Development. *Biological Psychiatry*. 62 (7). p.pp. 722–729.

Harris, J.M., Whalley, H., Yates, S., Miller, P., Johnstone, E.C. & Lawrie, S.M. (2004). Abnormal cortical folding in high-risk individuals: A predictor of the development of schizophrenia? *Biological Psychiatry*. 56 (3). p.pp. 182–189.

Harrisberger, F., Smieskova, R., Vogler, C., Egli, T., Schmidt, A., Lenz, C., Simon, A.E., Riecher-Rössler, A., Papassotiropoulos, A. & Borgwardt, S. (2016). Impact of polygenic schizophrenia-related risk and hippocampal volumes on the onset of psychosis. *Translational Psychiatry*. 6 (8). p.p. e868.

Hartigan, J.A. & Hartigan, P.M. (1985). The Dip Test of Unimodality. *The Annals of Statistics*. 13 (1). p.pp. 70–84.

Hartigan, P.M. (1985). Algorithm AS 217: Computation of the Dip Statistic to Test for Unimodality. *Applied Statistics*. 34 (3). p.pp. 320–325.

Herculano-Houzel, S., Mota, B., Wong, P. & Kaas, J.H. (2010). Connectivity-driven white matter scaling and folding in primate cerebral cortex. *Proceedings of the National Academy of Sciences of the United States of America*. 107 (44). p.pp. 19008–19013.

de Herdt, A., Wampers, M., Vancampfort, D., de Hert, M., Vanhees, L., Demunter, H., Van Bouwel, L., Brunner, E. & Probst, M. (2013). Neurocognition in clinical high risk young adults who did or did not convert to a first schizophrenic psychosis: A meta-analysis. *Schizophrenia Research*. 149 (1). p.pp. 48–55.

van den Heuvel, M.P. & Fornito, A. (2014). Brain networks in schizophrenia. *Neuropsychology Review*. 24 (1) p.pp. 32–48.

Hofer, S. & Frahm, J. (2006). Topography of the human corpus callosum revisited - Comprehensive fiber tractography using diffusion tensor magnetic resonance imaging. *NeuroImage*. 32 (3). p.pp. 989–994.

Hogstrom, L.J., Westlye, L.T., Walhovd, K.B. & Fjell, A.M. (2013). The Structure of the Cerebral Cortex Across Adult Life : Age-Related Patterns of Surface Area, Thickness, and Gyrification. *Cerebral Cortex*. 23 (11). p.pp. 2521–2530.

Honea, R., Crow, T.J., Passingham, D. & Mackay, C.E. (2005). Regional deficits in brain volume in schizophrenia: A meta-analysis of voxel-based morphometry studies. *American Journal of Psychiatry*. 162 (12) p.pp. 2233–2245.

Horwood, J., Salvi, G., Thomas, K., Duffy, L., Gunnell, D., Hollis, C., Lewis, G., Menezes, P., Thompson, A., Wolke, D., Zammit, S. & Harrison, G. (2008). IQ and non-clinical psychotic symptoms in 12-year-olds: Results from the ALSPAC birth cohort. *British Journal of Psychiatry*. 193 (3). p.pp. 185–191.

Huang, H., Zhang, J., Jiang, H., Wakana, S., Poetscher, L., Miller, M.I., Van Zijl, P.C.M., Hillis, A.E., Wytik, R. & Mori, S. (2005). DTI tractography based parcellation of white matter: Application to the mid-sagittal morphology of corpus callosum. *NeuroImage*. 26 (1). p.pp. 195–205.

Hubl, D., Koenig, T., Strik, W., Federspiel, A., Kreis, R., Boesch, C., Maier, S.E., Schroth, G., Lovblad, K. & Dierks, T. (2004). Pathways that make voices - White matter changes in auditory hallucinations. *Archives of General Psychiatry*. 61 (7). p.pp. 658–668.

International Early Psychosis Association Writing Group (2005). International Clinical Practice Guidelines for Early Psychosis. *The British Journal of Psychiatry*. 48. p.pp. s120–s124.

Jacobson, S., Kelleher, I., Harley, M., Murtagh, A., Clarke, M., Blanchard, M., Connolly, C., O'Hanlon, E., Garavan, H. & Cannon, M. (2010). Structural and functional brain correlates of subclinical psychotic symptoms in 11-13 year old schoolchildren. *NeuroImage*. 49 (2). p.pp. 1875–1885.

Johns, L.C., Cannon, M., Singleton, N., Murray, R.M., Farrell, M., Brugha, T., Bebbington, P., Jenkins, R., Meltzer, H. & Ay, R.M.M. (2004). Prevalence and correlates of self-reported psychotic symptoms in the British population. *British Journal of Psychiatry*. 185 (4). p.pp. 298–305.

Johns, L.C. & van Os, J. (2001). The continuity of psychotic experiences in the general population. *Clinical Psychology Review*. 21 (8) p.pp. 1125–1141.

Johnson, M.H., Jones, E.J.H. & Gliga, T. (2015). Brain adaptation and alternative developmental trajectories. *Development and Psychopathology*. 27 (2). p.pp. 425–442.

Jones, H.J., Stergiakouli, E., Tansey, K.E., Hubbard, L., Heron, J., Cannon, M., Holmans, P., Lewis, G., Linden, D.E.J., Jones, P.B., Davey Smith, G., O'Donovan, M.C., Owen, M.J., Walters, J.T. & Zammit, S. (2016). Phenotypic Manifestation of Genetic Risk for Schizophrenia During Adolescence in the General Population. *JAMA Psychiatry*. 73 (3). p.pp. 221–228.

Jung, W.H., Jang, J.H., Byun, M.S., An, S.K. & Kwon, J.S. (2010). Structural brain alterations in individuals at ultra-high risk for psychosis: A review of magnetic resonance imaging studies and future directions. *Journal of Korean Medical Science*. 25 (12). p.pp. 1700–1709.

Jung, W.H., Jang, J.H., Shin, N.Y., Kim, S.N., Choi, C.H., An, S.K. & Kwon, J.S. (2012). Regional Brain Atrophy and Functional Disconnection in Broca's Area in Individuals at Ultra-High Risk for Psychosis and Schizophrenia. *PLoS ONE*. 7 (12). p.p. e51975.

Jung, W.H., Kim, J.S., Jang, J.H., Choi, J.S., Jung, M.H., Park, J.Y., Han, J.Y., Choi, C.H., Kang, D.H., Chung, C.K. & Kwon, J.S. (2011). Cortical thickness reduction in individuals at ultra-high-risk for psychosis. *Schizophrenia Bulletin*. 37 (4). p.pp. 839–849.

Kambeitz, J., Kambeitz-Ilankovic, L., Leucht, S., Wood, S., Davatzikos, C., Malchow, B., Falkai, P. & Koutsouleris, N. (2015). Detecting neuroimaging biomarkers for schizophrenia: a meta-analysis of multivariate pattern recognition studies. *Neuropsychopharmacology*. 40 (7). p.pp. 1742–1751.

Kauppi, K., Westlye, L.T., Tesli, M., Bettella, F., Brandt, C.L., Mattingsdal, M., Ueland, T., Espeseth, T., Agartz, I., Melle, I., Djurovic, S. & Andreassen, O.A. (2015). Polygenic risk for schizophrenia associated with working memory-related prefrontal brain activation in patients with schizophrenia and healthy controls. *Schizophrenia Bulletin*. 41 (3). p.pp. 736–743.

Kaymaz, N., Drukker, M., Lieb, R., Wittchen, H.U., Werbeloff, N., Weiser, M., Lataster, T. & van Os, J. (2012). Do subthreshold psychotic experiences predict clinical outcomes in unselected non-help-seeking population-based samples? A systematic review and meta-analysis, enriched with new results. *Psychological Medicine*. 42 (11). p.pp. 2239–2253.

Kaymaz, N. & van Os, J. (2010). Extended psychosis phenotype – yes: single continuum – unlikely. *Psychological Medicine*. 40 (12). p.pp. 1963–1966.

Kelleher, I., Connor, D., Clarke, M.C., Devlin, N., Harley, M. & Cannon, M. (2012a). Prevalence of psychotic symptoms in childhood and adolescence: a systematic review and meta-analysis of population-based studies. *Psychological Medicine*. 42 (9). p.pp. 1857–1863.

Kelleher, I., Keeley, H., Corcoran, P., Lynch, F., Fitzpatrick, C., Devlin, N., Molloy, C., Roddy, S., Clarke, M.C., Harley, M., Arseneault, L., Wasserman, C., Carli, V., Sarchiapone, M., Hoven, C., Wasserman, D. & Cannon, M. (2012b). Clinicopathological significance of psychotic experiences in non-psychotic young people: Evidence from four population-based studies. *British Journal of Psychiatry*. 201 (1). p.pp. 26–32.

Kempton, M.J., Stahl, D., Williams, S.C.R. & DeLisi, L.E. (2010). Progressive lateral ventricular enlargement in schizophrenia: A meta-analysis of longitudinal MRI studies. *Schizophrenia Research*. 120 (1–3). p.pp. 54–62.

Klein, D., Rotarska-Jagiela, A., Genc, E., Sritharan, S., Mohr, H., Roux, F., Han, C.E., Kaiser, M., Singer, W. & Peter, J.U. (2014). Adolescent brain maturation and cortical folding: Evidence for reductions in gyrification. *PLoS ONE*. 9 (1). p.p. e84914.

Klein, S., Staring, M., Murphy, K., Viergever, M.A. & Pluim, J.P.W. (2010). Elastix: A toolbox for intensity-based medical image registration. *IEEE Transactions on Medical Imaging*. 29 (1). p.pp. 196–205.

Klingberg, T. (2006). Development of a superior frontal-intraparietal network for visuo-spatial working memory. *Neuropsychologia*. 44 (11). p.pp. 2171–2177.

van der Knaap, L.J. & van der Ham, I.J.M. (2011). How does the corpus callosum mediate interhemispheric transfer? A review. *Behavioural Brain Research*. 223 (1) p.pp. 211–221.

Kochunov, P., Mangin, J.F., Coyle, T., Lancaster, J., Thompson, P., Rivière, D., Cointepas, Y., Régis, J., Schlosser, A., Royall, D.R., Zilles, K., Mazziotta, J., Toga, A. & Fox, P.T. (2005). Age-related morphology trends of cortical sulci. *Human Brain Mapping*. 26 (3). p.pp. 210–220.

Krabbendam, L., Myin-Germeys, I., Bak, M. & van Os, J. (2005a). Explaining transitions over the hypothesized psychosis continuum. *Australian and New Zealand Journal of Psychiatry*. 39 (3). p.pp. 180–186.

Krabbendam, L., Myin-Germeys, I., Hanssen, M., de Graaf, R., Vollebergh, W., Bak, M. & van Os, J. (2005b). Development of depressed mood predicts onset of psychotic disorder in individuals who report hallucinatory experiences. *The British Journal of Clinical Psychology*. 44 (1). p.pp. 113–125.

Kuperberg, G. & Heckers, S. (2000). Schizophrenia and cognitive function. *Current Opinion in Neurobiology*. 10 (2) p.pp. 205–210.

Lancaster, T.M., Ihssen, N., Brindley, L.M., Tansey, K.E., Mantripragada, K., O'Donovan, M.C., Owen, M.J. & Linden, D.E.J. (2016). Associations between polygenic risk for schizophrenia and brain function during probabilistic learning in healthy individuals. *Human Brain Mapping*. 37 (2). p.pp. 491–500.

Lawrie, S.M., Hall, J., McIntosh, A.M., Owens, D.G.C. & Johnstone, E.C. (2010). The 'continuum of psychosis': Scientifically unproven and clinically impractical. *British Journal of Psychiatry*. 197 (6). p.pp. 423–425.

Lawrie, S.M., McIntosh, A.M., Hall, J., Owens, D.G.C. & Johnstone, E.C. (2008). Brain structure and function changes during the development of schizophrenia: the evidence from studies of subjects at increased genetic risk. *Schizophrenia Bulletin*. 34 (2). p.pp. 330–340.

Lebel, C., Walker, L., Leemans, A., Phillips, L. & Beaulieu, C. (2008). Microstructural maturation of the human brain from childhood to adulthood. *NeuroImage*. 40 (3). p.pp. 1044–1055.

Leemans, A., Jeurissen, B., Sijbers, J. & Jones, D. (2009). ExploreDTI: a graphical toolbox for processing, analyzing, and visualizing diffusion MR data. In: *Proceedings 17th Scientific Meeting, International Society for Magnetic Resonance in Medicine*. 2009, p. 3537.

Leemans, A. & Jones, D.K. (2009). The B-matrix must be rotated when correcting for subject motion in DTI data. *Magnetic Resonance in Medicine*. 61 (6). p.pp. 1336–1349.

Lenroot, R.K. & Giedd, J.N. (2006). Brain development in children and adolescents: Insights from anatomical magnetic resonance imaging. *Neuroscience and Biobehavioral Reviews*. 30 (6). p.pp. 718–729.

Lewis, D.A. & Levitt, P. (2002). Schzophrenia as a disorder of neurodevelopment. *Annual Review of Neuroscience*. 25 (1). p.pp. 409–432.

Lewis, G., Pelosi, A.J. & Araya, R. (1992). Measuring psychiatric disorder in the community a standardized assessment for use by lay interviewers. *Psychological Medicine*. 22 (2). p.pp. 465–486.

Leys, C. & Schumann, S. (2010). A nonparametric method to analyze interactions. *Journal of Experimental Social Psychology*. [Online]. 46 (4). p.pp. 684–688. Available from: http://dx.doi.org/10.1016/j.jesp.2010.02.007.

Liu, B., Zhang, X., Cui, Y., Qin, W., Tao, Y., Li, J., Yu, C. & Jiang, T. (2016). Polygenic Risk for Schizophrenia Influences Cortical Gyrification in 2 Independent General Populations. *Schizophrenia Bulletin*. 43 (3). p.pp. 673–680.

Liu, C., Wei, H., Gong, N.-J., Cronin, M., Dibb, R. & Decker, K. (2015). Quantitative Susceptibility Mapping: Contrast Mechanisms and Clinical Applications. *Tomography: a journal for imaging research*. 1 (1). p.pp. 3–17.

Luna, B., Padmanabhan, A., Hearn, K.O. & O'Hearn, K. (2010). What has fMRI told us about the Development of Cognitive Control through Adolescence? *Brain and Cognition*. 72 (1). p.pp. 1–28.

van Lutterveld, R., Diederen, K.M.J., Otte, W.M. & Sommer, I.E. (2014). Network analysis of auditory hallucinations in nonpsychotic individuals. *Human Brain Mapping*. 35 (4). p.pp. 1436–1445.

Ma, L., Steinberg, J.L., Hasan, K.M., Narayana, P. a., Kramer, L. a. & Moeller, F.G. (2012). Working memory load modulation of parieto-frontal connections: Evidence from dynamic causal modeling. *Human Brain Mapping*. 33 (8). p.pp. 1850–1867.

Malykhin, N., Vahidy, S., Michielse, S., Coupland, N., Camicioli, R., Seres, P. & Carter, R. (2011). Structural organization of the prefrontal white matter pathways in the adult and aging brain measured by diffusion tensor imaging. *Brain Structure and Function*. 216 (4). p.pp. 417–431.

Maric, N., Krabbendam, L., Vollebergh, W., de Graaf, R. & van Os, J. (2003). Sex differences in symptoms of psychosis in a non-selected, general population sample. *Schizophrenia Research*. 63 (1). p.pp. 89–95.

Martino, J., Brogna, C., Robles, S.G., Vergani, F. & Duffau, H. (2010). Anatomic dissection of the inferior fronto-occipital fasciculus revisited in the lights of brain stimulation data. *Cortex*. 46 (5). p.pp. 691–699.

McGorry, P.D., Killackey, E.J. & Yung, A.R. (2008). Early intervention in psychosis : concepts , evidence and future directions. *World Psychiatry*. 7 (3). p.pp. 148–156.

McGrath, J.J., Saha, S., Al-Hamzawi, A., Alonso, J., Bromet, E.J., Bruffaerts, R., Caldas-de-Almeida, J.M., Chiu, W.T., de Jonge, P., Fayyad, J., Florescu, S., Gureje, O., Haro, J.M., Hu, C., Kovess-Masfety, V., Lepine, J.P., Lim, C.C.W., Mora, M.E.M., Navarro-Mateu, F., Ochoa, S., Sampson, N., Scott, K., Viana, M.C. & Kessler, R.C. (2015). Psychotic Experiences in the General Population. *JAMA Psychiatry*. 72 (7). p.pp. 697–705.

McRobbie, D.W., Moore, E.A., Graves, M.J. & Prince, M.R. (2003). *MRI: From Picture to Proton*. New York, United States of America: Cambridge University Press.

Mechelli, A., Riecher-Rössler, Anita, Meisenzahl, Eva M., Tognin, Stefania, Wood, Stephen J., Borgwardt, Stefan J., Koutsouleris, Nikolaos, Yung, Alison R., Stone, J.M., Phillips, Lisa J., McGorry, Patrick D., Valli, Isabel, Velakoulis, Dennis, B., W.J., Pantelis, Christos & McGuire, P.K. (2011). Neuroanatomical Abnormalities That Predate the Onset of Psychosis. *Archives of General Psychiatry*. 68 (5). p.pp. 489–495.

Meier, M.H., Caspi, A., Reichenberg, A., Keefe, R.S.E., Fisher, H.L., Harrington, H., Houts, R., Poulton, R., Moffitt, T.E., Harrington, N., Houts, R., Poulton, R. & Moffitt, T.E. (2014). Neuropsychological Decline in Schizophrenia From the Premorbid to the Postonset Period: Evidence From a Population-Representative Longitudinal Study. *American Journal of Psychiatry*. 171 (1). p.pp. 91–101.

Melicher, T., Horacek, J., Hlinka, J., Spaniel, F., Tintera, J., Ibrahim, I., Mikolas, P., Novak, T., Mohr, P. & Hoschl, C. (2015). White matter changes in first episode psychosis and their relation to the size of sample studied: A DTI study. *Schizophrenia Research*. 162 (1). p.pp. 22–28.

Mills, K.L., Goddings, A.-L., Herting, M.M., Meuwese, R., Blakemore, S.-J., Crone, E.A., Dahl, R.E., Güroğlu, B., Raznahan, A., Sowell, E.R. & Tamnes, C.K. (2016). Structural brain development between childhood and adulthood: Convergence across four longitudinal samples. *NeuroImage*. 141. p.pp. 273–281.

Mitelman, S.A., Torosjan, Y., Newmark, R.E., Schneiderman, J.S., Chu, K.W., Brickman, A.M., Haznedar, M.M., Hazlett, E.A., Tang, C.Y., Shihabuddin, L. & Buchsbaum, M.S. (2007). Internal capsule, corpus callosum and long associative fibers in good and poor outcome schizophrenia: A diffusion tensor imaging survey. *Schizophrenia Research*. 92 (1–3). p.pp. 211–224.

Modinos, G., Mechelli, A., Ormel, J., Groenewold, N.A., Aleman, A. & McGuire, P.K. (2010a). Schizotypy and brain structure: a voxel-based morphometry study. *Psychological Medicine*. 40 (9). p.pp. 1423–1431.

Modinos, G., Ormel, J. & Aleman, A. (2010b). Altered activation and functional connectivity of neural systems supporting cognitive control of emotion in psychosis proneness. *Schizophrenia Research*. 118 (1). p.pp. 88–97.

Modinos, G., Pettersson-Yeo, W., Allen, P., McGuire, P.K., Aleman, A. & Mechelli, A. (2012). Multivariate pattern classification reveals differential brain activation during emotional processing in individuals with psychosis proneness. *NeuroImage*. 59 (3). p.pp. 3033–3041.

Modinos, G., Renken, R., Ormel, J. & Aleman, A. (2011). Self-reflection and the psychosis-prone brain: an fMRI study. *Neuropsychology*. 25 (3). p.pp. 295–305.

Mollon, J., David, A.S., Morgan, C., Frissa, S., Glahn, D., Pilecka, I., Hatch, S.L., Hotopf, M. & Reichenberg, A. (2016). Psychotic Experiences and Neuropsychological Functioning in a Population-based Sample. *JAMA Psychiatry*. 73 (2). p.pp. 129–138.

Nesvåg, R., Schaer, M., Haukvik, U.K., Westlye, L.T., Rimol, L.M., Lange, E.H., Hartberg, C.B., Ottet, M.C., Melle, I., Andreassen, O.A., Jönsson, E.G., Agartz, I. & Eliez, S. (2014). Reduced brain cortical folding in schizophrenia revealed in two independent samples. *Schizophrenia Research*. 152 (2). p.pp. 333–338.

Niarchou, M., Zammit, S., Walters, J., Lewis, G., Owen, M.J. & Van Den Bree, M.B. (2013). Defective Processing Speed and Nonclinical Psychotic Experiences in Children: Longitudinal Analyses in a Large Birth Cohort. *American Journal of Psychiatry*. 170 (5). p.pp. 550–557.

Nishida, A., Sasaki, T., Nishimura, Y., Tanii, H., Hara, N., Inoue, K., Yamada, T., Takami, T., Shimodera, S., Itokawa, M., Asukai, N. & Okazaki, Y. (2010). Psychotic-like experiences are associated with suicidal feelings and deliberate self-harm behaviors in adolescents aged 12-15 years. *Acta Psychiatrica Scandinavica*. 121 (4). p.pp. 301–307.

O'Hanlon, E., Leemans, A., Kelleher, I., Clarke, M.C., Roddy, S., Coughlan, H., Harley, M., Amico, F., Hoscheit, M.J., Tiedt, L., Tabish, J., McGettigan, A., Frodl, T. & Cannon, M. (2015). White Matter Differences Among Adolescents Reporting Psychotic Experiences. *JAMA Psychiatry*. 72 (7). p.pp. 668–677.

Orr, J.M., Turner, J.A. & Mittal, V.A. (2014). Widespread brain dysconnectivity associated with psychotic-like experiences in the general population. *NeuroImage: Clinical*. 4. p.pp. 343–351.

van Os, J. (2003). Is there a continuum of psychotic experiences in the general population? *Epidemiologia e Psichiatria Sociale*. 12 (4). p.pp. 242–252.

van Os, J., Hanssen, M., Bijl, R. V. & Ravelli, A. (2000). Strauss (1969) revisited: A psychosis continuum in the general population? *Schizophrenia Research*. 45 (1). p.pp. 11–20.

van Os, J., Linscott, R.J., Myin-Germeys, I., Delespaul, P. & Krabbendam, L. (2009). A systematic review and meta-analysis of the psychosis continuum: evidence for a psychosis proneness-persistence-impairment model of psychotic disorder. *Psychological Medicine*. 39 (2). p.pp. 179–195.

Østby, Y., Tamnes, C.K., Fjell, A.M., Walhovd, K.B., Ostby, Y., Tamnes, C.K., Fjell, A.M. & Walhovd, K.B. (2011). Morphometry and connectivity of the fronto-parietal verbal working memory network in development. *Neuropsychologia*. 49 (14). p.pp. 3854–3862.

Palaniyappan, L. & Liddle, P.F. (2012a). Aberrant cortical gyrification in schizophrenia: A surface-based morphometry study. *Journal of Psychiatry and Neuroscience*. 37 (6). p.pp. 399–406.

Palaniyappan, L. & Liddle, P.F. (2014). Diagnostic discontinuity in psychosis: A combined study of cortical gyrification and functional connectivity. *Schizophrenia Bulletin*. 40 (3). p.pp. 675–684.

Palaniyappan, L. & Liddle, P.F. (2012b). Differential effects of surface area, gyrification and cortical thickness on voxel based morphometric deficits in schizophrenia. *NeuroImage*. 60 (1). p.pp. 693–699.

Palaniyappan, L., Mallikarjun, P., Joseph, V., White, T.P. & Liddle, P.F. (2011). Folding of the prefrontal cortex in schizophrenia: Regional differences in gyrification. *Biological Psychiatry*. 69 (10). p.pp. 974–979.

Palaniyappan, L., Marques, T.R., Taylor, H., Handley, R., Mondelli, V., Bonaccorso, S., Giordano, A., McQueen, G., DiForti, M., Simmons, A., David, A.S., Pariante, C.M., Murray, R.M. & Dazzan, P. (2013). Cortical folding defects as markers of poor treatment response in first-episode psychosis. *JAMA psychiatry*. 70 (10). p.pp. 1031–40.

Pantelis, C., Velakoulis, D., Wood, S.J., Yücel, M., Yung, a R., Phillips, L.J., Sun, D.-Q. & McGorry, P.D. (2007). Neuroimaging and emerging psychotic disorders: the Melbourne ultra-high risk studies. *International Review of Psychiatry*. 19 (4). p.pp. 371–381.

Pantelis, C., Yücel, M., Bora, E., Fornito, A., Testa, R., Brewer, W.J., Velakoulis, D. & Wood, S.J. (2009). Neurobiological markers of illness onset in psychosis and schizophrenia: The search for a moving target. *Neuropsychology Review*. 19 (3). p.pp. 385–398.

Pantelis, C., Yücel, M., Wood, S.J., Velakoulis, D., Sun, D., Berger, G., Stuart, G.W., Yung, A., Phillips, L. & McGorry, P.D. (2005). Structural Brain Imaging Evidence for Multiple Pathological Processes at Different Stages of Brain Development in Schizophrenia. *Schizophrenia Bulletin*. 31 (3). p.pp. 672–696.

Parker, G. (2014). *Robust processing of diffusion weighted image data*. Cardiff University.

Parker, G., Marshall, D., Rosin, P.L., Drage, N., Richmond, S. & Jones, D.K. (2013). Fast and fully automated clustering of whole brain tractography results using shape-space analysis. In: *Proceedings of the International Society for Magnetic Resonance in Medicine*. 2013, Salt Lake City, p. 778.

Pasternak, O., Sochen, N., Gur, Y., Intrator, N. & Assaf, Y. (2009). Free water elimination and mapping from diffusion MRI. *Magnetic Resonance in Medicine*. 62 (3). p.pp. 717–730.

Paul, L.K. (2011). Developmental malformation of the corpus callosum: A review of typical callosal development and examples of developmental disorders with callosal involvement. *Journal of Neurodevelopmental Disorders*. 3 (1). p.pp. 3–27.

Paus, T., Keshavan, M. & Giedd, J.N. (2008). Why do many psychiatric disorders emerge during adolescence? *Nature Reviews Neuroscience*. 9 (12). p.pp. 947–957.

Pelletier-Baldelli, A., Dean, D.J., Lunsford-Avery, J.R., Smith Watts, A.K., Orr, J.M., Gupta, T., Millman, Z.B. & Mittal, V. a. (2014). Orbitofrontal cortex volume and intrinsic religiosity in non-clinical psychosis. *Psychiatry Research: Neuroimaging*. 222 (3). p.pp. 124–130.

Peng, Q., Schork, A., Bartsch, H., Lo, M.-T., Panizzon, M.S., Westlye, L.T., Kremen, W.S., Jernigan, T.L., Le Hellard, S., Steen, V.M., Espeseth, T., Huentelman, M., Håberg, A.K., Agartz, I., Djurovic, S., Andreassen, O.A., Dale, A.M., Schork, N.J. & Chen, C.-H. (2016). Conservation of Distinct Genetically-Mediated Human Cortical Pattern. *PLoS Genetics*. 12 (7). p.p. e1006143.

Perkins, D.O., Gu, H., Boteva, K. & Lieberman, J.A. (2005). Relationship between duration of untreated psychosis and outcome in first-episode schizophrenia: a critical review and meta-analysis. *The American Journal of Psychiatry*. 162 (10). p.pp. 1785–1804.

Peters, B.D., Dingemans, P.M., Dekker, N., Blaas, J., Akkerman, E., van Amelsvoort, T.A., Majoie, C.B., den Heeten, G.J., Linszen, D.H. & de Haan, L. (2010). White matter connectivity and psychosis in ultra-high-risk subjects: A diffusion tensor fiber tracking study. *Psychiatry Research: Neuroimaging*. 181 (1). p.pp. 44–50.

Peters, B.D., de Haan, L., Dekker, N., Blaas, J., Becker, H.E., Dingemans, P.M., Akkerman, E.M., Majoie, C.B., van Amelsvoort, T.A., den Heeten, G.J. & Linszen, D.H. (2008). White matter fibertracking in first-episode schizophrenia, schizoaffective patients and subjects at ultra-high risk of psychosis. *Neuropsychobiology*. 58 (1). p.pp. 19–28.

Peters, B.D., Ikuta, T., Derosse, P., John, M., Burdick, K.E., Gruner, P., Prendergast, D.M., Szeszko, P.R. & Malhotra, A.K. (2014). Age-Related Differences in White Matter Tract Microstructure Are Associated with Cognitive Performance from Childhood to Adulthood. *Biological Psychiatry*. 75 (3). p.pp. 248–256.

Peters, B.D. & Karlsgodt, K.H. (2015). White matter development in the early stages of psychosis. *Schizophrenia Research*. 161 (1). p.pp. 61–69.

Peters, B.D., Schmitz, N., Dingemans, P.M., van Amelsvoort, T.A., Linszen, D.H., de Haan, L., Majoie, C.B. & den Heeten, G.J. (2009). Preliminary evidence for reduced frontal white matter integrity in subjects at ultra-high-risk for psychosis. *Schizophrenia Research*. 111 (1–3) p.pp. 192–193.

Peters, B.D., Szeszko, P.R., Radua, J., Ikuta, T., Gruner, P., Derosse, P., James, A.C., Gallego, J.A. & Malhotra, A.K. (2012). White Matter Development in Adolescence : Diffusion Tensor Imaging and Meta- Analytic Results. *Schizophrenia Bulletin*. 38 (6). p.pp. 1308–1317.

Pettersson-Yeo, W., Allen, P., Benetti, S., McGuire, P. & Mechelli, A. (2011). Dysconnectivity in schizophrenia: Where are we now? *Neuroscience and Biobehavioral Reviews*. 35 (5). p.pp. 1110–1124.

Phillips, L.J., Yung, A.R. & McGorry, P.D. (2000). Identification of young people at risk of psychosis: validation of Personal Assessment and Crisis Evaluation Clinic intake criteria. *The Australian and New Zealand Journal of Psychiatry*. 34 (s2). p.pp. S164–S169.

Pinheiro, J., Bates, D., DebRoy, S., Sarkar, D. & R CoreTeam (2016). *nlme: Linear and Nonlinear Mixed Effects Models*.

Polanczyk, G., Moffitt, T.E., Arseneault, L., Cannon, M., Ambler, A., Keefe, R.S.E., Houts, R., Odgers, C.L. & Caspi, A. (2010). Etiological and clinical features of childhood psychotic symptoms: results from a birth cohort. *Archives of General Psychiatry*. 67 (4). p.pp. 328–338.

Putnam, M.C., Wig, G.S., Grafton, S.T., Kelley, W.M. & Gazzaniga, M.S. (2008). Structural organization of the corpus callosum predicts the extent and impact of cortical activity in the nondominant hemisphere. *The Journal of Neuroscience*. 28 (11). p.pp. 2912–2918.

R Core Team (2016). R: A Language and Environment for Statistical Computing. *R Foundation for Statistical Computing Vienna Austria*. [Online]. Available from: http://www.r-project.org/.

Raybaud, C. (2010). The corpus callosum, the other great forebrain commissures, and the septum pellucidum: Anatomy, development, and malformation. *Neuroradiology*. 52 (6) p.pp. 447–477.

Razlighi, Q.R., Oh, H., Habeck, C., O'Shea, D., Gazes, E., Eich, T., Parker, D.B., Lee, S. & Stern, Y. (2016). Dynamic Patterns of Brain Structure-Behavior Correlation Across the Lifespan. *Cerebral Cortex*. 27 (7). p.pp. 3586–3599.

Reichenberg, A., Caspi, A., Harrington, H., Houts, R., Keefe, R.S.E., Murray, R.M., Poulton, R. & Moffitt, T.E. (2010). Static and dynamic cognitive deficits in childhood preceding adult schizophrenia: A 30-year study. *American Journal of Psychiatry*. 167 (2). p.pp. 160–169.

Roalf, D.R., Quarmley, M., Calkins, M.E., Satterthwaite, T.D., Ruparel, K., Elliott, M. a, Moore, T.M., Gur, R.C.R.E., Gur, R.C.R.E., Moberg, P.J. & Turetsky, B.I. (2016). Temporal Lobe Volume Decrements in Psychosis Spectrum Youths. *Schizophrenia Bulletin*. 43 (3). p.pp. 13–15.

Rooney, W.D., Johnson, G., Li, X., Cohen, E.R., Kim, S.G., Ugurbil, K. & Springer, C.S. (2007). Magnetic field and tissue dependencies of human brain longitudinal 1H2O relaxation in vivo. *Magnetic Resonance in Medicine*. 57 (2). p.pp. 308–318.

Samartzis, L., Dima, D., Fusar-Poli, P. & Kyriakopoulos, M. (2014). White matter alterations in early stages of schizophrenia: A systematic review of diffusion tensor imaging studies. *Journal of Neuroimaging*. 24 (2). p.pp. 101–110.

Sandu, A.-L., Izard, E., Specht, K., Beneventi, H., Lundervold, A. & Ystad, M. (2014). Post-adolescent developmental changes in cortical complexity. *Behavioral and Brain Functions*. 10 (1). p.p. 44.

Sarubbo, S., De Benedictis, A., Maldonado, I.L., Basso, G. & Duffau, H. (2013). Frontal terminations for the inferior fronto-occipital fascicle: Anatomical dissection, DTI study and functional considerations on a multi-component bundle. *Brain Structure and Function*. 218 (1). p.pp. 21–37.

Satterthwaite, T.D., Elliott, M.A., Ruparel, K., Loughead, J., Prabhakaran, K., Calkins, M.E., Hopson, R., Jackson, C., Keefe, J., Riley, M., Mentch, F.D., Sleiman, P., Verma, R., Davatzikos, C., Hakonarson, H., Gur, R.C. & Gur, R.E. (2014). Neuroimaging of the Philadelphia Neurodevelopmental Cohort. *NeuroImage*. 86 p.pp. 544–553.

Satterthwaite, T.D., Vandekar, S.N., Wolf, D.H., Bassett, D.S., Ruparel, K., Shehzad, Z., Craddock, R.C., Shinohara, R.T., Moore, T.M., Gennatas, E.D., Jackson, C., Roalf, D.R., Milham, M.P., Calkins, M.E., Hakonarson, H., Gur, R.C. & Gur, R.E. (2015). Connectome-wide network analysis of youth with Psychosis-Spectrum symptoms. *Molecular psychiatry*. 20 (12). p.pp. 1508–1515.

Satterthwaite, T.D., Wolf, D.H., Calkins, M.E., Vandekar, S.N., Erus, G., Ruparel, K., Roalf, D.R., Linn, K.A., Elliott, M.A., Moore, T.M., Hakonarson, H., Shinohara, R.T., Davatzikos, C., Gur, R.E. & Gur, R.C. (2016). Structural Brain Abnormalities in Youth With Psychosis Spectrum Symptoms. *JAMA Psychiatry*. 73 (5). p.pp. 515–524.

Schaer, M., Cuadra, M.B., Schmansky, N., Fischl, B., Thiran, J.-P. & Eliez, S. (2012). How to Measure Cortical Folding from MR Images: a Step-by-Step Tutorial to Compute Local Gyrification Index. *Journal of Visualized Experiments*. (59). p.pp. e3417–e3417.

Schizophrenia Working Group of the Psychiatric Genomics Consortium (2014). Biological insights from 108 schizophrenia-associated genetic loci. *Nature*. 511 (7510). p.pp. 421–427.

Schlösser, R., Gesierich, T., Kaufmann, B., Vucurevic, G., Hunsche, S., Gawehn, J. & Stoeter, P. (2003). Altered effective connectivity during working memory performance in schizophrenia: A study with fMRI and structural equation modeling. *NeuroImage*. 19 (3). p.pp. 751–763.

Schmidt, A., Diwadkar, V.A., Smieskova, R., Harrisberger, F., Lang, U.E., McGuire, P., Fusar-Poli, P. & Borgwardt, S. (2014a). Approaching a network connectivity-driven classification of the psychosis continuum: a selective review and suggestions for future research. *Frontiers in Human Neuroscience*. 8. p.pp. 1–16.

Schmidt, A., Smieskova, R., Aston, J., Simon, A., Allen, P., Fusar-Poli, P., McGuire, P.K., Riecher-Rössler, A., Stephan, K.E., Borgwardt, S., Riecher-Rossler, A., Stephan, K.E. & Borgwardt, S. (2013). Brain connectivity abnormalities predating the onset of psychosis: correlation with the effect of medication. *JAMA Psychiatry*. 70 (9). p.pp. 903–912.

Schmidt, A., Smieskova, R., Simon, A., Allen, P., Fusar-Poli, P., McGuire, P.K., Bendfeldt, K., Aston, J., Lang, U.E., Walter, M., Radue, E.W., Riecher-Rössler, A., Borgwardt, S.J., Riecher-Rossler, A. & Borgwardt, S.J. (2014b). Abnormal effective connectivity and psychopathological symptoms in the psychosis high-risk state. *Journal of Psychiatry and Neuroscience*. 39 (4). p.pp. 239–248.

de Schotten, M.T., Dell'Acqua, F., Forkel, S.J., Simmons, A., Vergani, F., Murphy, D.G.M. & Catani, M. (2011). A lateralized brain network for visuospatial attention. *Nature Neuroscience*. 14 (10). p.pp. 1245–1246.

Schultz, C.C., Koch, K., Wagner, G., Roebel, M., Nenadic, I., Gaser, C., Schachtzabel, C., Reichenbach, J.R., Sauer, H. & Schlösser, R.G.M. (2010). Increased parahippocampal and lingual gyrification in first-episode schizophrenia. *Schizophrenia Research*. 123 (2). p.pp. 137–144.

Schultz, C.C., Wagner, G., Koch, K., Gaser, C., Roebel, M., Schachtzabel, C., Nenadic, I.,

Reichenbach, J.R., Sauer, H. & Schlösser, R.G.M. (2013). The visual cortex in schizophrenia: Alterations of gyrification rather than cortical thickness - A combined cortical shape analysis. *Brain Structure and Function*. 218 (1). p.pp. 51–58.

Seidman, L.J., Thermenos, H.W., Poldrack, R.A., Peace, N.K., Koch, J.K., Faraone, S. V & Tsuang, M.T. (2006). Altered brain activation in dorsolateral prefrontal cortex in adolescents and young adults at genetic risk for schizophrenia: An fMRI study of working memory. *Schizophrenia Research*. 85 (1–3). p.pp. 58–72.

Seitz, J., Zuo, J.X., Lyall, A.E., Makris, N., Kikinis, Z., Bouix, S., Pasternak, O., Fredman, E., Duskin, J., Goldstein, J.M., Petryshen, T.L., Mesholam-Gately, R.I., Wojcik, J., Mccarley, R.W., Seidman, L.J., Shenton, M.E., Koerte, I.K. & Kubicki, M. (2016). Tractography analysis of 5 white matter bundles and their clinical and cognitive correlates in early-course schizophrenia. *Schizophrenia Bulletin*. 42 (3). p.pp. 762–771.

Shaffer, D., Fisher, P., Lucas, C.P., Dulcan, M.K. & Schwab-Stone, M.E. (2000). NIMH Diagnostic Interview Schedule for Children Version IV (NIMH DISC-IV): description, differences from previous versions, and reliability of some common diagnoses. *Journal of the American Academy of Child and Adolescent Psychiatry*. 39 (1). p.pp. 28–38.

Shaw, P., Greenstein, D., Lerch, J., Clasen, L., Lenroot, R., Gogtay, N., Evans, a, Rapoport, J. & Giedd, J. (2006). Intellectual ability and cortical development in children and adolescents. *Nature*. 440 (7084). p.pp. 676–679.

Shaw, P., Kabani, N.J., Lerch, J.P., Eckstrand, K., Lenroot, R., Gogtay, N., Greenstein, D., Clasen, L., Evans, A., Rapoport, J.L., Giedd, J.N. & Wise, S.P. (2008). Neurodevelopmental trajectories of the human cerebral cortex. *The Journal of Neuroscience*. 28 (14). p.pp. 3586–3594.

Shim, G., Oh, J.S., Jung, W., Jang, J., Choi, C.-H., Kim, E., Park, H.-Y., Choi, J.-S., Jung, M. & Kwon, J. (2010). Altered resting-state connectivity in subjects at ultra-high risk for psychosis: an fMRI study. *Behavioral and Brain Functions*. 6 (1). p.p. 58.

Silva, P.A. (1990). The Dunedin Multidisciplinary Health and Development Study: a 15 year longitudinal study. *Paediatric and Perinatal Epidemiology*. 4 (1). p.pp. 76–107.

Simon, A.E., Cattapan-Ludewig, K., Zmilacher, S., Arbach, D., Gruber, K., Dvorsky, D.N., Roth, B., Isler, E., Zimmer, A. & Umbricht, D. (2007). Cognitive functioning in the schizophrenia prodrome. *Schizophrenia Bulletin*. 33 (3). p.pp. 761–771.

Smallman, R.P., Barkus, E., Azadbakht, H., Embleton, K. V., Haroon, H.A., Lewis, S.W., Morris, D.M., Parker, G.J. & Rushe, T.M. (2014). MRI diffusion tractography study in individuals with schizotypal features: A pilot study. *Psychiatry Research: Neuroimaging*. 221 (1). p.pp. 49–57.

Smieskova, R., Allen, P., Simon, A., Aston, J., Bendfeldt, K., Drewe, J., Gruber, K., Gschwandtner, U., Klarhoefer, M., Lenz, C., Scheffler, K., Stieglitz, R.D., Radue, E.W., Mcguire, P., Riecher-Rössler, A. & Borgwardt, S.J. (2012a). Different duration of at-risk mental state associated with neurofunctional abnormalities. A multimodal imaging study. *Human Brain Mapping*. 33 (10). p.pp. 2281–2294.

Smieskova, R., Fusar-Poli, P., Allen, P., Bendfeldt, K., Stieglitz, R.D., Drewe, J., Radue, E.W., McGuire, P.K., Riecher-Rössler, A. & Borgwardt, S.J. (2010). Neuroimaging predictors of transition to psychosis-A systematic review and meta-analysis. *Neuroscience and Biobehavioral Reviews*. 34 (8). p.pp. 1207–1222.

Smieskova, R., Fusar-Poli, P., Riecher-Rössler, A. & Borgwardt, S. (2012b). Neuroimaging and Resilience Factors - Staging of the At-risk Mental State? *Current Pharmaceutical Design*. 18 (4). p.pp. 416–421.

Smith, S.M., Jenkinson, M., Johansen-Berg, H., Rueckert, D., Nichols, T.E., Mackay, C.E., Watkins, K.E., Ciccarelli, O., Cader, M.Z., Matthews, P.M. & Behrens, T.E.J. (2006). Tract-based spatial statistics: Voxelwise analysis of multi-subject diffusion data. *NeuroImage*. 31 (4). p.pp. 1487–1505.

Sprooten, E., Papmeyer, M., Smyth, A.M., Vincenz, D., Honold, S., Conlon, G.A., Moorhead, T.W.J., Job, D., Whalley, H.C., Hall, J., McIntosh, A.M., Owens, D.C.G., Johnstone, E.C. & Lawrie, S.M. (2013). Cortical thickness in first-episode schizophrenia patients and individuals at high familial risk: A cross-sectional comparison. *Schizophrenia Research*. 151 (1). p.pp. 259–264.

Stanfield, A.C., Moorhead, T.W.J., Harris, J.M., Owens, D.G.C., Lawrie, S.M. & Johnstone, E.C. (2008). Increased Right Prefrontal Cortical Folding in Adolescents at Risk of Schizophrenia for Cognitive Reasons. *Biological Psychiatry*. 63 (1). p.pp. 80–85.

Stephan, K.E., Baldeweg, T. & Friston, K.J. (2006a). Synaptic Plasticity and Dysconnection in Schizophrenia. *Biological Psychiatry*. 59 (10) p.pp. 929–939.

Stephan, K.E., Friston, K.J., Frith, C.D., Baldeweg, T. & Friston, K.J. (2006b). Dysconnection in Schizophrenia: From abnormal synaptic plasticity to failures of self-monitoring. *Schizophrenia Bulletin*. 35 (10) p.pp. 509–527.

Stephan, K.E., Penny, W.D., Daunizeau, J., Moran, R.J. & Friston, K.J. (2009). Bayesian model selection for group studies. *Neuroimage*. 46 (4). p.pp. 1004–1017.

Tamnes, C.K., Østby, Y., Fjell, A.M., Westlye, L.T., Due-Tønnessen, P. & Walhovd, K.B. (2010). Brain maturation in adolescence and young adulthood: Regional age-related changes in cortical thickness and white matter volume and microstructure. *Cerebral Cortex*. 20 (3). p.pp. 534–548.

Tandon, R. (2016). Conceptualizing psychotic disorders: don't throw the baby out with the bathwater. *World Psychiatry*. 15 (2). p.pp. 133–134.

Tau, G.Z. & Peterson, B.S. (2010). Normal development of brain circuits. *Neuropsychopharmacology*. 35 (1). p.pp. 147–168.

Terwisscha van Scheltinga, A.F., Bakker, S.C., van Haren, N.E.M., Derks, E.M., Buizer-Voskamp, J.E., Boos, H.B.M., Cahn, W., Hulshoff Pol, H.E., Ripke, S., Ophoff, R.A. & Kahn, R.S. (2013). Genetic schizophrenia risk variants jointly modulate total brain and white matter volume. *Biological Psychiatry*. 73 (6). p.pp. 525–531.

The Mathworks Inc. (2016). *MATLAB - MathWorks*. [Online]. 2016. www.mathworks.com/products/matlab. Available from: http://www.mathworks.com/products/matlab/.

Tournier, J.D., Calamante, F., Gadian, D.G. & Connelly, A. (2004). Direct estimation of the fiber orientation density function from diffusion-weighted MRI data using spherical deconvolution. *NeuroImage*. 23 (3). p.pp. 1176–1185.

Tuch, D.S., Reese, T.G., Wiegell, M.R., Makris, N., Belliveau, J.W. & Van Wedeen, J. (2002). High angular resolution diffusion imaging reveals intravoxel white matter fiber heterogeneity. *Magnetic Resonance in Medicine*. 48 (4). p.pp. 577–582.

Valli, I., Tognin, S., Fusar-Poli, P. & Mechelli, A. (2012). Episodic Memory Dysfunction in Individuals at High-Risk of Psychosis: A Systematic Review of Neuropsychological and Neurofunctional Studies. *Current Pharmaceutical Design*. 18 (4). p.pp. 443–458.

Varghese, D., Scott, J., Welham, J., Bor, W., Najman, J., O'Callaghan, M., Williams, G. & McGrath, J. (2011). Psychotic-like experiences in major depression and anxiety disorders: A population-based survey in young adults. *Schizophrenia Bulletin*. 37 (2). p.pp. 389–393.

Vijayakumar, N., Bartholomeusz, C., Whitford, T., Hermens, D.F., Nelson, B., Rice, S., Whittle, S., Pantelis, C., McGorry, P. & Schäfer, M.R. (2016). White matter integrity in individuals at ultra-high risk for psychosis: a systematic review and discussion of the role of polyunsaturated fatty acids. *BMC Psychiatry*. 16 (1). p.p. 287.

Vita, A., De Peri, L., Deste, G. & Sacchetti, E. (2012). Progressive loss of cortical gray matter in schizophrenia: a meta-analysis and meta-regression of longitudinal MRI studies. *Translational psychiatry*. 2 (11). p.p. e190.

Wakana, S., Caprihan, A., Panzenboeck, M.M., Fallon, J.H., Perry, M., Gollub, R.L., Hua, K., Zhang, J., Jiang, H., Dubey, P., Blitz, A., van Zijl, P. & Mori, S. (2007). Reproducibility of quantitative tractography methods applied to cerebral white matter. *NeuroImage*. 36 (3). p.pp. 630–644.

Walker, E.F., Trotman, H.D., Goulding, S.M., Holtzman, C.W., Ryan, A.T., McDonald, A., Shapiro, D.I. & Brasfield, J.L. (2013). Developmental mechanisms in the prodrome to psychosis. *Development and Psychopathology*. 25 (4pt2). p.pp. 1585–1600.

Walterfang, M., Wood, A.G., Reutens, D.C., Wood, S.J., Chen, J., Velakoulis, D., McGorry, P.D. & Pantelis, C. (2008a). Morphology of the corpus callosum at different stages of schizophrenia: Cross-sectional study in first-episode and chronic illness. *British Journal of Psychiatry*. 192 (6). p.pp. 429–434.

Walterfang, M., Wood, S.J., Velakoulis, D. & Pantelis, C. (2006). Neuropathological, neurogenetic and neuroimaging evidence for white matter pathology in schizophrenia. *Neuroscience and Biobehavioral Reviews*. 30 (7) p.pp. 918–948.

Walterfang, M., Yung, A., Wood, A.G., Reutens, D.C., Phillips, L., Wood, S.J., Chen, J., Velakoulis, D., McGorry, P.D. & Pantelis, C. (2008b). Corpus callosum shape alterations in individuals prior to the onset of psychosis. *Schizophrenia Research*. 103 (1). p.pp. 1–10.

Walton, E., Geisler, D., Lee, P.H., Hass, J., Turner, J.A., Liu, J., Sponheim, S.R., White, T., Wassink, T.H., Roessner, V., Gollub, R.L., Calhoun, V.D. & Ehrlich, S. (2014). Prefrontal inefficiency is associated with polygenic risk for schizophrenia. *Schizophrenia Bulletin*. 40 (6). p.pp. 1263–1271.

Wechsler, D., Golombok, S. & Rust, J. (1992). *Wechsler Intelligence Scale for Children (WISC–III UK)*. Sidcup, United Kingdom: The Psychological Corporation.

Weinberger, D.R. (1993). A connectionist approach to the prefrontal cortex. *Journal of Neuropsychiatry & Clinical Neurosciences*. 5 (3). p.pp. 241–253.

Westbrook, C. & Kaut, C. (1998). *MRI in Practice*. Oxford: Wiley-Blackwell.

Whalley, H.C., Simonotto, E., Marshall, I., Owens, D.G.C., Goddard, N.H., Johnstone, E.C. & Lawrie, S.M. (2005). Functional disconnectivity in subjects at high genetic risk of schizophrenia. *Brain*. 128 (9). p.pp. 2097–2108.

Wheeler, A.L. & Voineskos, A.N. (2014). A review of structural neuroimaging in schizophrenia: from connectivity to connectomics. *Frontiers in Human Neuroscience*. 8. p.pp. 1–18.

White, T. & Gottesman, I. (2012). Brain connectivity and gyrification as endophenotypes for schizophrenia: weight of the evidence. *Current Topics in Medicinal Chemistry*. 12 (21). p.pp. 2393–403.

White, T. & Hilgetag, C.C. (2011). Gyrification and neural connectivity in schizophrenia. *Development and Psychopathology*. 23 (1). p.pp. 339–352.

White, T., Su, S., Schmidt, M., Kao, C.Y. & Sapiro, G. (2010). The development of gyrification in childhood and adolescence. *Brain and Cognition*. 72 (1) p.pp. 36–45.

Whitford, T.J., Kubicki, M., Schneiderman, J.S., O'Donnell, L.J., King, R., Alvarado, J.L., Khan, U., Markant, D., Nestor, P.G., Niznikiewicz, M., McCarley, R.W., Westin, C.-F. & Shenton, M.E. (2010). Corpus Callosum Abnormalities and Their Association with Psychotic Symptoms in Patients with Schizophrenia. *Biological Psychiatry*. 68 (1). p.pp. 70–77.

Wing, J.K., Babor, T., Brugha, T., Burke, J., Cooper, J.E., Giel, R., Jablenski, A., Regier, D. & Sartorius, N. (1990). SCAN. Schedules for Clinical Assessment in Neuropsychiatry. *Archives of General Psychiatry*. 47 (6). p.pp. 589–93.

Wolf, D.H., Gur, R.C., Valdez, J.N., Loughead, J., Elliott, M.A., Gur, R.E. & Ragland, J.D. (2007). Alterations of fronto-temporal connectivity during word encoding in schizophrenia. *Psychiatry Research: Neuroimaging*. 154 (3). p.pp. 221–232.

Wolf, D.H., Satterthwaite, T.D., Calkins, M.E., Ruparel, K., Elliott, M. a, Hopson, R.D., Jackson, C.T., Prabhakaran, K., Bilker, W.B., Hakonarson, H., Gur, R.C. & Gur, R.E. (2015). Functional neuroimaging abnormalities in youth with psychosis spectrum symptoms. *JAMA psychiatry*. 72 (5). p.pp. 456–65.

Wood, S.J., Pantelis, C., Velakoulis, D., Yücel, M., Fornito, A. & McGorry, P.D. (2008). Progressive changes in the development toward schizophrenia: Studies in subjects at increased symptomatic risk. *Schizophrenia Bulletin*. 34 (2). p.pp. 322–329.

Woodberry, K. a., Giuliano, A.J. & Seidman, L.J. (2008). Premorbid IQ in schizophrenia: a meta-analytic review. *American Journal of Psychiatry*. 165 (5). p.pp. 579–587.

Worsley, K.J., Marrett, S., Neelin, P., Vandal, A.C., Friston, K.J. & Evans, A.C. (1996). A unified statistical approach for determining significant signals in images of cerebral activation. *Human Brain Mapping*. 4 (1). p.pp. 58–73.

Wu, Y., Sun, D., Wang, Y. & Wang, Y. (2016). Subcomponents and Connectivity of the Inferior Fronto-Occipital Fasciculus Revealed by Diffusion Spectrum Imaging Fiber Tracking. *Frontiers in Neuroanatomy*. 10. p.pp. 1–13.

Yung, A., Phillips, L., McGorry, P., McFarlane, C., Francey, S., Harrigan, S., Patton, G. & Jackson, H. (1998). Prediction of psychosis: A step towards indicated prevention of schizophrenia. *British Journal of Psychiatry. Supplement*. 172 (33). p.pp. 14–20.

Yung, A.R., Buckby, J.A., Cosgrave, E.M., Killackey, E.J., Baker, K., Cotton, S.M. & McGorry, P.D. (2007). Association between psychotic experiences and depression in a clinical sample over 6 months. *Schizophrenia Research*. 91 (1). p.pp. 246–53.

Yung, A.R. & Lin, A. (2016). Psychotic experiences and their significance. *World Psychiatry*. 15 (2) p.pp. 130–131.

Zammit, S., Hamshere, M., Dwyer, S., Georgiva, L., Timpson, N., Moskvina, V., Richards, A., Evans, D.M., Lewis, G., Jones, P., Owen, M.J. & O'Donovan, M.C. (2013a). A Population-Based Study of Genetic Variation and Psychotic Experiences in Adolescents. *Schizophrenia Bulletin*. 40 (6). p.pp. 1254–1262.

Zammit, S., Kounali, D., Cannon, M., David, A.S., Gunnell, D., Heron, J., Jones, P.B., Lewis, S., Sullivan, S., Wolke, D. & Lewis, G. (2013b). Psychotic Experiences and Psychotic Disorders at Age 18 in Relation to Psychotic Experiences at Age 12 in a Longitudinal Population-Based Cohort Study. *American Journal of Psychiatry*. 170 (7). p.pp. 742–750.

Zhang, H., Wei, X., Tao, H., Mwansisya, T.E., Pu, W., He, Z., Hu, A., Xu, L., Liu, Z., Shan, B. & Xue, Z. (2013). Opposite Effective Connectivity in the Posterior Cingulate and Medial Prefrontal Cortex between First-Episode Schizophrenic Patients with Suicide Risk and Healthy Controls. *PLoS ONE*. 8 (5). p.p. e63477.

Zilles, K., Palomero-gallagher, N. & Amunts, K. (2013). Development of cortical folding during evolution and ontogeny. *Trends in Neurosciences*. 36 (5). p.pp. 275–284.

Appendix A

A.1 Reported psychotic experiences in individuals with transient or persistent PEs per domain

Table A.1.1. Reported psychotic experiences (PEs) at ages 18 and 20 in each group. Individuals with transient PEs had PEs at either age 18 or age 20. Those with persistent PEs had PEs at both age 18 and age 20.

	Transient PEs (n = 36)		Persistent PEs (n = 35)	
Age	18	20	18	20
n	27 (75%)	9 (25%)	35 (100%)	35 (100%)
Rated Psychotic Experiences				
Thought Interference (TI)	3 (11.1%)	0 (0%)	1 (2.9%)	1 (2.9%)
Delusions (DL)	2 (7.4%)	7 (77.8%)	4 (11.4%)	2 (5.7%)
Hallucinations (HAL)	14 (51.9%)	1 (11.1%)	20 (57.1%)	20 (57.1%)
TI and DL	0 (0%)	0 (0%)	0 (0%)	0 (0%)
TI and HAL	5 (18.6%)	1 (11.1%)	5 (14.3)	5 (14.3)
DL and HAL	2 (7.4%)	0 (0%)	2 (5.7%)	3 (8.6%)
TI and DL and HAL	1 (3.7%)	0 (0%)	3 (8.6%)	4 (11.4%)

A.2 N-back task performance

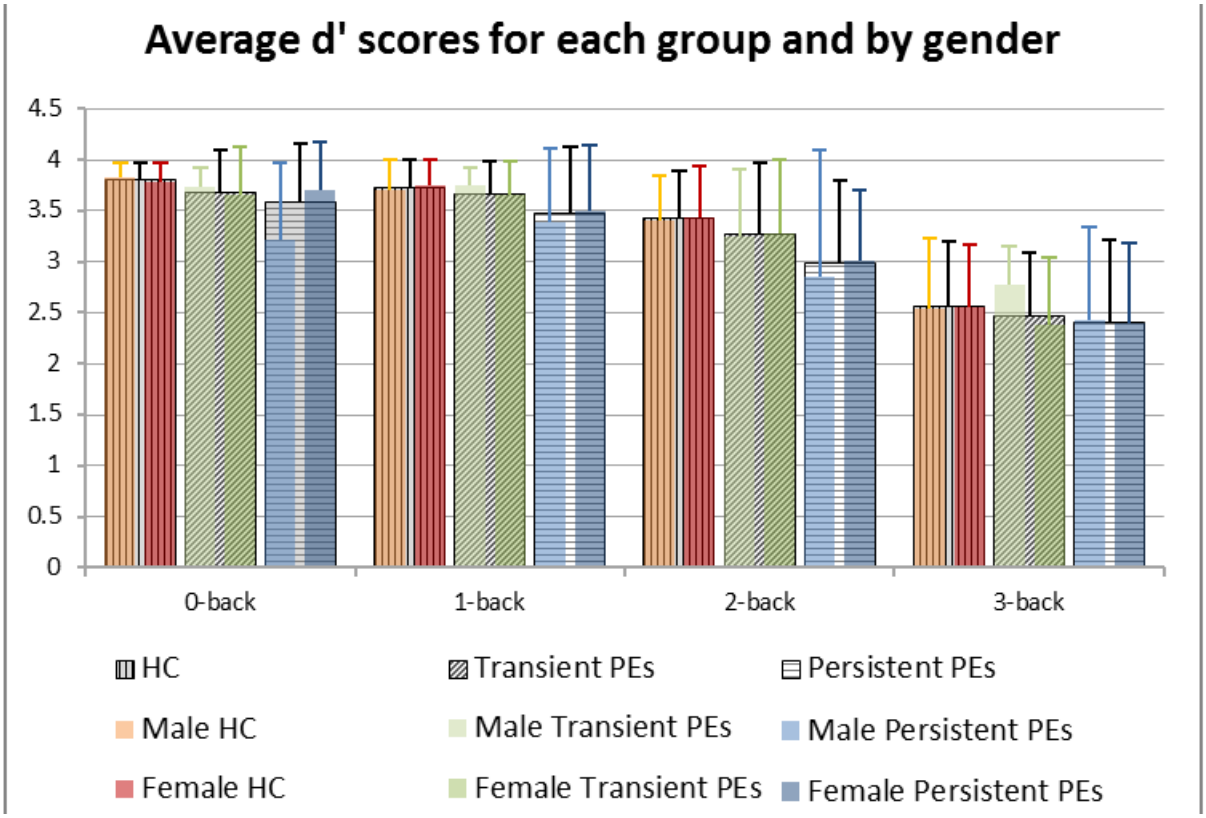

Figure A.2.1 Average performance on the n-back task as a measure of d' (range -3.85 to 3.85) per condition for each group and further split by gender within each group.

A.3 Increased BOLD Signal during the N-back task

Table A.3.1. Task-elicited increases in BOLD response across conditions and groups. Statistics are provided for cluster peak coordinates and local maxima in each cluster that are more than 8mm apart are noted underneath.

Region	Size (voxels)	MNI Coordinates			t-value	p-value[a]
		X	Y	Z		
R Inferior Parietal Lobule	353670	46	-46	47	22.46	<0.001
R Inferior Parietal Lobule		38	-55	42		
R Superior Occipital Lobule		33	-64	41		
R Inferior Frontal Gyrus	141970	33	20	-2	20.99	<0.001
R Anterior Cingulate Cortex		5	19	45		
L Supplementary Motor Area		-5	17	44		
L Inferior Parietal Lobule	288650	-36	-47	38	19.70	<0.001
L Inferior Parietal Lobule		-30	-57	42		
L Inferior Parietal Lobule		-39	-55	50		
R Cerebellum Crus I	135570	32	-64	-34	16.45	<0.001
L Cerebellum Crus I		-31	-65	-36		
L Cerebellum Crus II		-8	-78	-33		
L Putamen	3030	-17	0	14	8.24	<0.001
L Pallidum		-15	-1	3		
L Thalamus		-14	-10	0		

[a] Family-wise error corrected p-value to account for multiple comparisons

Table A.3.1. Continued from previous page

Region	Size (voxels)	MNI Coordinates			t-value	p-value[a]
		X	Y	Z		
R Inferior Temporal Gyrus	885	58	-44	-15	7.47	<0.001
R Middle Temporal Gyrus		64	-36	-10		
R Middle Temporal Gyrus		46	-30	-13		
R Caudate Nucleus	4013	16	-2	16	7.44	<0.001
R Pallidum		16	2	-1		
R Thalamus		13	-8	1		
R Cerebellum Vermis	7489	1	-47	-22	7.22	<0.001
L Cerebellum Anterior Lobe		-7	-51	-35		
R Cerebellum Anterior Lobe		5	-40	-25		
L Inferior Occipital Gyrus	416	-35	-91	-14	5.99	0.002
L Middle Occipital Gyrus	558	-44	-67	-16	5.73	0.001

[a] Family-wise error corrected p-value to account for multiple comparisons

Table A.3.2. Clusters that show a quadratic increase in BOLD response within the functionally defined working memory network that is strongest during the 2-back condition. Cluster p-values are provided and t-statistics for cluster peak coordinates. Local maxima in each cluster more than 8mm apart are noted underneath.

Region	Size (voxels)	MNI Coordinates			t-value	p-value[a]
		X	Y	Z		
L Middle Frontal Gyrus	116052	-27	0	52	11.86	<0.001
R Middle Frontal Gyrus		29	7	52		
L Precentral Gyrus		-43	0	43		
L Inferior Parietal Lobule	278500	-36	-46	38	11.72	<0.001
L Superior Parietal Lobule		-30	-64	44		
L Inferior Parietal Lobule		-38	-56	50		
R Inferior Parietal Lobule	30202	44	-45	48	10.97	<0.001
R Supramarginal Gyrus		41	-44	37		
R Superior Parietal Lobule		32	-66	44		
L Cerebellum Crus I	10882	-31	-65	-36	9.59	<0.001
R Cerebellum Crus I		30	-65	-33		
L Cerebellum Crus II		-7	-79	-32		
L Putamen	2702	-18	0	15	7.64	<0.001
L Pallidum		-18	1	0		

[a] Family-wise error corrected p-value to account for multiple comparisons

Table A.3.2. Continued from previous page

Region	Size (voxels)	MNI Coordinates			t-value	p-value[a]
		X	Y	Z		
R Caudate Nucleus	1076	19	-1	16	7.23	<0.001
R Thalamus		15	-9	8		
L Inferior Occipital Gyrus	556	-48	-65	-15	7.22	0.001
R Cerebellum Vermis	318	0	-50	-22	5.00	0.004
R Globus Pallidus	201	15	-3	-3	4.89	0.008
R Pallidum		19	5	3		
R Inferior Temporal Gyrus	94	52	-55	-16	5.50	0.017
R Inferior Temporal Gyrus		57	-47	-15		

[a] Family-wise error corrected p-value to account for multiple comparisons

Table A.3.3. Clusters that show a linear increase in BOLD response within the functionally defined working memory network where the response is stronger during the 3-back condition relative to the 1-back condition and the 2-back condition is assumed to lie intermediate. Cluster p-values are provided and t-statistics for cluster peak coordinates. Local maxima more than 8mm apart are noted underneath.

Region	Size (voxels)	MNI Coordinates			t-value	p-value[a]
		X	Y	Z		
R Middle Frontal Gyrus	134500	27	10	53	20.42	<0.001
R Medial Superior Frontal Gyrus		5	21	43		
L Supplementary Motor Area		-6	18	44		
R Inferior Parietal Lobule	344740	47	-45	41	17.30	<0.001
R Precuneus		12	-68	48		
R Superior Occipital Gyrus		33	-67	40		
L Inferior Parietal Lobule	267600	-37	-50	38	16.22	<0.001
L Inferior Parietal Lobule		-32	-60	42		
L Precuneus		-9	-68	47		
L Cerebellum Crus I	4821	-32	-65	-35	12.65	<0.001
L Cerebellum Crus II		-9	-79	-32		
R Cerebellum Crus II		9	-78	-31		
R Cerebellum Crus I	3405	33	-64	-34	11.49	<0.001
L Putamen	2845	-15	1	15	10.55	<0.001
L Pallidum		-15	0	-1		

[a] Family-wise error corrected p-value to account for multiple comparisons

Table A.3.3. Continued from previous page

Region	Size (voxels)	MNI Coordinates			t-value	p-value[a]
		X	Y	Z		
R Pallidum	3832	15	2	-2	9.28	<0.001
R Caudate Nucleus		14	1	16		
R Pallidum		15	0	6		
L Mesencaphalon	2040	-4	-31	-21	7.13	<0.001
R Mesencaphalon		4	-30	-21		
L Substantia Nigra		-7	-15	-12		
R Inferior Temporal Lobe	483	57	-42	-15	6.45	0.002
R Middle Temporal Lobe		64	-36	-10		
R Cerebellum Vermis	127	0	-48	-22	5.06	0.013

[a] Family-wise error corrected p-value to account for multiple comparisons

Appendix B

B.1 Summary of additional findings on cortical morphometry

As mentioned in chapter 4, this section of the appendix provides detailed information on the results from the initial vertex-based analysis of gyrification in relation to psychotic experiences (PEs), and provides the output from the different general linear model (GLM) that were used to assess the microstructure of the tracts segmented using atlas-based tractography.

Table B.1.1. Summary of brain regions where gyrification was associated with PEs

Effect	Region	Cluster Size (mm^2)	MNI Coordinates			CWP-value[a]	Z-score[b]
			X	Y	Z		
PEs	L Middle Temporal Gyrus	505.1	-54.7	0.4	-28.5	0.0066	1.92
PEs & TBV	R Caudal Middle Frontal Gyrus	2233.6	29.0	24.1	41.8	0.0002	2.63
PEs & TBV	L Lingual Gyrus	1476.4	-12.1	-90.9	-8.4	0.0002	2.63
PEs & TBV	L Lateral Occipital Gyrus	467.9	-26.6	-65.2	3.4	0.0100	1.82

[a] Cluster-wise corrected p-value based on a precomputed Monte Carlo simulation with a z-distribution with a vertex-wise threshold of $p < 0.001$ and a cluster threshold of $p < 0.05$.

[b] Computed based on the cluster-wise p-value

B.2 Output from Initial Model Testing for Streamlines Identified using Atlas-based Tractography

Table B.2.1. Summary of the diffusion metrics in each group, reported as median and interquartile range. Test statistic is given for an F test comparing the linear fit of the general linear model to the constant model.

		Healthy Controls	Transient PEs	Persistent PEs	Test Statistic	
		n = 78	n = 52	n = 48	$F_{(1)}$	p
L Lateral Occipital Gyrus	Length (mm)	113.5±36.5	117.3±35.5	127.5±36.5	1.47	0.149
	Streamlines	939±378	931±393	951±423.5	1.80	0.057
	Volume (mm^3)	36911.1 ±13565.1	36386.3 ±11438.2	36858.4 ±14300.9	2.24	0.015
	FA ($x10^{-1}$)	3.94±0.79	3.82±0.65	3.99±0.58	1.23	0.272
	MD ($x10^{-4}$ mm^2/s^{-1})	8.14±0.26	8.17±0.39	8.18±0.32	1.33	0.214
	AD ($x10^{-3}$ mm^2/s^{-1})	1.23±0.09	1.24±0.05	1.26±0.08	2.85	0.002
	RD ($x10^{-4}mm^2/s^{-1}$)	6.27±0.50	6.28±0.53	6.25±0.45	0.92	0.524
L Precentral Gyrus	Length(mm)	40.0±8.0	40.0±6.3	42.0±5.3	3.29	<0.001
	Streamlines	558±194	542±170.5	586±162	8.11	<0.001
	Volume (mm^3)	16452.9 ±6378.3	15483.6 ±5386.4	16995.3 ±4510.0	8.84	<0.001
	FA ($x10^{-1}$)	2.47±0.48	2.46±0.39	2.44±0.31	2.79	0.002
	MD ($x10^{-4}$ mm^2/s^{-1})	8.08±0.28	8.13±0.38	8.14±0.33	1.54	0.120
	AD ($x10^{-3}$ mm^2/s^{-1})	1.05±0.03	1.06±0.04	1.05±0.03	1.06	0.394
	RD ($x10^{-4}mm^2/s^{-1}$)	7.01±0.34	7.06±0.46	7.02±0.31	2.13	0.021

Table B.2.1. Continued from previous page

		Healthy Controls	Transient PEs	Persistent PEs	Test Statistic	
		n = 78	n = 52	n = 48	$F_{(1)}$	p
R Caudal Middle Frontal Gyrus	Length (mm)	58.0±16.0	57.8±17.5	57.5±16.5	1.27	0.245
	Streamlines	624±154	600±256	591±191	1.54	0.122
	Volume (mm^3)	19360.8 ±5680.2	18406.6 ±7076.4	18313.7 ±5594.8	1.56	0.117
	FA ($x10^{-1}$)	2.98±0.38	3.02±0.42*	2.96±0.49	1.99	0.032
	MD ($x10^{-4}$ mm^2/s^{-1})	6.54±0.31	6.53±0.47	6.66±0.34	1.29	0.235
	AD ($x10^{-3}$ mm^2/s^{-1})	1.09±0.05	1.09±0.05	1.10±0.06	1.89	0.043
	RD ($x10^{-4}mm^2/s^{-1}$)	7.80±0.37	7.85±0.48	7.87±0.46	1.53	0.126
R Rostral Middle Frontal Gyrus	Length (mm)	45.5±14.0	48.8±14.8	45.5±14.3	1.68	0.081
	Streamlines	691±230	738±316	679±199	10.1	<0.001
	Volume (mm^3)	19622.0 ±8246.6	21241.7 ±8982.3	19157.4 ±7026.2	4.47	<0.001
	FA ($x10^{-1}$)	2.96±0.45	2.97±0.34	2.98±0.38	1.85	0.049
	MD ($x10^{-4}$ mm^2/s^{-1})	6.67±0.33	6.64±0.29	6.62±0.29	1.02	0.433
	AD ($x10^{-3}$ mm^2/s^{-1})	1.10±0.06	1.08±0.04	1.10±0.05	3.84	<0.001
	RD ($x10^{-4}mm^2/s^{-1}$)	7.96±0.34	7.88±0.36	7.96±0.40	0.84	0.604
L Middle Temporal Gyrus	Length (mm)	71.8±51.0	72.0±36.0	74.8±45.0	2.16	0.027
	Streamlines	576±208	588±209.5	643±278	5.22	<0.001
	Volume (mm^3)	20711.8 ±9467.0	20716.8 ±7026.2	21738.9 ±8344.5	4.34	<0.001
	FA ($x10^{-1}$)	3.56±0.58	3.57±0.63	3.51±0.46	2.89	0.003
	MD ($x10^{-4}$ mm^2/s^{-1})	8.15±0.27	8.16±0.24	8.12±0.27	0.45	0.909
	AD ($x10^{-3}$ mm^2/s^{-1})	1.14±0.06	1.13±0.05	1.14±0.06	2.52	<0.001
	RD ($x10^{-4}mm^2/s^{-1}$)	6.43±0.42	6.47±0.46	6.47±0.39	1.47	0.161

Table B.2.1 Continued from previous pages

		Healthy Controls	Transient PEs	Persistent PEs	Test Statistic	
		n = 78	n = 52	n = 48	$F_{(1)}$	p
L Medial Orbito-frontal Gyrus	Length (mm)	55.5±13.0	54.3±12.8	60.5±14.0*	2.48	0.007
	Streamlines	875.5±264	790±274	872±271	8.37	<0.001
	Volume (mm^3)	29091.5 ±8733.7	27928.8 ±7626.3	30964.8 ±9575.0	7.67	<0.001
	FA ($x10^{-1}$)	2.45±0.43	2.45±0.37	2.64±0.41*	3.24	<0.001
	MD ($x10^{-4}$ mm^2/s^{-1})	8.32±0.37	8.32±0.31	8.29±0.29	0.74	0.696
	AD ($x10^{-3}$ mm^2/s^{-1})	1.11±0.04	1.11±0.05	1.13±0.05	1.68	0.081
	RD ($x10^{-4}mm^2/s^{-1}$)	7.19±0.44	7.19±0.30	7.04±0.32*	1.88	0.046
L Inferior Parietal Lobule	Length (mm)	45.3±11.5	47.3±10.0	48.0±12.0	0.37	0.966
	Streamlines	406±204	413±196	383±155	3.50	<0.001
	Volume (mm^3)	12917.3 ±6860.4	13359.2 ±6516.4	12661.1 ±6009.1	2.57	0.005
	FA ($x10^{-1}$)	2.86±0.63	3.04±0.65	3.05±0.48	1.89	0.045
	MD ($x10^{-4}$ mm^2/s^{-1})	7.73±0.26	7.79±0.29	7.73±0.26	0.43	0.940
	AD ($x10^{-3}$ mm^2/s^{-1})	1.02±0.07	1.03±0.06	1.04±0.05	1.62	0.098
	RD ($x10^{-4}mm^2/s^{-1}$)	6.47±0.40	6.46±0.39	6.36±0.47	0.87	0.574
L Post-central Gyrus	Length (mm)	114.0±17.0	113.5±15.3	115.0±13.0	2.04	0.028
	Streamlines	2357±626	2341±606	2423±410	8.65	<0.001
	Volume (mm^3)	65686.2 ±16322.4	64385.4 ±15338.0	67160.2 ±12342.2	10.8	<0.001
	FA ($x10^{-1}$)	3.93±0.31	3.92±0.39	3.95±0.37	1.44	0.161
	MD ($x10^{-4}$ mm^2/s^{-1})	7.70±0.22	7.72±0.27	7.72±0.31	0.84	0.600
	AD ($x10^{-3}$ mm^2/s^{-1})	1.17±0.04	1.18±0.03	1.17±0.04	2.08	0.025
	RD ($x10^{-4}mm^2/s^{-1}$)	5.88±0.31	5.95±0.36	5.93±0.34	0.73	0.709

B.3 Visualisation of Streamlines Projecting from Clusters that show Significant Differences in Diffusion Scalars and Plotted Group-by-Gyrification Interaction Effects

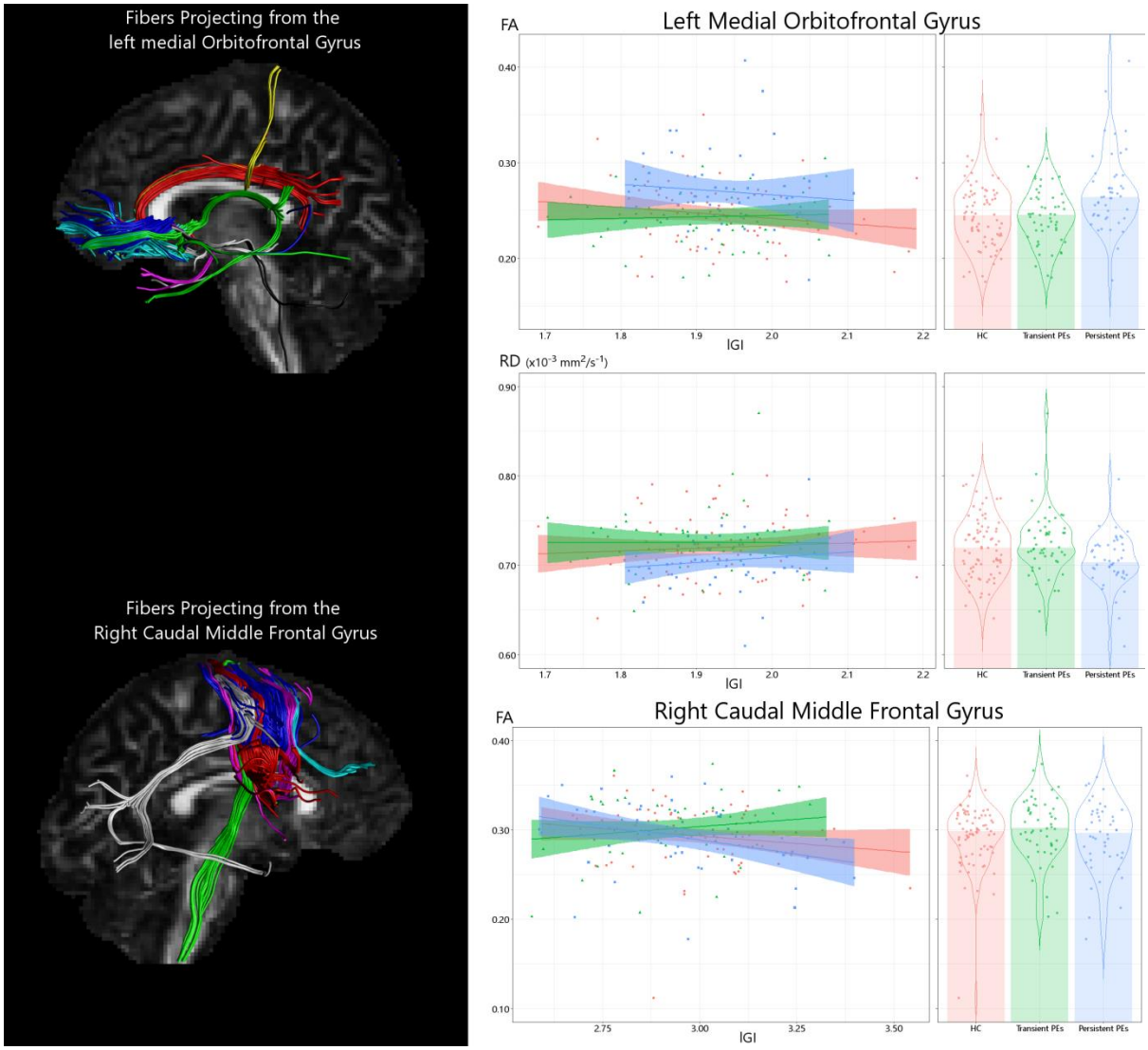

Figure B.3.1. Significant effects identified from atlas-based tractography. Left: Visualisation of streamlines projecting from clusters that were found to differ in terms of gyrification (lGI) as well as fractional anisotropy (FA) and radial diffusivity (RD). Brain maps and streamlines are shown for a single individual. Right: Illustration of the significant effects of group and group-by-gyrification interaction.

Appendix C

C.1 Precision and Recall across Model Configurations

A total of 27 different configurations were applied to the training data and voxel-based comparisons were carried out. The 27 configurations comprised of step-wise increments in the cluster intersect frequency, which represents the frequency of streamlines being assigned to shape in feature space, and the spatial masking thresholds. Frequency cut-off ranged from 0.80 up to 0.95 in steps of 0.05. A different type of masking was applied based on the type of tract; for the Corpus Callosum (CC) we specified spatial masking for the middle of the tract and for the Superior Longitudinal Fasciculus (SLF) and the Inferior Fronto-Occipital Fasciculus (IFOF) we set spatial masking to the terminal points of the streamlines in feature space. The spatial masking thresholds specified how much of the streamlines assigned to the clusters can be found either on the ends of the tract (for the SLF and IFOF) or in the middle (for the CC). The masking threshold was set to 0.6 and increased in steps of 0.05 up to 0.8. A binary threshold, which specifies the masking threshold where each voxel, rather than each streamline, is treated as one unit was set to 0.008 and increased in step of 0.001 up to 0.01. Thus there are 3 settings for each parameter leading to 27 different combinations to be tested. The following figures highlight the precision and recall statistics for each configuration when comparing the results to the manual tractography. As a reminder, precision was calculated as the true positives divided by the total number of positives (true and false) and thus represents the probability that a retrieved voxel is relevant. The recall was calculated as the true positives divided by the true positives and false negatives and represents the probability that a relevant voxel is retrieved.

Table C.1.1. Average Precision (Recall) Statistics for the Corpus Callosum Sections for each of the 27 Model Configurations

Model	Orbito-frontal	Frontal Anterior	Frontal Superior	Frontal Lateral	Parietal	Occipital	Temporal
1	0.567 (0.737)	0.567 (0.737)	0.662 (0.801)	0.378 (0.564)	0.705 (0.712)	0.641 (0.722)	0.387 (0.692)
2	0.568 (0.736)	0.568 (0.736)	0.664 (0.801)	0.389 (0.556)	0.710 (0.710)	0.644 (0.721)	0.390 (0.693)
3	0.573 (0.735)	0.573 (0.735)	0.665 (0.801)	0.397 (0.551)	0.713 (0.709)	0.647 (0.720)	0.390 (0.693)
4	0.609 (0.720)	0.609 (0.720)	0.677 (0.794)	0.421 (0.520)	0.724 (0.698)	0.659 (0.707)	0.418 (0.672)
5	0.607 (0.720)	0.607 (0.721)	0.681 (0.794)	0.435 (0.510)	0.728 (0.695)	0.662 (0.705)	0.424 (0.673)
6	0.604 (0.722)	0.604 (0.722)	0.684 (0.793)	0.447 (0.504)	0.729 (0.694)	0.666 (0.703)	0.432 (0.672)
7	0.645 (0.687)	0.645 (0.687)	0.706 (0.778)	0.495 (0.464)	0.746 (0.674)	0.690 (0.681)	0.467 (0.633)
8	0.646 (0.691)	0.646 (0.691)	0.712 (0.775)	0.510 (0.444)	0.750 (0.668)	0.696 (0.678)	0.478 (0.635)
9	0.646 (0.690)	0.646 (0.690)	0.718 (0.772)	0.534 (0.432)	0.753 (0.664)	0.701 (0.676)	0.482 (0.631)
10	0.539 (0.759)	0.539 (0.759)	0.645 (0.817)	0.338 (0.617)	0.691 (0.724)	0.612 (0.745)	0.365 (0.736)
11	0.541 (0.756)	0.541 (0.756)	0.646 (0.817)	0.349 (0.614)	0.697 (0.721)	0.614 (0.743)	0.367 (0.733)
12	0.543 (0.755)	0.543 (0.755)	0.648 (0.817)	0.358 (0.605)	0.700 (0.721)	0.616 (0.741)	0.367 (0.734)

Table C.1.1. Continued from previous page

Model	Orbito-frontal	Frontal Anterior	Frontal Superior	Frontal Lateral	Parietal	Occipital	Temporal
13	0.574 (0.739)	0.574 (0.739)	0.660 (0.812)	0.388 (0.575)	0.709 (0.713)	0.633 (0.730)	0.399 (0.713)
14	0.576 (0.739)	0.576 (0.739)	0.662 (0.811)	0.398 (0.560)	0.713 (0.709)	0.637 (0.727)	0.400 (0.712)
15	0.575 (0.740)	0.575 (0.740)	0.664 (0.811)	0.407 (0.553)	0.715 (0.707)	0.640 (0.725)	0.410 (0.713)
16	0.607 (0.711)	0.607 (0.711)	0.685 (0.798)	0.451 (0.516)	0.729 (0.691)	0.667 (0.703)	0.454 (0.671)
17	0.608 (0.714)	0.608 (0.714)	0.691 (0.795)	0.467 (0.503)	0.733 (0.684)	0.676 (0.701)	0.465 (0.672)
18	0.611 (0.712)	0.611 (0.712)	0.696 (0.794)	0.484 (0.495)	0.737 (0.680)	0.681 (0.698)	0.467 (0.668)
19	0.507 (0.777)	0.507 (0.777)	0.620 (0.828)	0.309 (0.658)	0.666 (0.739)	0.586 (0.772)	0.354 (0.748)
20	0.508 (0.779)	0.508 (0.779)	0.621 (0.828)	0.319 (0.655)	0.672 (0.738)	0.590 (0.770)	0.358 (0.747)
21	0.509 (0.778)	0.509 (0.778)	0.622 (0.828)	0.328 (0.651)	0.677 (0.737)	0.592 (0.770)	0.359 (0.747)
22	0.535 (0.761)	0.535 (0.761)	0.636 (0.824)	0.368 (0.613)	0.689 (0.731)	0.609 (0.758)	0.389 (0.728)
23	0.542 (0.761)	0.542 (0.761)	0.638 (0.824)	0.380 (0.602)	0.693 (0.727)	0.613 (0.756)	0.395 (0.727)
24	0.543 (0.761)	0.543 (0.761)	0.640 (0.823)	0.388 (0.598)	0.697 (0.727)	0.616 (0.755)	0.400 (0.728)

Table C.1.1. Continued from previous pages

Model	Orbito-frontal	Frontal Anterior	Frontal Superior	Frontal Lateral	Parietal	Occipital	Temporal
25	0.578 (0.737)	0.578 (0.737)	0.660 (0.813)	0.433 (0.554)	0.711 (0.711)	0.646 (0.731)	0.444 (0.694)
26	0.577 (0.738)	0.577 (0.738)	0.666 (0.812)	0.45 (0.542)	0.716 (0.706)	0.656 (0.727)	0.455 (0.691)
27	0.580 (0.736)	0.580 (0.736)	0.671 (0.811)	0.460 (0.534)	0.719 (0.701)	0.661 (0.726)	0.458 (0.687)

Table C.1.2. Precision (Recall) Statistics for the Left and Right Inferior Fronto-Occipital (IFOF) and Superior Longitudinal Fasciculi (SLF) for each of the 27 Model Configurations

Model	Left IFOF	Right IFOF	Left SLF	Right SLF
1	0.685 (0.472)	0.741 (0.598)	0.440 (0.651)	0.445 (0.719)
2	0.699 (0.450)	0.746 (0.574)	0.443 (0.652)	0.446 (0.721)
3	0.710 (0.422)	0.750 (0.575)	0.441 (0.654)	0.444 (0.720)
4	0.723 (0.407)	0.764 (0.543)	0.489 (0.634)	0.496 (0.695)
5	0.725 (0.386)	0.769 (0.522)	0.492 (0.635)	0.495 (0.695)
6	0.752 (0.357)	0.772 (0.524)	0.494 (0.636)	0.496 (0.695)
7	0.770 (0.322)	0.795 (0.472)	0.545 (0.602)	0.558 (0.663)
8	0.772 (0.307)	0.802 (0.448)	0.551 (0.600)	0.565 (0.658)
9	0.783 (0.273)	0.798 (0.455)	0.551 (0.601)	0.563 (0.659)
10	0.679 (0.507)	0.731 (0.608)	0.405 (0.671)	0.415 (0.746)
11	0.69 (0.475)	0.738 (0.585)	0.406 (0.672)	0.417 (0.748)
12	0.697 (0.447)	0.741 (0.585)	0.406 (0.674)	0.413 (0.749)
13	0.709 (0.432)	0.758 (0.550)	0.457 (0.654)	0.468 (0.724)
14	0.718 (0.406)	0.763 (0.530)	0.460 (0.653)	0.467 (0.724)
15	0.736 (0.376)	0.763 (0.533)	0.461 (0.654)	0.467 (0.723)
16	0.756 (0.345)	0.788 (0.480)	0.516 (0.624)	0.530 (0.690)
17	0.754 (0.326)	0.797 (0.458)	0.519 (0.623)	0.535 (0.689)
18	0.77 (0.295)	0.791 (0.464)	0.521 (0.624)	0.533 (0.689)
19	0.664 (0.550)	0.721 (0.629)	0.347 (0.707)	0.383 (0.771)
20	0.675 (0.522)	0.727 (0.604)	0.344 (0.709)	0.383 (0.773)
21	0.684 (0.499)	0.733 (0.609)	0.343 (0.711)	0.38 (0.774)
22	0.695 (0.483)	0.748 (0.570)	0.402 (0.685)	0.438 (0.748)
23	0.703 (0.462)	0.755 (0.551)	0.399 (0.686)	0.436 (0.750)

Table C.1.2. Continued from previous page

Model	Left IFOF	Right IFOF	Left SLF	Right SLF
24	0.717 (0.432)	0.755 (0.553)	0.400 (0.688)	0.435 (0.750)
25	0.740 (0.393)	0.780 (0.503)	0.464 (0.655)	0.502 (0.718)
26	0.737 (0.372)	0.786 (0.483)	0.466 (0.655)	0.503 (0.718)
27	0.751 (0.346)	0.782 (0.486)	0.465 (0.657)	0.502 (0.717)

C.2 Statistical Output for models testing the Effects of PEs and PEs-by-Position Interaction Effects for each Tract

Table C.2.1. Statistical Output for the Corpus Callosum testing for a main effect of group, group-by-position interaction effects and post-hoc testing of significant effects.

		Main Effect of Group	Group x Position Interaction	Transient PEs vs. HC	Persistent PEs vs. HC
Orbito-frontal	FA	$F_{(2, 236)} = 2.63$, $p = 0.075$	$F_{(118, 14101)} = 1.09$, $p = 0.246$		
	MD	$F_{(2, 236)} = 0.86$, 0.424	$F_{(118, 14101)} = 0.76$, P = 0.976		
	AD	$F_{(2, 236)} = 1.56$, $p = 0.213$	$F_{(118, 14101)} = 0.83$, P = 0.912		
	RD	$F_{(2, 236)} = 1.20$, $p = 0.302$	$F_{(118, 14101)} = 0.89$, $p = 0.794$		
Frontal Anterior	FA	$F_{(2, 236)} = 0.77$, $p = 0.463$	$F_{(122, 14579)} = 1.26$, $p = 0.029$		
	MD	$F_{(2, 236)} = 0.19$, $p = 0.827$	$F_{(122, 14579)} = 0.47$, $p = 1.000$		
	AD	$F_{(2, 236)} = 0.55$, $p = 0.579$	$F_{(122, 14579)} = 0.53$, $p = 1.000$		
	RD	$F_{(2, 236)} = 0.17$, $p = 0.845$	$F_{(122, 14579)} = 0.60$, $p = 1.000$		

Table C.2.1 Continued from previous page

		Main Effect of Group	Group x Position Interaction	Transient PEs vs. HC	Persistent PEs vs. HC
Frontal Superior	FA	$F_{(2, 236)} = 0.14$, $p = 0.873$	$F_{(136, 16252)} = 1.45$, $p < 0.001$	$F_{(68, 11832)} = 1.14$, $p = 0.205$	$F_{(68, 11832)} = 2.04$, $p < 0.001$
	MD	$F_{(2, 236)} = 1.02$, $p = 0.362$	$F_{(136, 16252)} = 0.84$, $p = 0.913$		
	AD	$F_{(2, 236)} = 1.50$, $p = 0.226$	$F_{(136, 16252)} = 0.71$, $p = 0.996$		
	RD	$F_{(2, 236)} = 0.79$, $p = 0.456$	$F_{(136, 16252)} = 0.97$, $p = 0.585$		
Frontal Lateral	FA	$F_{(2, 233)} = 2.56$, $p = 0.079$	$F_{(90, 10620)} = 0.834$, $p = 0.870$		
	MD	$F_{(2, 233)} = 0.11$, $p = 0.900$	$F_{(90, 10620)} = 1.07$, $p = 0.316$		
	AD	$F_{(2, 233)} = 0.13$, $p = 0.876$	$F_{(90, 10620)} = 1.29$, $p = 0.035$		
	RD	$F_{(2, 233)} = 0.42$, $p = 0.656$	$F_{(90, 10620)} = 0.94$, $p = 0.641$		
Parietal	FA	$F_{(2, 236)} = 1.56$, $p = 0.213$	$F_{(152, 18164)} = 0.79$, $p = 0.971$		
	MD	$F_{(2, 236)} = 0.75$, $p = 0.471$	$F_{(152, 18164)} = 1.06$, $p = 0.303$		
	AD	$F_{(2, 236)} = 1.03$, $p = 0.360$	$F_{(152, 18164)} = 1.13$, $p = 0.136$		
	RD	$F_{(2, 236)} = 0.87$, $p = 0.421$	$F_{(152, 18164)} = 0.97$, $p = 0.602$		

Table C.2.1 Continued from previous pages

		Main Effect of Group	Group x Position Interaction	Transient PEs vs. HC	Persistent PEs vs. HC
Occipital	FA	$F_{(2, 236)} = 1.34$, $p = 0.263$	$F_{(182, 21749)} = 1.35$, $p = 0.001$	$F_{(91, 15834)} = 2.21$, $p < 0.001$	$F_{(91, 15834)} = 0.70$, $p = 0.986$
	MD	$F_{(2, 236)} = 2.35$, $p = 0.097$	$F_{(182, 21749)} = 1.30$, $p = 0.004$	$F_{(91, 15834)} = 2.21$, $p < 0.001$	$F_{(91, 15834)} = 0.97$, $p = 0.576$
	AD	$F_{(2, 236)} = 2.19$, $p = 0.114$	$F_{(182, 21749)} = 1.10$, $p = 0.169$		
	RD	$F_{(2, 236)} = 2.23$, $p = 0.110$	$F_{(182, 21749)} = 1.34$, $p = 0.001$	$F_{(91, 15834)} = 2.35$ $p < 0.001$	$F_{(91, 15834)} = 0.91$, $p = 0.726$
Temporal	FA	$F_{(2, 233)} = 0.34$, $p = 0.717$	$F_{(170, 20060)} = 0.51$, $p = 1.000$		
	MD	$F_{(2, 233)} = 0.90$, $p = 0.407$	$F_{(170, 20060)} = 1.14$, $p = 0.102$		
	AD	$F_{(2, 233)} = 0.95$, $p = 0.386$	$F_{(170, 20060)} = 1.23$, $p = 0.024$		
	RD	$F_{(2, 233)} = 0.82$, $p = 0.441$	$F_{(170, 20060)} = 1.01$, $p = 0.447$		

Table C.2.2. Statistical Output for the Inferior Fronto-Occipital Fasciculus (IFOF) testing for a main effect of group, group-by-position interaction effects and post-hoc testing of significant effects.

		Main Effect of Group	Group x Position Interaction	Transient PEs vs. HC	Persistent PEs vs. HC
L IFOF	FA	$F_{(2, 235)} = 1.09$, $p = 0.338$	$F_{(188, 22466)} = 1.26$, $p = 0.010$	$F_{(94, 16356)} = 0.40$ $p = 1.000$	$F_{(94, 16356)} = 2.09$, $p < 0.001$
	MD	$F_{(2, 235)} = 2.29$, $p = 0.104$	$F_{(188, 22466)} = 0.98$, $p = 0.557$		
	AD	$F_{(2, 235)} = 0.69$, $p = 0.502$	$F_{(188, 22466)} = 0.88$, $p = 0.890$		
	RD	$F_{(2, 235)} = 2.49$, $p = 0.085$	$F_{(188, 22466)} = 1.39$, $p < 0.001$	$F_{(94, 16356)} = 0.79$, $p = 0.936$	$F_{(94, 16356)} = 2.16$, $p < 0.001$
R IFOF	FA	$F_{(2, 235)} = 0.32$, $p = 0.728$	$F_{(188, 22372)} = 0.50$, $p = 1.000$		
	MD	$F_{(2, 235)} = 0.15$, $p = 0.859$	$F_{(188, 22372)} = 0.76$, $p = 0.994$		
	AD	$F_{(2, 235)} = 0.15$, $p = 0.861$	$F_{(188, 22372)} = 0.60$, $p = 1.000$		
	RD	$F_{(2, 235)} = 0.21$, $p = 0.813$	$F_{(188, 22372)} = 0.74$, $p = 0.997$		

Table C.2.3. Statistical Output for the Superior Longitudinal Fasciculus (SLF) testing for a main effect of group, group-by-position interaction effects and post-hoc testing of significant effects.

		Main Effect of Group	Group x Position Interaction	Transient PEs vs. HC	Persistent PEs vs. HC
L SLF	FA	$F_{(2, 236)} = 1.74$, $p = 0.178$	$F_{(78, 9321)} = 1.60$, $p < 0.001$	$F_{(39, 6786)} = 1.34$, $p = 0.077$	$F_{(39, 6786)} = 1.98$, $p < 0.001$
	MD	$F_{(2, 236)} = 0.31$, $p = 0.733$	$F_{(78, 9321)} = 1.30$, $p = 0.039$		
	AD	$F_{(2, 236)} = 0.3$, $p = 0.707$	$F_{(78, 9321)} = 0.90$, $p = 0.715$		
	RD	$F_{(2, 236)} = 0.60$, $p = 0.550$	$F_{(78, 9321)} = 1.41$, $p = 0.010$	$F_{(39, 6786)} = 1.46$, $p = 0.033$	$F_{(39, 6786)} = 0.90$, $p = 0.658$
R SLF	FA	$F_{(2, 236)} = 2.93$, $p = 0.056$	$F_{(78, 9321)} = 1.16$, $p = 0.163$		
	MD	$F_{(2, 236)} = 1.91$, $p = 0.150$	$F_{(78, 9321)} = 1.59$, $p = 0.001$	$F_{(39, 6786)} = 2.03$, $p < 0.001$	$F_{(39, 6786)} = 0.45$, $p = 0.999$
	AD	$F_{(2, 236)} = 0.82$, $p = 0.442$	$F_{(78, 9321)} = 1.48$, $p = 0.004$	$F_{(39, 6786)} = 1.89$, $p < 0.001$	$F_{(39, 6786)} = 0.47$, $p = 0.998$
	RD	$F_{(2, 236)} = 2.33$, $p = 0.100$	$F_{(78, 9321)} = 1.57$, $p = 0.001$	$F_{(39, 6786)} = 1.9$, $p < 0.001$	$F_{(39, 6786)} = 0.52$, $p = 0.994$

Appendix C.3 Visualisation of the Diffusion Scalars Averaged both per Group and per Individual for the Corpus Callosum, Inferior Fronto-Occipital Fasciculus, and Superior Longitudinal Fasciculus

The following plots highlight the fractional anisotropy (FA; top left), mean diffusivity (MD; top right), axial diffusivity (AD; bottom left), and radial diffusivity (RD; bottom right) along each segmented white matter bundle. The diffusion scalars are depicted in red for healthy controls, green for transient PEs, and blue for persistent PEs. This applies to the individual average diffusion indices along the tract (*the thin lines*), the average taken across the tract (*the dotted lines*), and for the average per group along the tract (*the thicker lines*).

The first seven pages depict the different segmentations of the Corpus Callosum based on the projections of the streamlines (figures C.3.1 - C.3.7). The 1st page denotes the orbitofrontal projections of the corpus callosum, the next three pages give the anterior, superior, and lateral projections to the frontal lobe, the 5th page provides the parietal projections, the 6th page gives the occipital projections, and finally the 7th page denotes the temporal projections of the Corpus Callosum.

The following four pages show the plots for the segmented association tracts, namely the Inferior Fronto-Occipital Fasciculus (figures C.3.8 & C.3.9) and the Superior Longitudinal Fasciculus (figures C.3.10 & C.3.11). The first two of these pages show the left and right Inferior Fronto-Occipital Fasciculus, respectively. The final two pages display the left and right Superior Longitudinal Fasciculus, respectively.

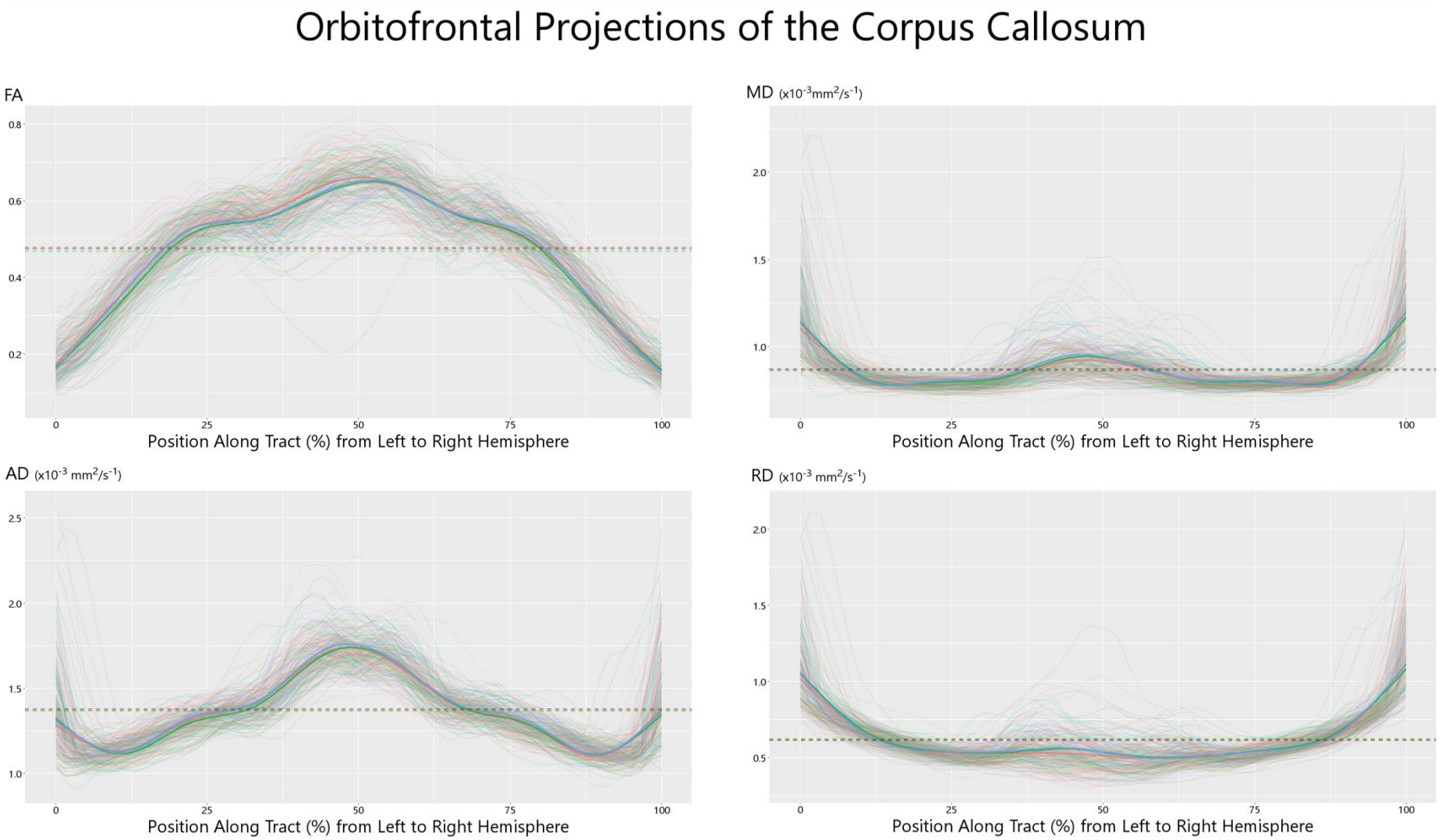

Figure C.3.1. Diffusion Indices along the Orbitofrontal Projections of the Corpus Callosum.

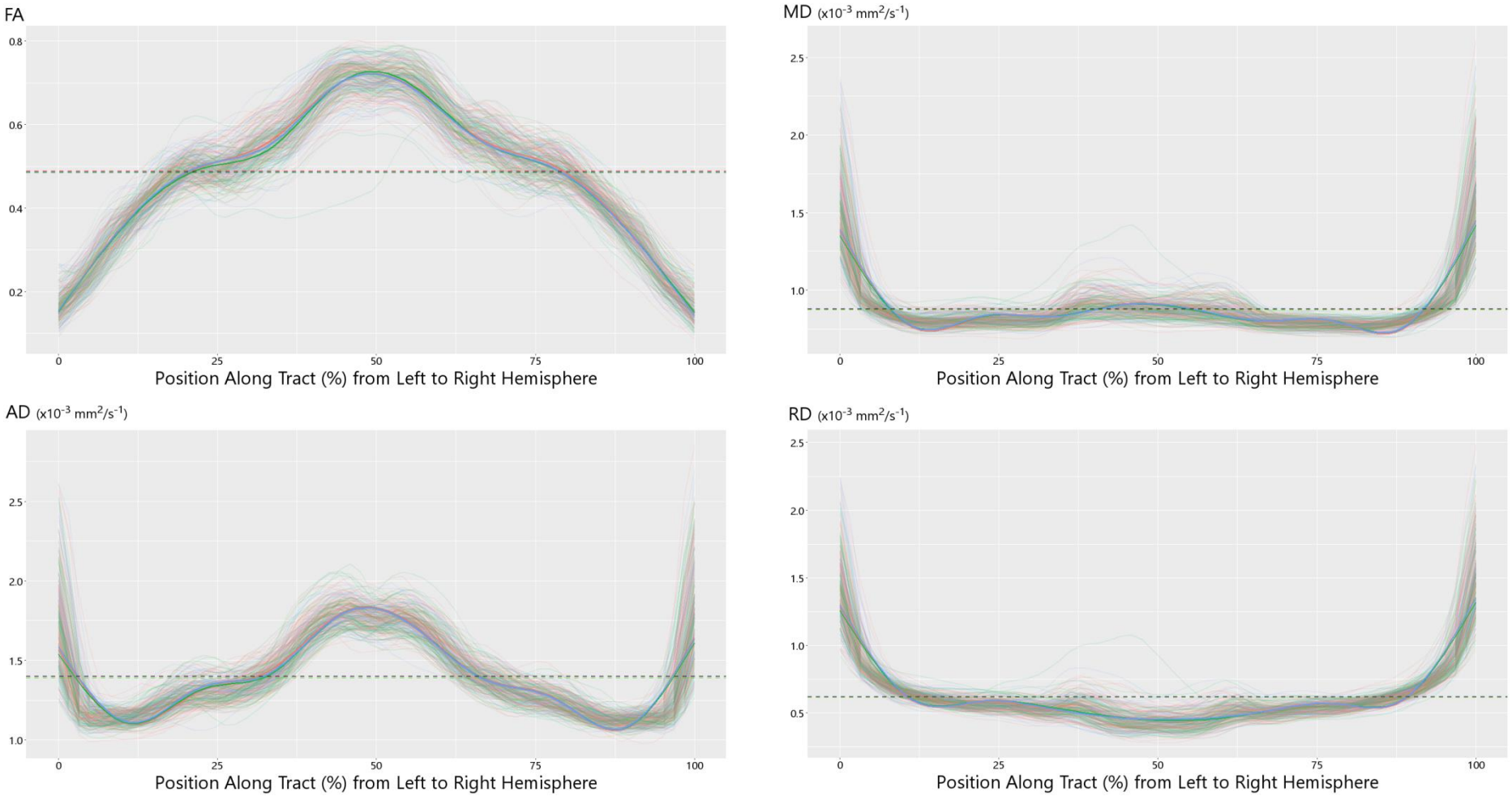

Figure C.3.2. Diffusion Indices along the Frontal Anterior Projections of the Corpus Callosum.

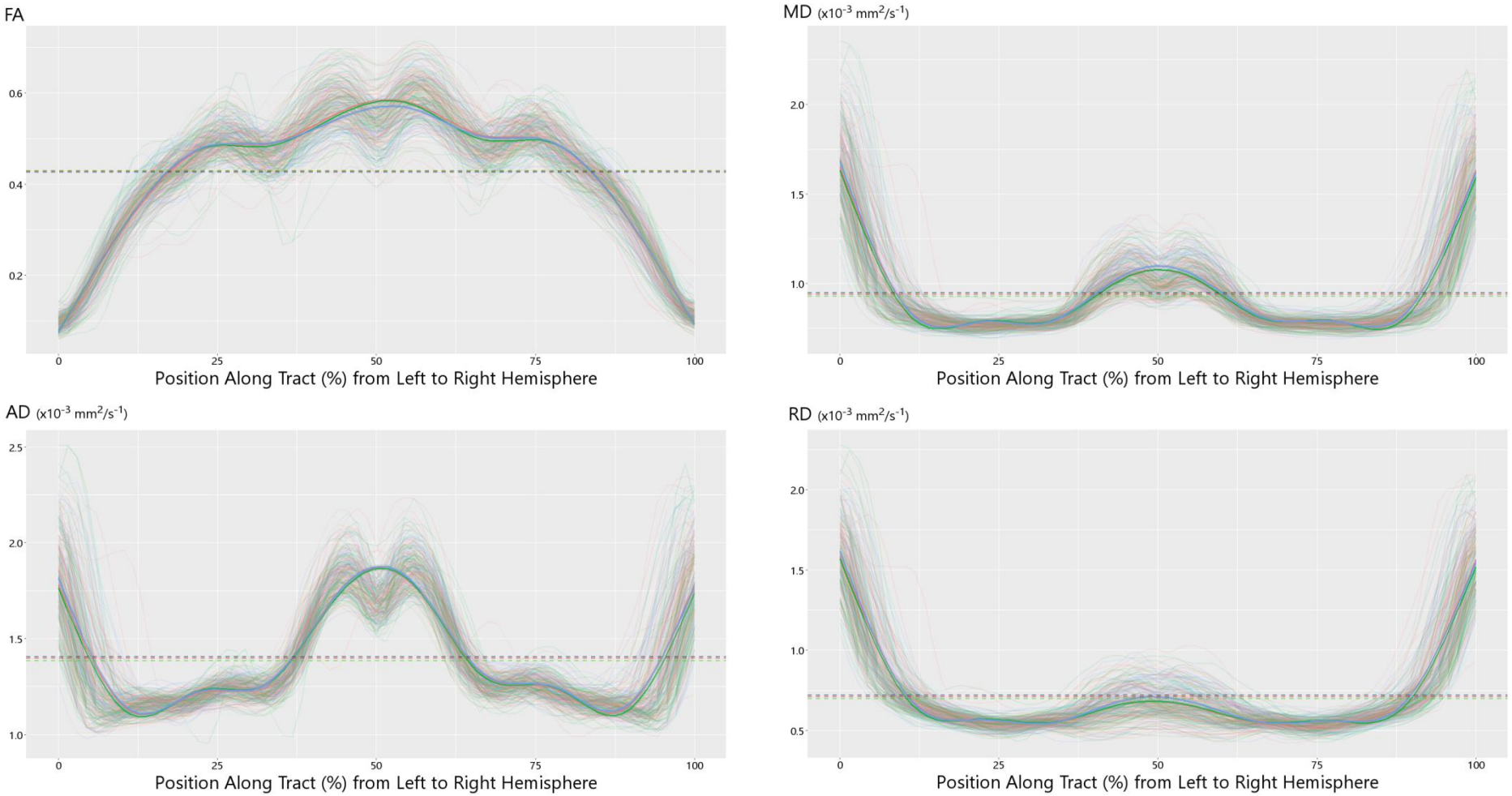

Figure C.3.3. Diffusion Indices along the Frontal Superior Projections of the Corpus Callosum.

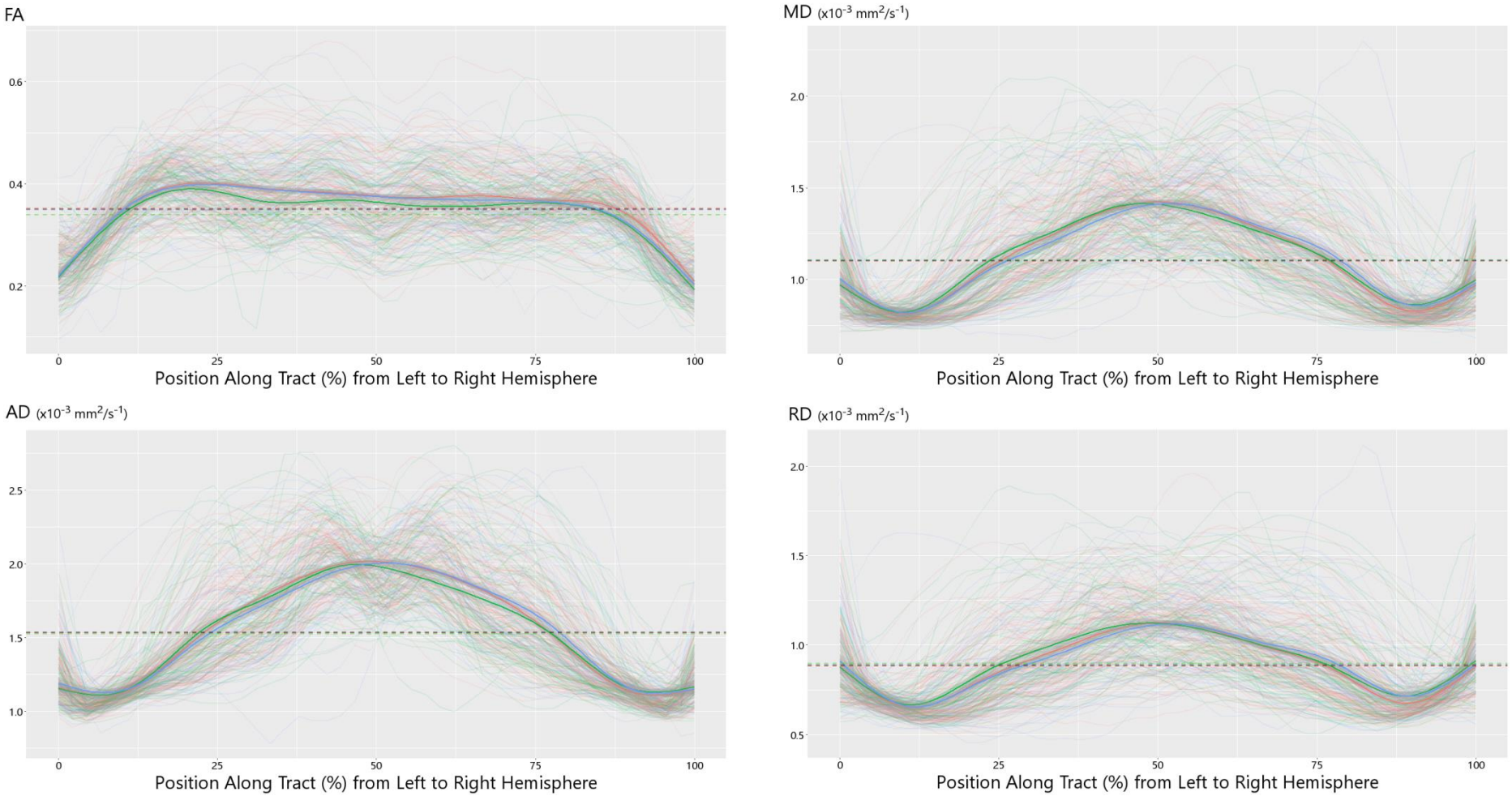

Figure C.3.4. Diffusion Indices along the Frontal Lateral Projections of the Corpus Callosum.

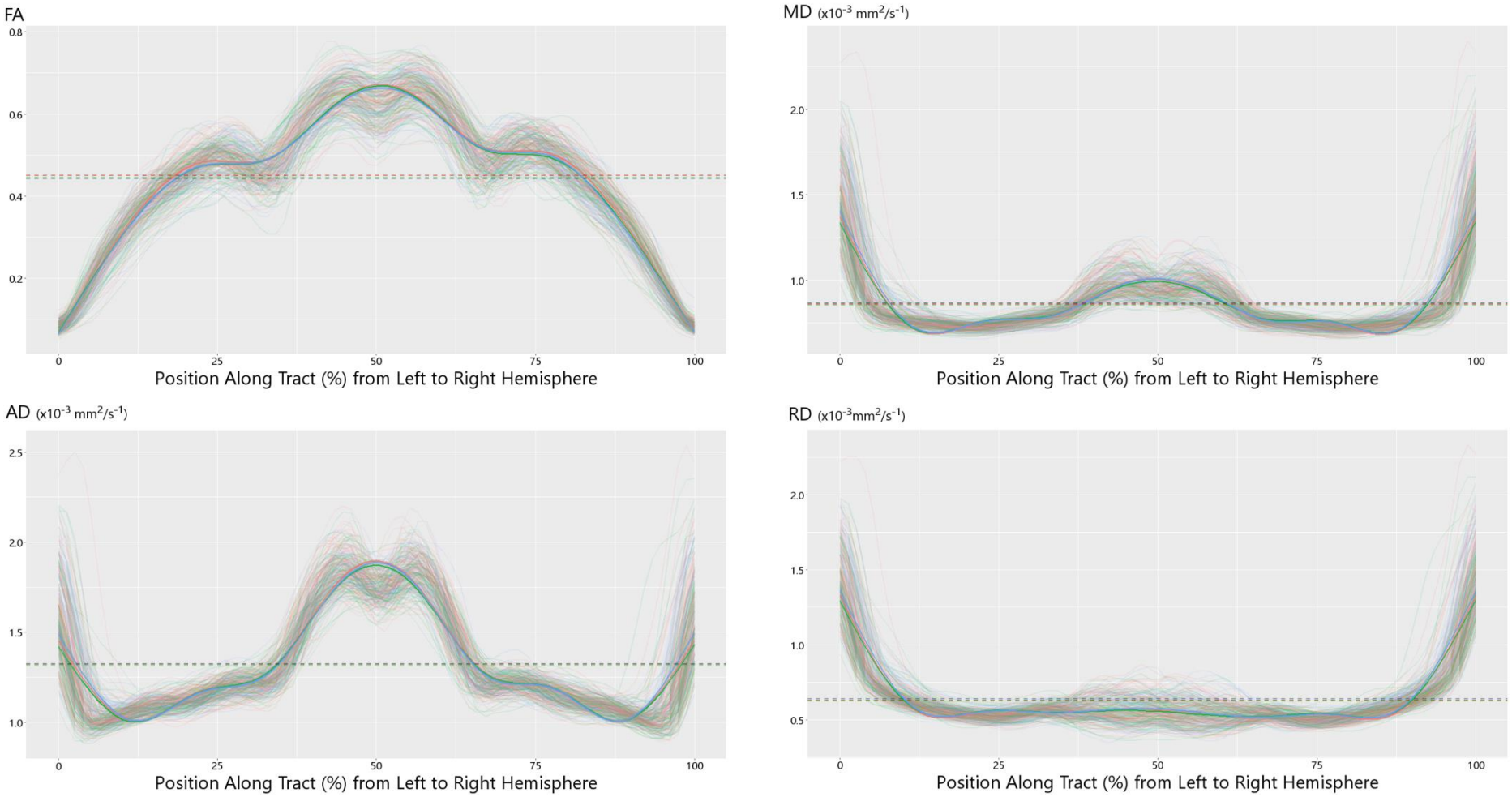

Figure C.3.5. Diffusion Indices along the Parietal Projections of the Corpus Callosum.

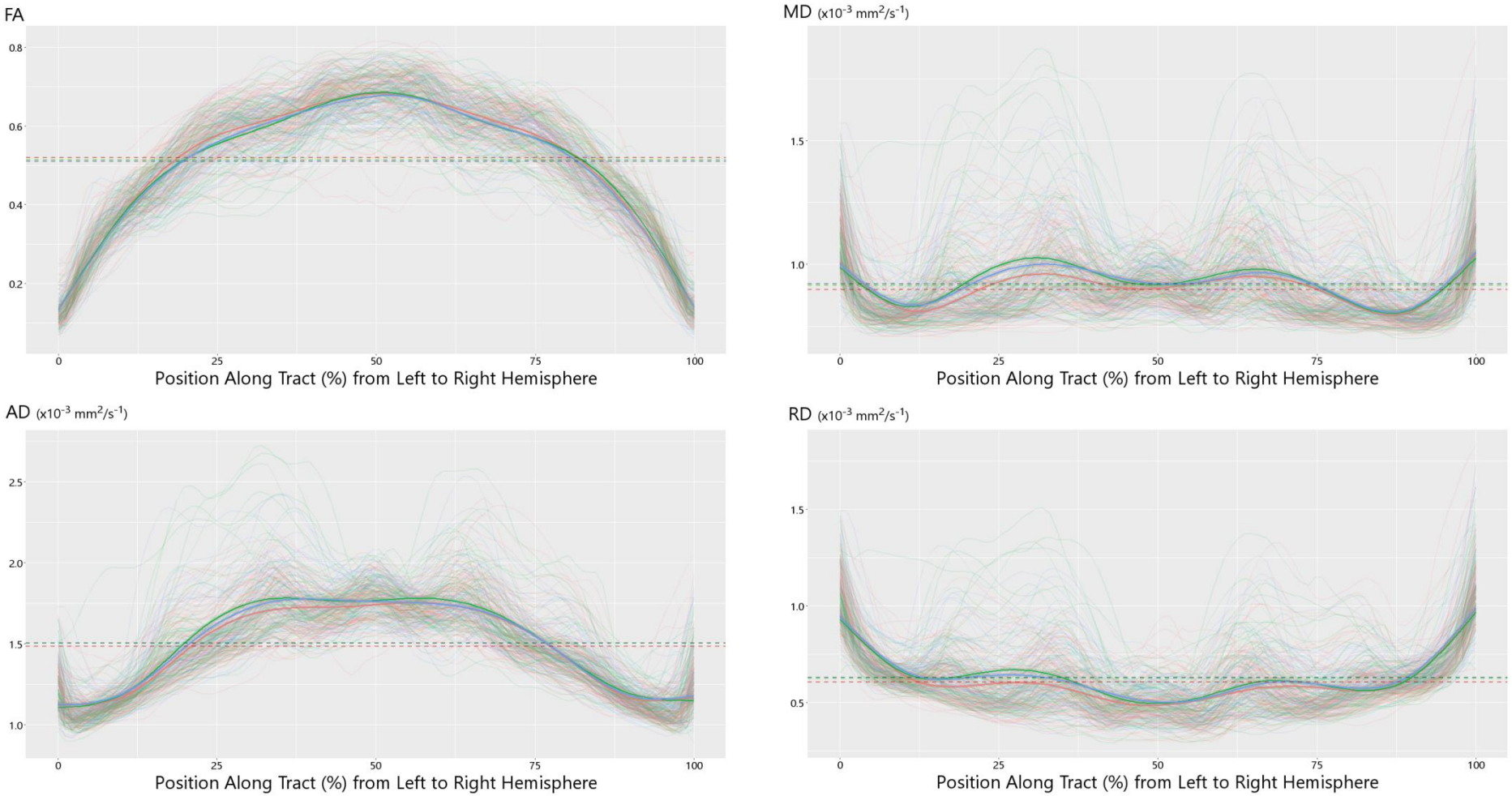

Figure C.3.6. Diffusion Indices along the Occipital Projections of the Corpus Callosum.

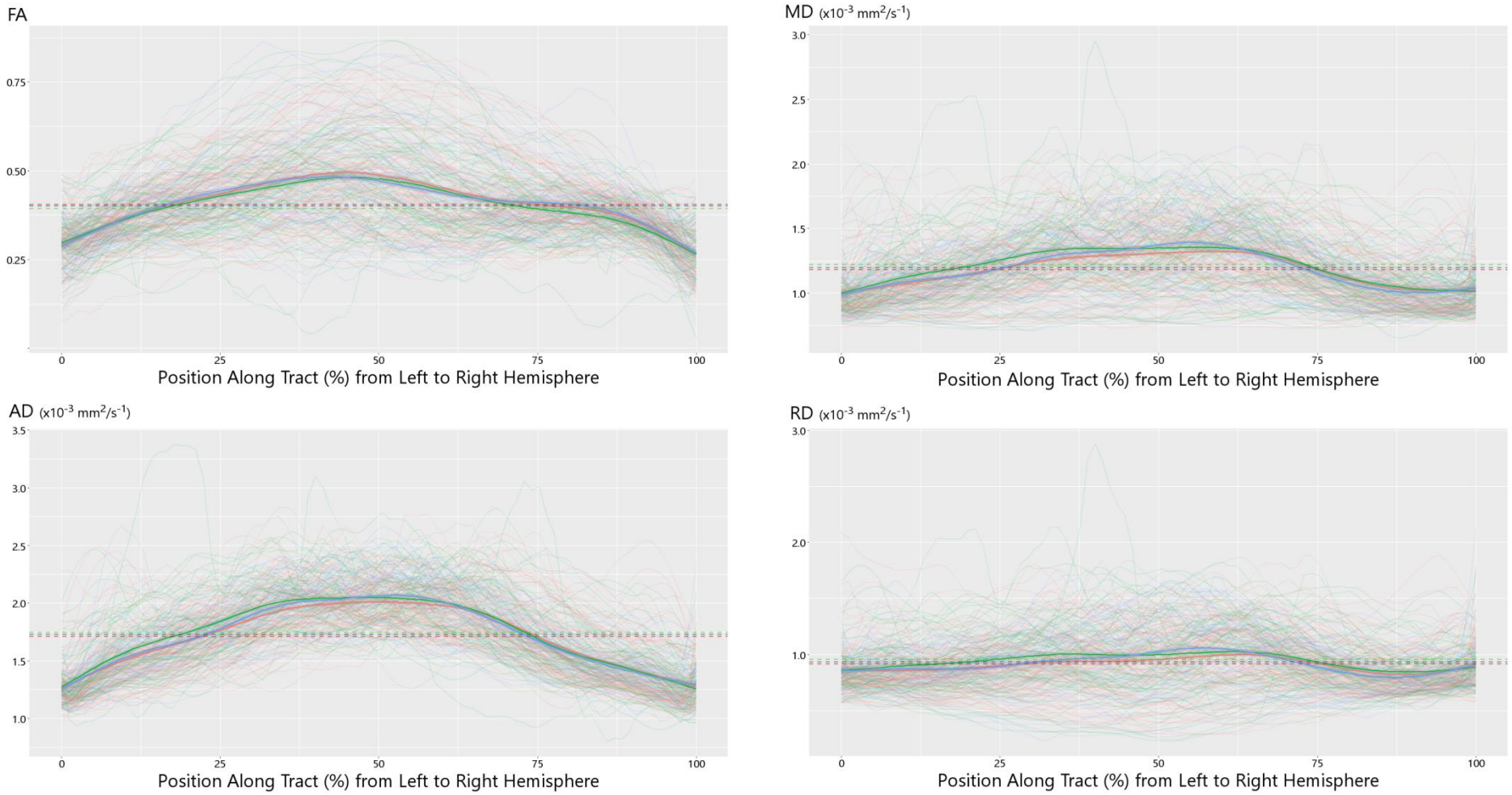

Figure C.3.7. Diffusion Indices along the Temporal Projections of the Corpus Callosum.

Left Inferior Fronto-Occipital Fasciculus

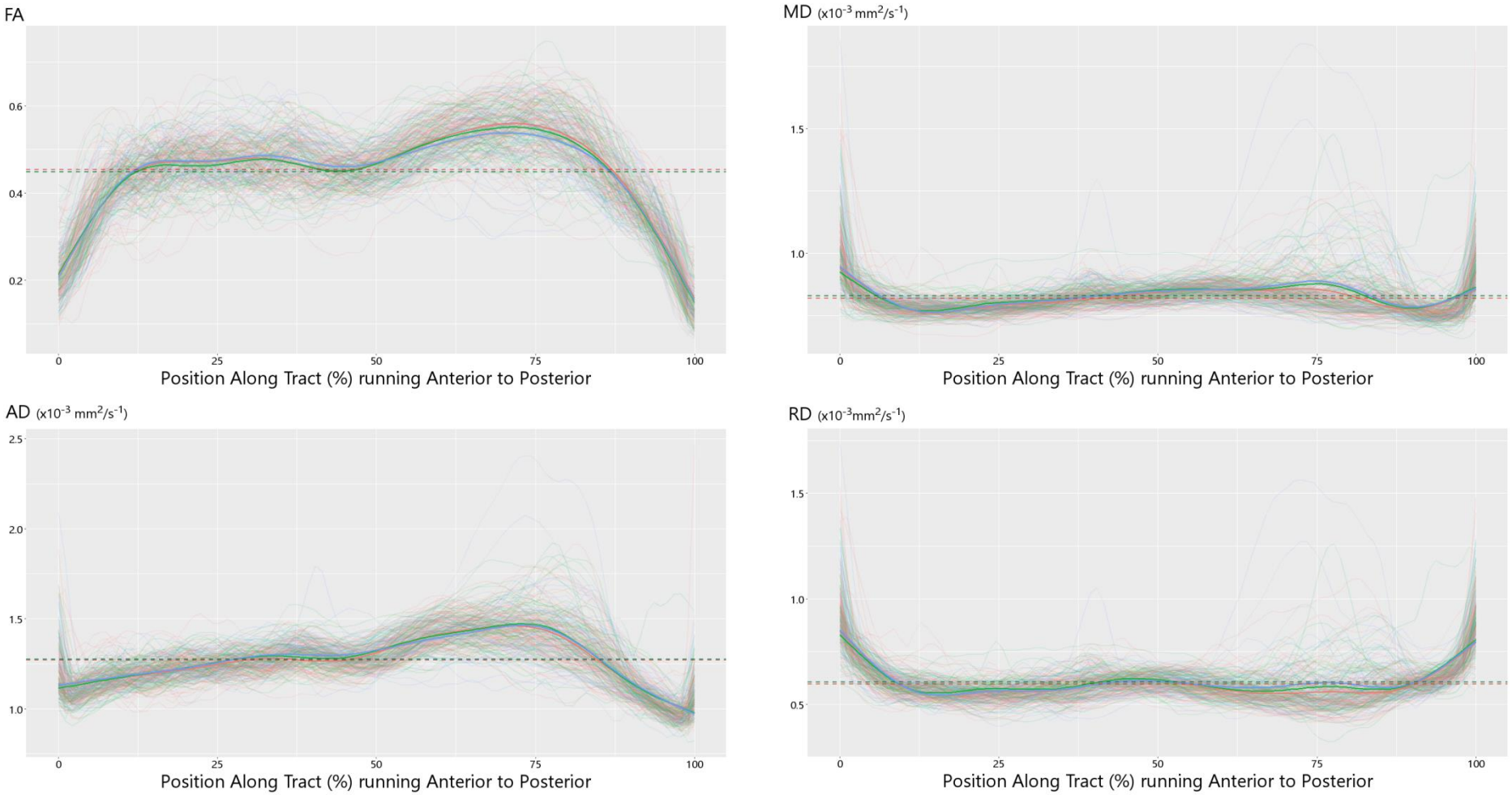

Figure C.3.8. Diffusion Indices along the Left Inferior Fronto-Occipital Fasciculus.

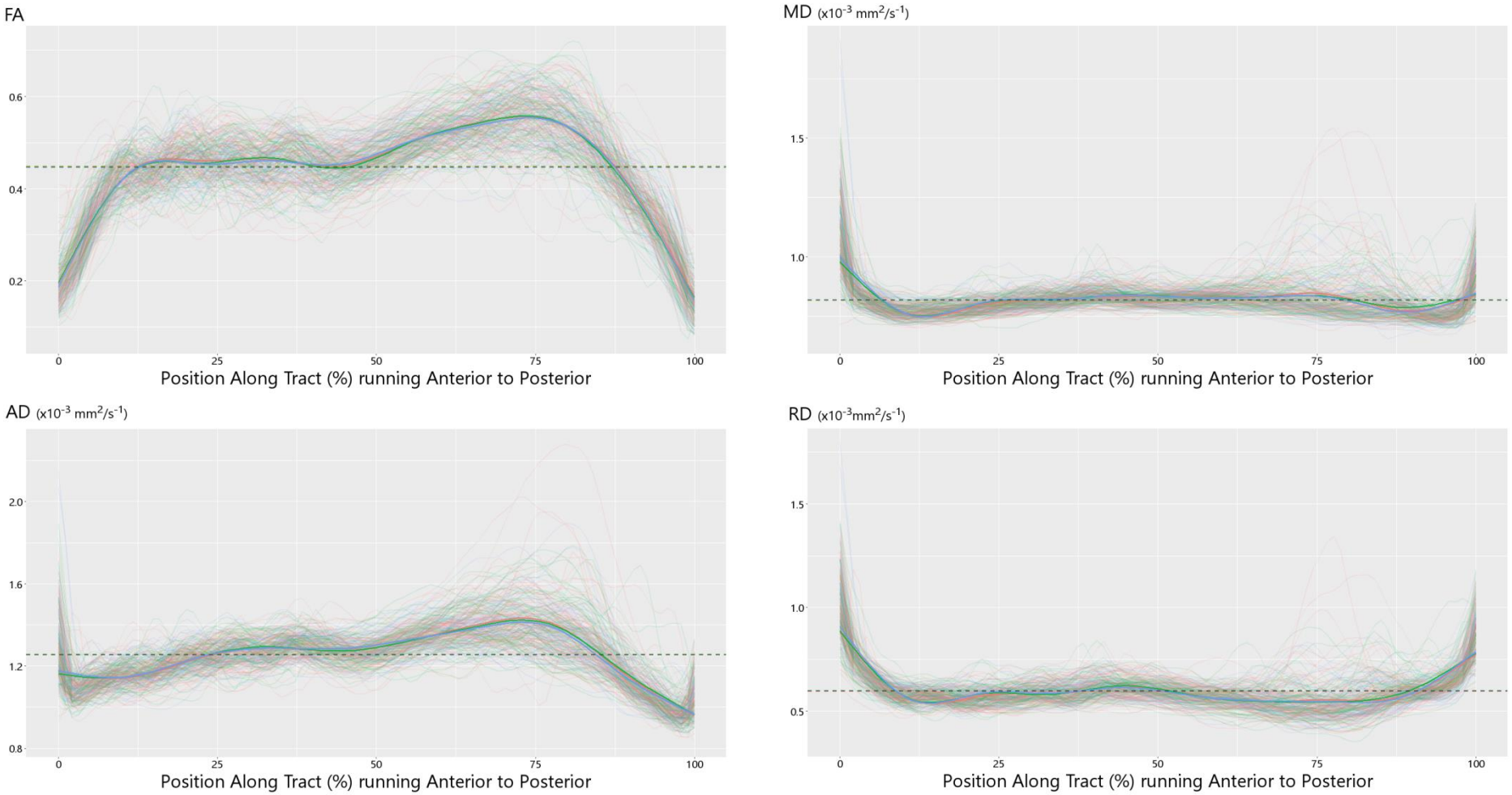

Figure C.3.9. Diffusion Indices along the Right Inferior Fronto-Occipital Fasciculus.

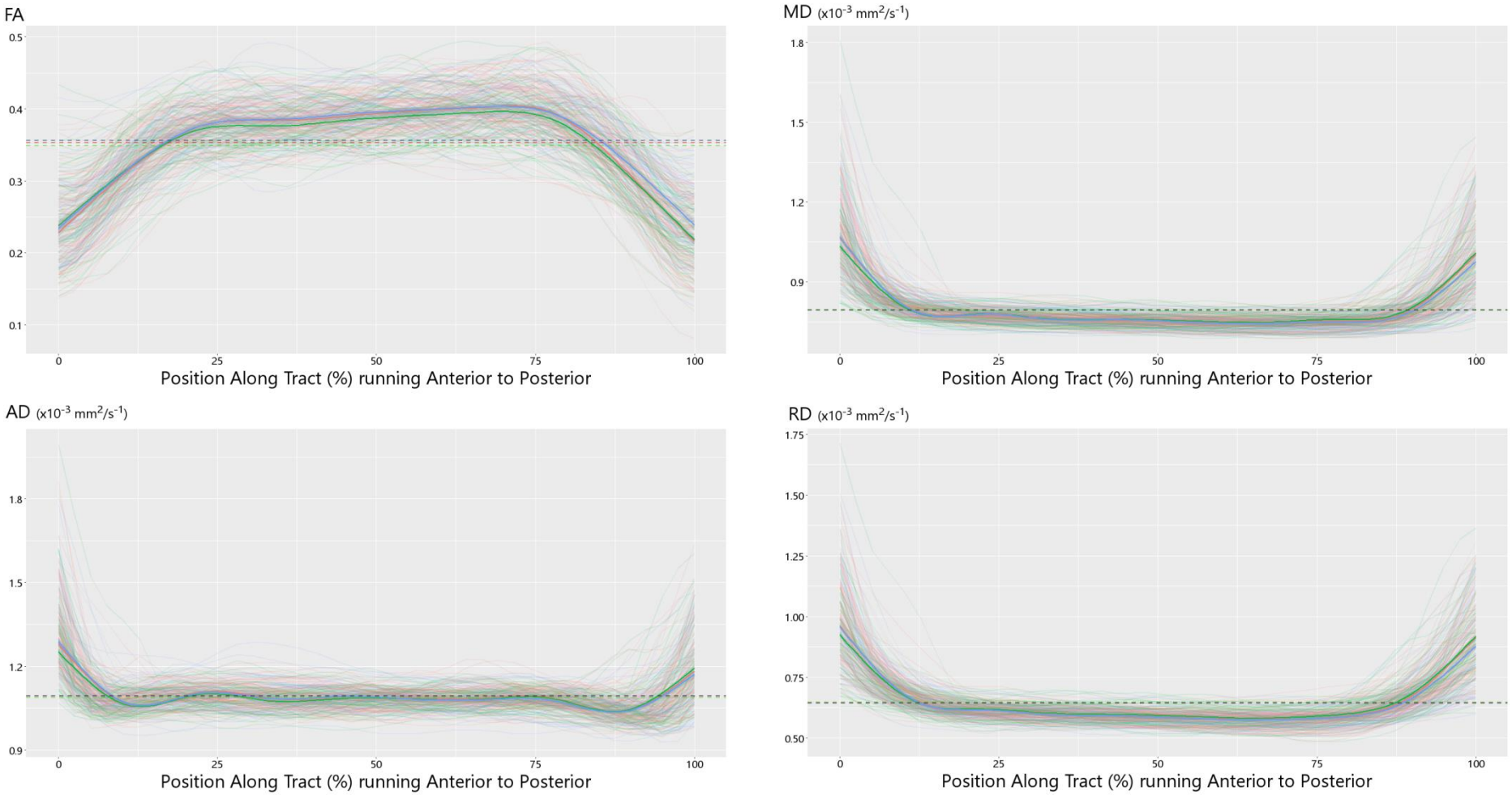

Figure C.3.10. Diffusion Indices along the Left Superior Longitudinal Fasciculus.

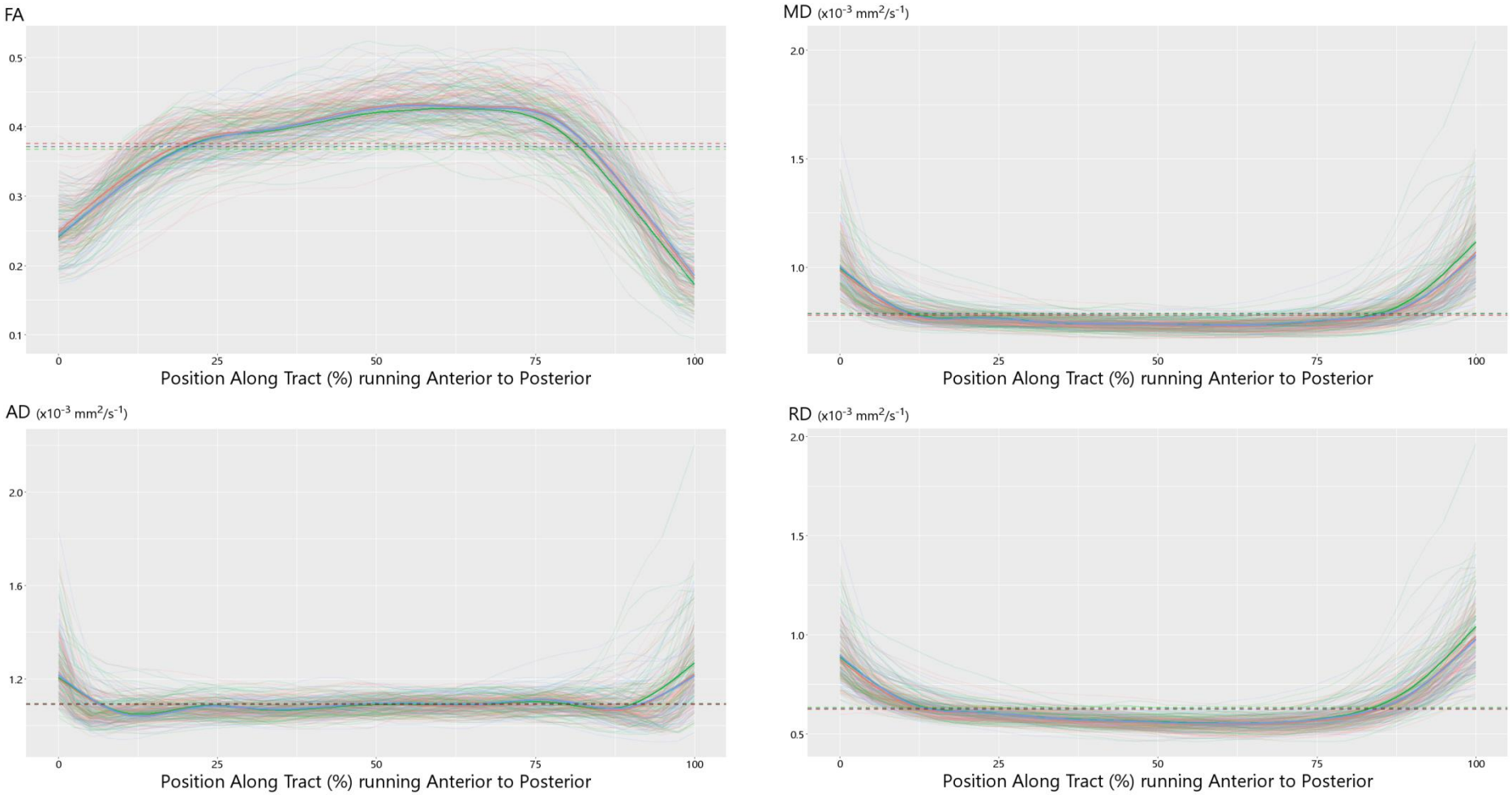

Figure C.3.11. Diffusion Indices along the Right Superior Longitudinal Fasciculus.